ISTANBUL TECHNICAL UNIVERSITY ★ GRADUATE SCHOOL

MICROWAVE DIELECTRIC PROPERTY CHARACTERIZATION WITH OPEN-ENDED COAXIAL PROBE AND SENSING DEPTH ANALYSIS OF THE PROBES FOR BIOLOGICAL TISSUES

Ph.D. THESIS

Cemanur AYDINALP

Department of Electronics and Communication Engineering

Telecommunications Engineering Programme

MARCH 2022

ISTANBUL TECHNICAL UNIVERSITY ★ GRADUATE SCHOOL

MICROWAVE DIELECTRIC PROPERTY CHARACTERIZATION WITH OPEN-ENDED COAXIAL PROBE AND SENSING DEPTH ANALYSIS OF THE PROBES FOR BIOLOGICAL TISSUES

Ph.D. THESIS

Cemanur AYDINALP
(504162302)

Department of Electronics and Communication Engineering

Telecommunications Engineering Programme

Thesis Advisor: Assoc. Prof. Tuba YILMAZ ABDOLSAHEB

MARCH 2022

İSTANBUL TEKNİK ÜNİVERSİTESİ ★ LİSANSÜSTÜ EĞİTİM ENSTİTÜSÜ

AÇIK UÇLU KOAKSİYEL PROB İLE MİKRODALGA DİELEKTRİK ÖZELLİK TANIMLAMASI VE BİYOLOJİK DOKULAR İÇİN PROBLARIN ALGILAMA DERİNLİK ANALİZİ

DOKTORA TEZİ

Cemanur AYDINALP
(504162302)

Elektronik ve Haberleşme Mühendisliği Anabilim Dalı

Telekomünikasyon Mühendisliği Programı

Tez Danışmanı: Assoc. Prof. Tuba YILMAZ ABDOLSAHEB

MART 2022

Cemanur AYDINALP, a Ph.D. student of ITU Graduate School student ID 504162302 successfully defended the thesis entitled "MICROWAVE DIELECTRIC PROPERTY CHARACTERIZATION WITH OPEN-ENDED COAXIAL PROBE AND SENSING DEPTH ANALYSIS OF THE PROBES FOR BIOLOGICAL TISSUES", which he/she prepared after fulfilling the requirements specified in the associated legislations, before the jury whose signatures are below.

Thesis Advisor :	**Assoc. Prof. Tuba YILMAZ ABDOLSAHEB** Istanbul Technical University	.....
Jury Members :	**Prof. Dr. Mehmet ÇAYÖREN** Istanbul Technical University	.....
	Prof. Dr. Ali YAPAR Istanbul Technical University	.....
	Asst. Prof. Evrim TETİK Arel University	.....
	Asst. Prof. Egemen BİLGİN MEF University	.....

Date of Submission : **16 February 2022**
Date of Defense : **28 March 2022**

To my parents İbrahim and Emine Dudu,

FOREWORD

Gratitude is owed to many individuals who have helped me over the past six years. I am very grateful to my advisor Associate Prof. Tuba YILMAZ ABDOLSAHEB more for her supportive and thoughtful suggestions during the period of my study. I extend my gratitude to my father İbrahim, mother Emine Dudu, and siblings, who gave me tremendous support and deserve much more than a simple thank you. I wish to thank several friends who worked closely with me during my study. Associate Prof. Mehmet Nuri AKINCI, my colleagues Sulayman JOOF, İsmail DİLMAN, PhD. candidates and Agah Oktay ERTAY, PhD. many thanks for your helpful friendship.

March 2022

Cemanur AYDINALP
(Research Assistant)

TABLE OF CONTENTS

Page

ABBREVIATIONS

ADS : Advanced Design System
ANN : Artificial Neural Network
BN : Batch Normalization
CST : Computer Simulation Technology
CT : Computed Tomography
DAK : Dielectric Assessment Kit
DL : Deep Learning
DMBA : Dimethylbenz(a)anthracene
DMEM : Dulbecco's Modified Eagle Medium
DMSO : Dimethyl Sulfoxide
DN : Dense Layer
DP : Dielectric Property
ESWL : Extracorporeal Shockwave Therapy
FBS : Fetal Bovine Serum
IR : Infrared Radiation
k-NN : k-Nearest Neighborhood
LUT : Look Up Table
mm : milimeter
MPE : Mean of Percent relative Error
MRI : Magnetic Resonance Imaging
MTI : Microwave Tomography Imaging
MUT : Material Under Test
MWI : Microwave Imaging
NIST : National Institute for Standard and Technology
NN : Neural Network
OECP : Open-Ended Coaxial Probe
PCNL : Percutaneous Nephrolithotomy
PET : Positron Emission Tomography
PSO : Particle Swarm Optimization
RBF : Radial Basis Function
ReLu : Relu Layer
RL : Regression Layer
SD : Standard Deviation
SEM : Scanning Electron Microscopy
SPE : Standard deviation of Percent relative Error
XRD : X-Ray Powder Diffraction

SYMBOLS

a and b	**:** The inner and outer radius of the conductors
α	**:** The linear model parameters
$\mathbf{B^{p_i}}$	**:** The size of a single hidden layer
$\mathbf{d_k}$,	**:** The thickness of specified layer
$\mathbf{D_n}$	**:** The distance from the probe tip to the surface of the first layer.
$\mathbf{E_{v,L}}$, $\mathbf{E_{t,L}}$	**:** The validation and training error for L many hidden layers
ε_c	**:** The complex permittivity
ε_∞	**:** The high-frequency permittivity
ε'	**:** The real-part for the complex permittivity
ε''	**:** The imaginary-part for the complex permittivity
ε_r	**:** The Relative permittivity
ε_s	**:** The static permittivity
Γ	**:** The reflection coefficient
Γ_c	**:** The calibrated reflection coefficient of measured material
$J_0(\cdot)$	**:** The first order Bessel function
$\mathbf{k_d}$	**:** The wave number of the dielectric material
$\mathbf{k_0}$	**:** The free space wave number
L	**:** The number of hidden layers
ω	**:** The angular frequency
σ	**:** The conductivity
ρ_k	**:** the reflection coefficients of measured material
$\mathbf{S_{11,22}}$, $\mathbf{S_{12,21}}$	**:** The scattering parameters
τ	**:** The relaxation time
$\mathbf{X_1}$, $\mathbf{X_2}$	**:** The displayed value of caliper for positions of probe
Y	**:** Admittance
$\mathbf{Y_0}$	**:** The probe characteristic admittance

LIST OF TABLES

Page

LIST OF FIGURES

Page

MICROWAVE DIELECTRIC PROPERTY CHARACTERIZATION WITH OPEN-ENDED COAXIAL PROBE AND SENSING DEPTH ANALYSIS OF THE PROBES FOR BIOLOGICAL TISSUES

SUMMARY

Inherent dielectric property discrepancy at microwave frequencies between the healthy and malignant tissues enabled many different microwave diagnostic technologies among these microwave breast cancer imaging, microwave hyperthermia, and microwave ablation are popular research topics. To develop and test such technologies the dielectric properties of the biological tissues must be quantified. This is mostly done with the open-ended coaxial probes in the laboratory environment due to advantages of the technique including but not limited to minimal sample preparation requirements, commercial availability and broadband measurement capabilities. Despite being commercially available, the technique suffers from high error rates and remains overlooked as a potential diagnostic technology.

The error sources can be categorized as the sample and equipment related complications. The sample related error sources can be mitigated via the selection of an appropriate probe for dielectric property characterization. Particularly, biological tissues are known to be heterogeneous contributing to the high measurement error due to sample. Hence, it is important to analyze the sensing depth of the probes under different conditions including using samples with varying dielectric properties and probes with different aperture diameters. Next, the equipment related errors mostly due to the mathematical approach which can potentially be diminished via the introduction of new retrieval methodologies. Towards this end, in an attempt to enable diagnostics applications of the open-ended coaxial probe technique, this thesis focuses on the improvement of the two shortcomings by sensing depth characterization and introducing a deep learning based model for dielectric property retrieval.

In the first part of the thesis, sensing depth analysis of the 2.2 mm diameter open-ended coaxial probe was performed using two different double-layered configurations to mimic the tissue heterogeneity. The double-layered configurations are used to mimic the heterogeneous skin tissue in order to establish the potential use of the open-ended coaxial probe method for skin cancer diagnosis. To this end, the sensing depth analysis was performed via simulations and measurements. The double-layered sample configurations are composed using skin-mimicking phantom and olive oil or triton X-100 liquids. In addition, the experiments were carried out by following a newly proposed measurement protocol, which can be easily applied to any tissue type. The results show that the sensing depth was independent of the frequency of operation (0.5-6 GHz) and was affected by the following conditions: by the material located immediately at the probe tip, and by the dielectric property contrast between the two layers. Thus, in order to accurately obtain dielectric property measurement

results using the open-ended coaxial probe method, there is a need to establish a pre-measurement protocol to minimize the error due to the skin tissue diversity.

The second part of thesis reports the sensing depth analysis of the open-ended coaxial probe for ex vivo experiments on real heterogeneous tissue. The knowledge on the sensing depth of the probe can help eliminate the errors due to tissue heterogeneity. Accurate classification of tissues with similar dielectric properties can be obtained by minimizing the measurement errors. Therefore, this method can be applied in practical applications, such as microwave biopsy. In this work, double-layered sample configuration consisting of an ex vivo rat's breast or wet skin as first layer and pure liquids olive oil or triton X-100 as second layer was utilized to perform the sensing depth analysis of the probe from 0.5 to 6 GHz frequency range. A straight forward, adoptable experimental protocol was established and employed in this study. The analysis was performed by determining five different the percent change in measured dielectric property values. The results indicate a discrepancy of 52%-84% of the measured dielectric property when a membrane layer (between 0.4-0.8 mm thickness) was present on the wet skin tissue and breast tissue.

The aim of the third part of this thesis is to analyze and to specify the sensing depth of the open-ended coaxial probe in order to employ the appropriate probe aperture dimension for any given measurement set-up. The proposed method has the potential to reduce the errors due to tissue heterogeneity for skin cancer diagnosis. This work presents the sensing depth comparison of three different probes with different aperture sizes. Simulations of the probes with 0.5, 0.9 and 2.2 mm-diameters terminated with a double-layered skin tissue and olive oil sample configuration were performed. It should be noted that probes with different aperture diameters were investigated in the literature but no information was reported on probes with small aperture sizes. An experimental validation of the simulated scenario was performed with the 2.2 mm-diameter probe and the fully developed double-layered configuration. The acquired simulations and experimental results indicate a proportional relation between the sensing depth and the aperture of the probe. From this relation, it can be concluded that probes with smaller aperture size can possibly help to obtain more precise results from the heterogeneous tissues which can lead to the accurate characterization of thin skin tissue layers. In order to obtained more accurate results especially for tissues with multi-layered structures or membrane-like layers, it is recommended to a establish measurement protocols to prepare the surface of the tissue.

In the fourth and last part of the thesis, a novel approach for the determination of material dielectric properties from the reflection coefficient response of the open-ended coaxial probe is proposed. This technique retrieves the Debye parameters of the material under test using a deep learning model which is trained with numerically generated data. The ability to train the deep learning model with synthetic data provide the advantage of rapid generation of a large variety of materials as a dataset. Additionally, the presented method can be easily adapted to any type of probe with desired dimensions and materials. An experimental verification of the trained deep learning model was performed by testing the network with measured reflection coefficients obtained from five different standard liquids, four mixtures, and a gel-like material. A comparison of the acquired results from the deep learning model with literature values is also performed. Finally, a large-scale statistical verification of the retrieved dielectric property from the proposed technique is presented.

AÇIK UÇLU KOAKSİYEL PROB İLE MİKRODALGA DİELEKTRİK ÖZELLİK TANIMLAMASI VE BİYOLOJİK DOKULAR İÇİN PROBLARIN ALGILAMA DERİNLİK ANALİZİ

ÖZET

Kanser çağımızda sık görülen hastalık türlerinden biridir. Her ne kadar hastalığın sebebi tam olarak belirlenememiş olsa da tanı ve teşhis yöntemleri geliştirilmeye devam etmektedir. Kanser, anormal doku hücrelerinin kontrolsüz bir şekilde çoğalıp büyümesi ve diğer sağlıklı dokulara yayılması sonucunda ortaya çıkan ve hayati riskin oldukça yüksek olduğu bir hastalık türüdür. Bu hastalığın erken teşhis edilmesi ve tedaviye erken başlanması ölüm riskini önemli ölçüde düşürmektedir. Sağlıklı ve sağlıksız dokular arasındaki mikrodalga frekanslarında görülen dielektrik özellik farklılığı, mikrodalga meme kanseri görüntüleme, mikrodalga hipertermi ve mikrodalga ablasyon gibi birçok farklı mikrodalga tanı ve tedavi teknolojisinin gelistirilmesini mümkün kılmıştır. Böylelikle, hastalığın erken teşhisi mümkün hale gelip tedavi sürecine hemen başlanabilmektedir. Bu tür teknolojileri geliştirmek ve test etmek için biyolojik dokuların dielektrik özelliklerinin ölçülmesi gerekmektedir. Dielektrik özellikleri bilinen dokular sayesinde daha güvenilir ve kapsamlı tanı, teşhis ve tedavi yöntemleri geliştirilebilmektedir. Bu ölçümler, minimum numune hazırlama gereksinimi, piyasadan kolaylıkla satın alınabilir olması ve geniş bant ölçüm özelliği gibi daha fazla avantajlara sahip olması nedeniyle laboratuvar ortamında çoğunlukla açık uçlu koaksiyel problarla yapılır. Piyasada kolay ulaşılabilir olmasına rağmen, bu tür ölçüm teknikleri yüksek hata oranlara sahip olduklarından dolayı, potansiyel bir teşhis teknolojisi olarak kullanılmaktan kaçınılmaktadır. Hata kaynakları, numune ve ekipmanla ilintili olmak üzere iki sınıfa ayrılabilir.

Ekipmanla ilişkili hatalar seçilen ölçüm ekipmanından, ölçüm belirsizliklerinden, ölçüm esnasındaki kalibrasyondan veya kullanılan matematiksel yaklaşımlardan kaynaklanabilmektedir. Ölçüm ekipmanı seçimi, yöntemin avantaj ve dezavantajları göz önünde bulundurularak yapılmalıdır. Ölçüm sisteminin belirsizliği, ölçülen numunenin aynı ölçüm koşullar altında birden fazla ölçüm yapılarak tekrarlanabilirliği ve doğruluğu saptanarak giderilmelidir. Standart bir ölçüm kalibrasyon prosedürü (açık devre, kısa devre ve bilinen dielektrik özelliklere sahip bir sıvı olan saf su ölçümü) kullanılmalıdır. Kalibrasyon başarıyla tamamlandığında, hata oranı düşük dielektrik özellik ölçümleri alınabilir. Ayrıca, ölçüm sisteminin doğru çalıştığının önceden teyit edilmesi için bilinen referans sıvının dielektrik özelliklerinin de ölçülmesi gerekmektedir. Doğrulama yoluyla, kalibrasyon kalitesi kontrol edilebilir ve sistematik hatalar giderilebilir. Ayrıca, ekipmanla ilgili hatalar matematiksel yaklaşımlardan da kaynaklanabilir. Yeni yaklaşımlardan olan makine veya derin öğrenme yöntemleri ile bu hatalar giderilebilir.

Dokuyla ilişkili hatalar, sıcaklıktan, prob ile numunenin temasının tam olarak gerçekleştirilemediğinden, probun numune üzerine uyguladığı basınçtan, in vivo ve ex

vivo deneylerin farklılığından, doku numunesinin özelliklerinden ve heterojenliğinden kaynaklanabilir. Sıcaklığın dielektrik özellikler üzerinde etkisinin olduğu bildirilmektedir. Açık uçlu koaksiyel probun biyolojik dokuların dielektrik özelliklerini doğru bir şekilde ölçmek için prob-numune temasının tam olarak gerçekleştirilmesi önem arz etmektedir. Ölçüm esnasında prob ile numune arasında herhangi bir hava boşluğu olmaması gerekmektedir. Doku yüzeyinin özelliklerine bağlı olarak, prob-doku teması tam olarak gerçekleştirilemiyorsa, daha küçük bir prob seçilerek temas tam olarak sağlanmalıdır. Biyolojik dokuların dielektrik özelliklerini ölçerken, prob ucunun doku üzerine uyguladığı baskıdan dolayı prob ucunda doku sıvısı birikebilir, bu da ölçüm sonuçlarını büyük ölçüde etkilemektedir. In vivo ve ex vivo deneylerde dielektrik özelliklerinin birbirinden farklı olması da medikal alanda kullanılacak olan bu yöntemin karşılaştığı zorluklardandır. Canlı ve cansız doku özellikleri su içeriği, sıcaklık ve damarlardaki kan akışı, kalp hızı gibi fizyolojik farklılıklara sahip olmasından dolayı ölçüm sonuçları etkilenmektedir. Dokunun heterojenliği, dielektrik özelliklerin ölçümü sırasında yöntemin karşılaştığı zorluklarından biridir.

En kritik hata kaynaklarından biri olan numunelerin heterojenliğinin etkisi, dokuların dielektrik özelliklerini ölçerken uygun bir prob seçilerek azaltılabileceği ön görülmektedir. Bu nedenle, yaygın olarak kullanılan 2.2 mm çaplı probun algılama derinliğinin analiz edilmesi ve ölçüm sistemiyle ilgili problemlerin tanımlanarak 0.9 ve 0.5 mm çaplı probların algılama derinliğinin detaylıca analiz edilmesi önemlidir. Bu probların algılama derinliğinin farklı koşullar altında (numune heterojenliği açısından) analiz edilmesi hata kaynağının saptanmasında yardımcı olacaktır. Ayrıca, probun boyutlarına bakılmaksızın ölçümlerden elde edilen yansıma katsayılarını doğrudan kullanarak her tür malzemenin dielektrik özelliğini hesaplayabilen uyarlanabilir bir hesaplama yöntemine sahip olmak önemlidir. Böylece, ekipmanla ilgili hatalardan olan matematiksel yaklaşımlardan kaynaklı olan hataların, önerilen yeni yaklaşım ile azaltılabileceği ön görülmektedir.

Tezin ilk bölümünde, doku heterojenliğini benzetmek için iki farklı çift katmanlı numune konfigürasyonları kullanılarak 2.2 mm çaplı açık uçlu koaksiyel probun algılama derinliği analizi yapılmştır. Böylece, cilt kanseri teşhisi için açık uçlu koaksiyel prob yönteminin potansiyel kullanımını belirlemek için cilt dokusu heterojenliğinin 2.2 mm çapındaki probun algılama derinliği üzerindeki etkisi araştırılmıştır. Çalışmada, benzetimler ve deneysel ölçümler yoluyla algılama derinliği analizi yapılmıştır. Cilt dokusunun heterojenliği, cilt benzeri fantom ve zeytinyağı veya triton X-100 sıvılarından oluşan çift katmanlı numune konfigürasyonları kullanılarak gerçekleştirilmiştir. Ayrıca deneyler her algılama derinliği, prob ve doku çalışmasına kolaylıkla uygulanabilen bir ölçüm protokolü izlenerek gerçekleştirilmiştir. Bağıl dielektrik (yalıtkanlık) sabiti, 5, 20 ve 80 yüzdesel değişikliklerinde, birden fazla frekans noktalarında analiz edilmiştir. Sonuçlar, algılama derinliğinin çalışma frekansından (0.5-6 GHz) bağımsız olduğunu; prob ucu ile doğrudan temas halinde olan malzemeden ve iki katman arasındaki dielektrik özellik kontrasttan etkilendiğini göstermektedir. Hem benzetim hem de deney sonuçları zeytinyağı ve triton X-100'ün dielektrik özelliklerinin 2 GHz'de %5, %20 ve %80 değişimlerine göre analiz edilmiş ve 0.36-0.86 mm 0.14-0.42 mm ve 0.66–1.2 mm kalınlıklarındaki zeytin yağı ve triton X-100'de %5, %20 ve %80 değişimleri sırasıyla gözlemlenmiştir. Sonuçlara dayanarak deri dokusu üzerindeki bir membran veya keratin tabakasının ölçüm dielektrik özellik sonuçlarını potansiyel olarak %80 etkileyeceği söylenebilmektedir. Bu nedenle, açık uçlu koaksiyel prob yöntemini kullanarak dielektrik özellik ölçüm

sonuçlarını doğru bir şekilde elde etmek için, cilt dokusu çeşitliliğinden kaynaklanan hatayı en aza indirecek bir hazırlık protokolünün oluşturulmasına ihtiyaç vardır.

Tezin ikinci kısmında, ex vivo deneylerde ölçümü yapılan gerçek heterojen dokular için açık uçlu koaksiyel probun algılama derinliği analizleri sunulmuştur. Probun algılama derinliği hakkında bilgi sahibi olmak, hayvan deneyleri esnasında doku heterojenliğinden kaynaklanan hataların ortadan kaldırılmasında yardımcı olacağı ön görülmektedir. Benzer dielektrik özelliklere sahip dokuların doğru sınıflandırılması için ölçüm hatalarını en aza indirmek gerekmektedir. Bu sayede, bu yöntem mikrodalga biyopsisi gibi pratik uygulamalarda uygulanabilir. Bu çalışmada, 0.5-6 GHz çalışma frekansları arasında, probun algılama derinliği analizini gerçekleştirmek üzere ilk katmanı bir ex vivo sıçanın göğsü veya ıslak derisi ve ikinci katmanı saf sıvı zeytinyağı veya triton X-100'den oluşan çift katmanlı numune konfigürasyonları tasarlanmıştır. Bu çalışmada kolaylıkla uyarlanabilir bir deney protokolü oluşturulmuş ve kullanılmıştır. Analiz gerçekleştirilirken ölçülen dielektrik özellik değerlerinin beş farklı yüzde değişimi göz önünde bulundurulmuş ve analiz hesaplamaları bu değişimler üzerinden yapılmıştır. Sonuçlara göre, dielektrik özelliği ölçülen ıslak cilt dokusu ve meme dokusu üzerinde herhangi bir membran tabakası (0.4-0.8 mm kalınlık arasında) bulunması durumunda ölçüm sonuçlarının %52-%84 oranında etkinlendiği saptanmıştır.

Tezin üçüncü bölümünde, herhangi bir ölçüm düzeneğinde kullanılmak üzere uygun prob boyutunu belirlemek için açık uçlu koaksiyel probun algılama derinliği analiz edilmiştir. Önerilen bu yöntem, cilt kanseri teşhisi için doku heterojenliğinden kaynaklanan hataları azaltma potansiyeline sahiptir. Bu çalışmada, farklı açıklık boyutlarına sahip üç adet probun algılama derinliğinin karşılaştırması yapılmıştır. Çift katmanlı deri dokusu ve zeytinyağı numune konfigürasyonu içeren 0.5, 0.9 ve 2.2 mm çaplı probların benzetimleri gerçekleştirilmiştir. Literatürde farklı açıklık çaplarına sahip probların çalışmaları yapılmıştır ancak küçük açıklık boyutlarına sahip problar hakkında detaylı bilgi belirtilmemiştir. Benzetim ile gerçekleştirilen senaryonun deneysel doğrulaması, 2.2 mm çapındaki prob ve birebir benzetimi yapılan çift katmanlı konfigürasyon ile gerçekleştirilmiştir. Benzetimlerin ve deneylerin sonuçları, algılama derinliği ile probun açıklığı arasında orantılı bir ilişki olduğunu göstermektedir. Bu orantısal ilişki sayesinde, daha küçük yarıçapa sahip problar ile heterojen dokuların ölçümünün daha hassas yapılacağı ve böylece ince cilt dokusu katmanlarının daha yanlışsız karakterizasyonunun yapılacağı sonucuna varılmaktadır. Özellikle çok katmanlı yapılara veya zar benzeri katmanlara sahip dokularda daha doğru sonuçlar elde edebilmek için doku yüzeyini hazırlayacak ölçüm protokollerinin oluşturulması bu çalışma sonucunda önerilmektedir.

Tezin dördüncü ve son bölümünde, açık uçlu koaksiyel probun yansıma katsayısı ölçümlerinden malzemelerin dielektrik özelliklerinin belirlenmesi için yeni bir yaklaşım önerilmiştir. Bu teknik, sayısal olarak üretilen verilerle eğitilmiş bir derin öğrenme modeli kullanarak deneysel verilerle test edilen bir modeldir. Bu derin öğrenme modeli, malzemenin yansıma katsayısılarından Debye parametreleri elde edebilmektedir. Teorik olarak üretilen verilerle derin öğrenme modelini eğitme yöntemi, çok çeşitli materyallerin bilgisini barındıran büyük bir veri setini hızlı bir şekilde üretilmesi avantajını sağlamaktadır. Ek olarak, önerilen bu yöntem, istenilen boyut ve malzemeye sahip herhangi bir prob tipine kolayca uyarlanabilmektedir. Eğitilmiş bu derin öğrenme modelinin deneysel doğrulanması,

beş farklı standart sıvıdan, dört karışımdan ve bir jel-benzeri bir malzemeden elde edilen yansıma katsayıları ölçümleriyle ile test edilerek gerçekleştirilmiştir. Derin öğrenme modelinden elde edilen Debye parametresi sonuçları, literatürdeki sonuçlarla karşılaştırılmıştır. Son olarak, önerilen modelden elde edilen dielektrik özellikleri için büyük-ölçekli istatistiksel doğrulama yapılmıştır.

1. PRE-INTRODUCTION

In order to develop innovative diagnostic and therapeutic tools for medical applications, researchers have developed an immense interest to study the interaction of electromagnetic fields with biological tissues over the past century. [1–3]. The most common method of characterizing biological tissues with electromagnetic waves is through determining the dielectric properties of the tissues. [4, 5]. Thus, accurately measuring the dielectric properties of biological tissues is a paramount step in the development of medical devices [6]. Several methods are available for the measurement of dielectric properties of different material types including : resonant cavity perturbation, parallel plate, free space, transmission line and open-ended coaxial probe [7]. The open-end coaxial probe technique is the most widely used amongst the methods mentioned above due to its non-destructive measurement capabilities, broadband measurement capabilities and ad-lib sample requirements (in vivo or ex vivo) [8–10].

The following sections provide detail description of all the studies conducted during the period of this thesis which includes the classification of renal calculi, characterization of normal and cancer bone cell lines and categorization of healthy and tumor breast tissues. The machine learning-aided algorithms and the statistical analysis implemented on these studies provided some quite promising results in dielectric property characterization of tissues.

1.1 Cole-Cole Parameters-based Classification of Renal Calculi Using Machine Learning

When medicine is not an option to pass the kidney stone, the most recommended type of treatment methods are Extracorporeal Shockwave Therapy (ESWL), Percutaneous Nephrolithotomy (PCNL), ureteroscopy and open surgery. [11]. After the treatment is completed by removing the kidney stones, the patients are advised to take the necessary precautions in order to avoid the reformation of the stone.

The formation of kidney stones in the kidney, bladder and urinary tract is referred to as urolithiasis and its known to affect 5-10% of the world's population. It has an 80% recurrence rate associated with genetic factors, geographical environment and eating habits [12]. The most common types kidney stone formed are calcium oxalate, struvite, cystine and uric acid [11]. The formation of calcium oxalate is known to be a pre-existing or a post-existing condition in patients with renal tubular acidosis, steroid treatment, Vitamin D intoxication and immobilization. Struvite stones (Magnesium Ammonium Phosphate) are usually formed by urease-splitting bacteria during urinary tract infections. Due to the poor solubility of Cystine (amino acid), formation of stone and occur when cystine is reabsorbed from the renal tubular genetic owing to genetic defect. Uric acid stones are related with obesity, diabetes, gout and low urine pH [11]. Generally, after the stone is diagnosed, an appropriate treatment is decided based on the type, size and location of the stone.

The analysis of the stone can be performed via Chemical Analysis, Thermogravimetry, Optic Polarizing Microscopy, Scanning Electron Microscopy (SEM), Infrared Radiation (IR) Spectroscopy and X-Ray Powder Diffraction (XRD) [13]. Chemical Analysis is implemented by a commercial kit to determine the ions (uric acid, ammonium urate, cystine, calcium carbonate, calcium oxalate and calcium phosphate) in the kidney stones. Even though the technique is cost-effective, it requires long processing time [13]. In thermogravimetry analysis, the stones are classified according to their weight changes with respect to increase in temperature. This method suffers from insensitivity, and causes an irreversible changes on the stones [13]. In the optic polarizing microscopy method, the interaction of polarized light with the fragmented stones are analyzed. This method does not provide accurate component information of the stones [13]. In the SEM technique, the stones are examined by sending a beam of high energy electrons to the stone. In the Infrared Radiation (IR) Spectroscopy method, the classification of the stones performed via the information acquired from the image of the stone sample. The energy generated from vibration of the stones is used to analyze the samples and the energy absorbance spectrum is calculated for each stone [13]. In XRD method, monochromatic X-rays are used to examine stones.This method provides accurate data but it is not cost-effective [13]. The above mentioned methods are already been implemented to classify the kidney stones. However, they

have some disadvantages in terms of cost, usability, efficiency, sensitivity and an irreversible effects on the samples. For these reasons, we proposed that the Cole-Cole parameters of kidney stones can be exploited to categorize the samples through the used of an Artificial Neural Network (ANN) and the k-Nearest Neighborhood (k-NN) [14]. Furthermore, the microwave dielectric spectroscopy of renal calculi is performed for a large scale study on dielectric properties from 500 MHz to 18 GHz [15].

To this end, dielectric properties of the stones are measured with the open-ended coaxial probe. A total of 105 stones obtained from 40 patients (from the Department of Urology, Cerrahpasa Medical School, Istanbul, Turkey.) are measured for classification based on the types: calcium oxalate, cystine and struvite. Each type includes 35 samples extracted with ESWL, PCNL, ureteroscopy and open surgery. The samples were previously classified by Directorate of Mineral Research and Exploration. The range of the size of the samples is from 0.25-1 cm. The samples were prepared before the measurement by sanding and smoothing some faces of the stones in order to facilitate the open-ended coaxial probe to have a direct contact with sample without having any air gap. The experiment setup consists of Agilent N5242A PNA-X Microwave Network Analyzer, Agilent N1501A Dielectric Slim Form Probe, Agilent 85070E software and an external computer. The dielectric properties were measured within 0.5–6 GHz frequency range with 100 MHz intervals. The standard calibration setup described by the software instruction was performed for the experiment: air (open circuit), a conductive textile (short circuit) and deionized water (known load). The calibration was verified by measuring pure methanol at 23°C. Five measurements were performed for each stone. The Cole-Cole parameters (ε_s, ε_∞, τ, α and σ) for the kidney stones were calculated from the medians of the measurements and by implementing the generalized Newton-Raphson method. These parameters were used to classify the kidney stones with the help of machine learning algorithms. First, an ANN was designed to classify the kidney stones. Five input vectors were formed for each stone type, and the corresponding output vector was comprised of their types (Calcium oxalat=1,cystine=2, and struvite=3). The input vectors were normalized in the range of (-1, 1) to obtain a faster convergence criteria and better transfer function. The dataset was split into five folds in order to perform k-fold cross validation. Four folds were used as training sets and the remaining was used as a test set. The structure

of the ANN is a 1-15-1 network with tangent sigmoid transfer function for hidden layer: $HL = \frac{1}{(1+e^{-S})}$ where S is the input of the hidden layer neuron and Y is the output of the hidden layer neurons in the range of (-1, 1). Also, linear transfer function was applied at the output layer: $HL_k = ActivationFunction(\sum_{j=1}^{n} HL_i W_{jk})$ where n is the number of inputs of neuron k in output layer. The training of the network was performed with the gradient descent algorithm. Second, k-NN was designed by selecting the parameter k as 5 in order to classify kidney stones.

For both networks, the outputs were examined in terms of accuracy, sensitivity, specificity, precision, recall and F1 score. The relative permittivities were measured for calcium oxalate, cystine and struvite as 2.31, 2.51 and 3.38 at 2 GHz, respectively. The conductivities of calcium oxalate, cystine and struvite were found as 0.0079, 0.0481 and 0.0269 at 2 GHz, respectively. The Cole-Cole parameters of calcium oxalate (ε_s=12.84, ε_∞=1.96, τ=1.41e-6 s, α=0.73 and σ=8.11e-5 S/m), cystine (ε_s=16.78, ε_∞=1.93, τ=6.04e-7 s, α=0.62 and σ=0.0071 S/m) and struvite (ε_s=14.66, ε_∞=3.50, τ=1.80e-7 s, α=0.39 and σ=0.0365 S/m) were computed with generalized Newton-Raphson numerical method. The ANN results among three kidney stone were calculated as 98.1%, 94.3%, 97.1%, 94.6%, 97.2% and 93.1% for minimum accuracy, sensitivity, specificity, precision, recall and F1 score, respectively. The k-NN minimum results of accuracy, sensitivity, specificity, precision, recall and F1 score were found as 99.1%, 97.1%, 98.6%, 97.2%, 98.6% and 98.1%, respectively.

1.2 Characterization of Human Fetal Osteoblastic (hFOB) and Osteosarcoma (SaOS-2) Cell Lines Based on Dielectric Property

Osteosarcoma is a type of cancer that commonly occurs in the long bones. These cancerous cells are usually similar to early forms of bone cells that aid in the formation of new bone tissues, but are not as strong as healthy bone tissue. This type cancer is most common in young people especially within the period of rapid bone growth [16]. The reported incidence rates are approximately 4.0 for children within 0–14 years of age and 5.0 for the ones within 0–19 years per year per million persons [17]. One of the causal factors is exposure to radiation [18]. For instance, long-term cancer survivors treated with radiation therapy are prone to osteosarcoma [16]. Osteosarcoma can be diagnosed by an X-ray, Computed Tomography (CT) scan, Positron Emission

Tomography (PET) scan, bone scan, Magnetic Resonance Imaging (MRI) and a surgical biopsy [16]. The histological examination of tissues is performed by the use of needle or open biopsies. Due to the resistance of the tumor structure to radiation, radiation therapy is not recommended treatment for osteosarcoma. [16]. The current treatment methods for osteosarcoma are Surgical resection with wide margins, along with preoperative and postoperative chemotherapy [19]. Since osteosarcoma is a type of cancer that are usually found in children, there are ongoing studies to develop new diagnostic and therapeutic methods [19]. In this respect, the interaction between bone tissue and electromagnetic field was also examined by measuring the dielectric properties of bone tissues [20]. In vitro porcine cortical bone was analyzed via the open-ended coaxial probe method in the frequency range of 0.05-20 GHz. The reported dielectric property for a 10 kg porcine were ε_r = 28.1 $\pm$ 2.0, σ = 0.34 $\pm$ 0.04 S/m at 450 MHz [20]. Human trabecular calcaneus bone was examined using Microwave Tomography Imaging (MTI) method over the frequency range of 900–1700 MHz. The results obtained from two patients were ε_r = 13.6, σ = 0.84 at 1300 MHz [21]. Extensive studies for interactions microwave with biological tissues were conducted for the analysis of dielectric properties of biological tissues [20–22]. However, there are limited studies on the interaction between electromagnetic fields and biological cells, which are constituent of tissues [23–25]. The dielectric property of human breast cancer cell lines (MDA-MB-231, Hs578T, MCF-7 and T47D) were characterized using the open-ended coaxial probe technique over the frequency range of 0.2– 13.6 GHz [23]. They concluded that the results are in good agreement with other reported results comparable in literature for breast tissues. In [24], dielectric property of normal (SK-MES) and malignant (NL-20) human lung cells were measured via a the open-ended coaxial probe with a flange over the frequency range of 0.2-2 GHz. They deduced that there is a slight difference between two cell lines in terms of dielectric properties for the composites gels form. Although this difference was statistically meaningful for the imaginary part. In [25], the dielectric property measurements of healthy (osteoblast hFOB 1.19) and unhealthy human bone (osteosarcoma SaOS-2) cell lines, and the dielectric property of mouse myoblast (C2C12) were measured in order to develop experimental procedure for cell lines over the frequency range of 2-50 GHz. To examine the effect of cell concentration on the

dielectric property measurements, the concentration of hFOB 1.19 was increased from 33,500 to 1,350,000 cells/ml. Thus, the lack of sufficient and valid data for biological solutions and cells is still one of the scientific gaps in the dielectric property research. Consequently, Normal bone cell line (hFOB 1.19) and unhealthy cell lines (SaOS-2) were prepared with high concentrations in order to measure the dielectric property of pellets and the solutions within the frequency range of 0.5-10 GHz. [26, 27]. The measurements were performed with the 2.2 mm-diameter probe. From the obtained results, the Debye and the Cole-Cole parameters were calculated by the Particle Swarm Optimization (PSO) algorithm. The human osteoblast (hFOB 1.19) and osteosarcoma (SaOS-2) cell lines were prepared in department of Molecular Biology and Genetics, Istanbul Technical University, Istanbul, Turkey.

Standard adherent cell culture protocol was implemented to prepare the cell pellets. The protocol details are given as follows:

- Three cell lines (two of the cell lines were SaOS-2 and one was hFOB 1.19) were cultured in a growth medium consisting of Dulbecco's Modified Eagle Medium (DMEM), 10% Fetal Bovine Serum (FBS) and 1% Penicillin-Streptomycin.
- The cell cultures were stored in an incubator at 37 °C.
- Trypsin was used to passage the cells when the confluency amounted to nearly 80% of the flask.
- Removal of the cell line was performed under the microscope to verify that the cells were separated from the flask.
- The cell lines were isolated by placing in a falcon tube.
- They were centrifuged for 5 minutes at 1000 rpm.
- Number of SaOS-2 cells in the falcon tubes were 12,500,000 cells/ml and 22,500,000 cells/ml.
- Number of hFOB 1.19 cells in the falcon tube was 17,800,000 cells/ml.

The experiment setup consisted of the Agilent N5230A PNA-L Microwave Network Analyzer, Agilent N1501A Dielectric Slim Form Probe, Agilent 85070E software

Table 1.1 : The Cole-Cole parameters of SaOS-2 and hFOB 1.19 for the measurements of cell pellet and suspension forms.

Samples		Cole-Cole Parameters				
		ε_s	ε_∞	τ (ps)	α	σ
Cell Pellet	SaOS-2*	64.04	1.01	5.15	0.01	0.01
	SaOS-2**	58.85	1.01	4.97	0.01	0.01
	hFOB 1.19	60.81	1.01	4.97	0.01	0.01
Cell Suspension	SaOS-2*	69.91	1	5.2	0.01	0.01
	SaOS-2**	68.57	1.1	5.39	0.01	0.01
	hFOB 1.19	68.17	1.03	4.98	0.01	0.01
Growth medium without serum		69.67	1.02	5.08	0.01	0.01

* SaOS-2 sample includes 12,500,000 cells/ml. * * SaOS-2 sample includes 22,500,000 cells/ml.

and a laptop. The standard three steps calibration procedure instructed by software was followed: air (open circuit), a conductive textile (short circuit) and deionized water (known load). The calibration was validated by measuring pure methanol at 23 °C. Afterwards, Ten measurements were performed for each sample. The dielectric property measurements of the cell pellets were performed between 500 MHz to 18 GHz with 250 MHz intervals. After completing the measurements of each cell pellet, we added 3 ml growth medium without serum in each falcon tube in order to form cell suspensions and the dielectric property measurements were performed for each suspension. Additionally, the dielectric property of the growth medium without serum was also measured. The Cole-Cole parameters (ε_s, ε_∞, τ, α and σ) were calculated from the medians of ten measurements by implementing the particle swarm optimization (PSO) algorithm.The calculated the Cole-Cole parameters for each sample are listed in Table 1.1 [28]. According to the results, the difference between hFOB and SaOS-2 cell suspensions through out the measurement frequency are 0.1480% and 2.8267% for the relative permittivity and conductivity, respectively. For the pellet measurements, the calculated percent discrepancy is 2.1895% for the relative permittivity and 3.6766% for the conductivity.

1.3 Classification of Rat Healthy Breast Tissues and Malignant Tumors Based on Dielectric Property Through Support Vector Machines

Breast cancer is a disease that can emerge when the cells in the breast begin to exponentially grow. This type of cancer is common amongst women and more deathly than other malignant cancer types. [29]. It is estimated that approximately 500,000

people lose thier lives annually from breast cancer in the world. [29]. Therefore, enormous research has been put towards breast cancer due to its lethal consequences [30–32]. The aim these studies mainly focuses on protection, early detection and treatment of breast cancer.One of the most common diagnostic methods for breast cancer is X-ray mammography. Although this technique produces low sensitivity and specificity results [33]. In addition, due to the harmful effects of X-rays, multiple repetitions of X-ray mammography on a single case detection are not recommended for patients under the age of forty. MRI method is also used for the diagnosis of breast cancer. However, the high sensitivity of the MRI in detecting suspicious tissues causes a high positive rate due to the heterogeneity of the breast structure [34]. Owing to its advantages such as low-cost and safety, the research on microwave imaging (MWI) for breast cancer diagnosis has recently gained a wide interest [35]. In addition to the diagnostic approach of the MWI method, knowledge of the dielectric properties of the tissues can provide the surgeon with cancer-free surgical margins during resection of tumor tissues. Therefore, the recurrence probability of the cancer can be reduced to almost zero by completely removing all the cancerous tissue. The significance of increasing the dielectric property data reservoir for biological tissues apparent since the MWI technique is mainly based on the inherent dielectric property difference between healthy and malignant tissues [36–39]. In [36], ex vivo infiltrating tumor and surrounding tissues obtained from seven patients were measured in the frequency range of 0.02-100 MHz. Three sections of tissues (the central part of the tumor, the tumor surrounding tissue, and the peripheral tissue) were analyzed based on their Cole-Cole parameters. The relative permittivity values of tumor tissues are higher than peripheral tissues result. In [37], ex vivo human breast tissues (fat, normal, benign tumor and malignant tumor tissues) were examined at 3.2 GHz. The difference in dielectric property between benign and malign tumors tissues was reported. In [38], a MWI prototype for breast cancer diagnosis was established using the inherent difference of the dielectric properties between normal and malignant tumor tissues. The prototype was tested in vivo with 5 patients within 300-1000 MHz frequency range. In [39], human breast tissues (155 samples) obtained from 119 patients were classified based on glandular content, fibroglandular and adipose tissues in order to understand the heterogeneity of breast tissues structure. The dielectric property of

normal, benign and malignant tumor tissues was reported for each class over the 0.5-20 GHz frequency range. Moreover, the Cole-Cole parameters were calculated from the complex permittivity dataset for each category. From the studies reported above, it can seen that accurately obtaining the dielectric property in a broadband range is important to develop a new treatment and diagnostic for the medical industries. For testing and verification of microwave techniques techniques, the ability to repeat the experiments is very useful. Furthermore, the availability of human breast tissue samples to researchers is limited. Therefore, rat breast tissue play a crucial role as an alternative. Rat breast tissues posses similar characteristic to that of humans to the extent of having more hormone responsiveness with histopathology and premalignant stages which is comparable to the human breast cancer model [40]. Therefore, the dielectric properties of in vivo rat tissue of both healthy breast and breast tumors were measured using the open-ended coaxial probe form 0.5 GHz to 6 GHz. Support Vector Machines (SVM) algorithm was implemented for the classification of the tissues based on dielectric properties [41]. A total of 30 adult albino Sprague Dawley strain female rats were acquired from the Center for Life Sciences and Technologies, Boğaziçi University. The rats were divided into two groups, one as the control (6 specimens) and the other as the experiment (24 specimens). A 12 h light/dark cycle was provided as an environmental condition. Moreover, free access to a regular laboratory pellet nutrition as well as tap water was provided to the animals. A single dose carcinogenic solution was prepared by dissolving 20 mg/kg 7,12-dimethylbenz (a)anthracene (DMBA) in 1 mL olive oil using an ultrasound bath. This solution was feed to the experiment group by oral gavage when they were 47 days old. At the same time, a dummy solution of 1 ml olive oil was given to the control group in order to maintain same conditions in both groups and both groups were kept on a two weeks rest period after the oral gavage process. After the resting period, the weights and tumors of the animals were checked by hand weekly. The experiment setup includes Agilent Fieldfox N9923A Network Analyzer, Keysight flexible cable, Agilent N1501A Dielectric Slim Form Probe, Agilent 85070E software and a laptop. The three step calibration procedure instructed by the software was followed: air (open circuit), a conductive textile (short circuit) and deionized water (known load). The calibration was verified by measuring pure methanol at 25 °C. The animals were prepared for dielectric property measurements

by performing anesthesia with injection of 80ml/kg ketamine and 10mg/kg xylazine mixture. Five measurements were performed from the targeted part of the tissues with restricting the movement of the probe. After the measurement is completed , the animal was euthanized. The tumor tissues were resected and kept in tissue cassettes with 10% formalin solution for pathological analysis. After the results were obtained from the pathological analysis, we generate a dataset from 5 control (325 samples) and 5 experiment (325 samples). The dataset consisted the mean of five measurements calculated form dielectric property of each sample. The mean values were comprised of 101 individual complex numbers (ε' and ε'') in the frequency range of 0.5-6 GHz. A total of 202 features were used for each sample for the classification of normal and tumor tissue with the help SVM algorithm. The accuracy results obtained from different scenarios are given as follows:

- Using all 202 features, relative permittivity and conductivity were tested separately and 100% accuracy was obtained from SVM algorithm for each test.
- The relative permittivity and conductivity were combined to perform SVM algorithm as well. In combined dataset, 100% accuracy was also achieved when distinguishing normal and tumor tissues.
- 100 features were determined from 202 dielectric property features through inf-FS feature selection algorithm and 100% accuracy was obtained permittivity data.
- 50 features were selected 202 dielectric property features with inf-FS feature selection algorithm and 99.23% accuracy was resulted with combined dataset.
- Selecting 1 feature with linear kernel gave 90.31% accuracy on logarithm of the conductivity data. The selected feature was conductivity data at 0.505 GHz.
- Selecting 1 feature with Radial Basis Function (RBF) kernel resulted in 90% accuracy on logarithm of the conductivity data.
- 70-feature selection for conductivity data provided 98% accuracy.

In conclusion, the obtained dielectric measurement data has the potential to become acceptable diagnostic tool for breast cancer diagnosis.Hence, development of EM medical technologies requires more information on tissues based on dielectric data.

This study provides significant dielectric data to the literature and it offers a perspective for analyzing the dielectric data for classification purposes.

2. INTRODUCTION

Dielectric properties of biological tissues at microwave frequencies have been widely investigated for medical diagnostic, monitoring, and therapeutic technologies. In order to precisely measure the dielectric properties of biological tissues, it is important to eliminate the equipment-related errors and tissue-related errors which can severely alter the measurement results. The equipment-related errors stem from equipment of choice, measurement uncertainties, and the calibration procedure. The choice of the device to use for measurement should be chosen based on the type of material under test while also considering the advantages and drawbacks related to the applied method. Amongst the several techniques available, the most prevalent applied method for the determination of dielectric properties of biological tissues is the open-ended coaxial probe. The uncertainty of the measurement system can be established in terms the repeatability and accuracy of the system by maintaining similar conditions and conducting numerous measurement on the same material. In practice, a standard three steps calibration procedure: open circuit, short circuit, and a broadband load (distilled water) is generally used. Correctly performing the system calibration procedure leads to reliable dielectric property measurements. A common practice used to verify the calibration is to measure the dielectric properties of a known reference liquid and while verifying the calibration, the quality and systematic errors of system the can be monitored.

Tissue-related errors usually arise from the temperature, probe-sample contact, probe-sample pressure, in vivo versus ex vivo experiments, sample handling procedure, tissue sample properties, and heterogeneity [42]. Temperature is known to affect the results of permittivity and conductivity as reported in [43, 44].Accurately measuring the dielectric properties of biological tissues with the open-ended coaxial probe requires no air-gap between the probe and the tissue sample. Depending on the surface properties of the tissue, choosing a probe with small dimension can solve this issue [42]. When pressure is applied on the biological tissue sample during

measurement, fluid can accumulate at the tip of the probe which is the confounder of the probe-sample pressure related errors in the determination of dielectric properties of biological tissues. [43–46]. Apparent features such as the water content, temperature and physiological variations such as blood flow in vessels, heart rate are various distinctions in an vivo and ex vivo experiments.In an ex vivo measurement settings, appropriate sample handling procedures are to be applied to maintains minimum dehydration, contamination and damage to the tissue. Tissue heterogeneity is one of the challenges encountered dielectric spectroscopy and in order to overcome this problem, it is recommended that only the targeted tissue part should be included inside the sensing volume [39].

Recent advances in technology especially in the field of machine learning is paving the way for us to determine the unseen relation between the input output of a system and for data classification [47]. In [48], multiclass classification of hepatic anomalies with dielectric properties is studied using k-nearest neighbors (kNN), logistic regression (LR), and random forests (RF) classification algorithms. The classification of rat healthy breast tissues and malignant tumors was performed based on dielectric property through support vector machines [41]. In [14], ANN and k-NN were implemented for classification of kidney stones. ANNs and deep learning models are also effectively utilized in high dimensional microwave modelling including extracting the parameters of microwave filters [49]. Therefore, machine learning algorithms can be implemented in electromagnetic nonlinear inverse problems in order to minimize the measurement system complexity and enhance the measured results for the characterization of biological tissues.

This thesis focuses on the microwave dielectric property characterization with open-ended coaxial probe and sensing depth analysis of the probes for biological tissues. The thesis consists of four sections. The first and second sections focuses on the sensing depth analysis of the 2.2 mm-diameter open-ended coaxial probe. The third section, presents the comparison and sensing depth analysis of the 0.5, 0.9 and 2.2 mm-diameter probes. In the fourth section, a deep learning model to retrieve the Debye parameters from reflection coefficients is presented.

2.1 Purpose of Thesis

In the context described above, the general aim of this thesis is to examine the sensing depth the open-ended coaxial probe, which is one of its source of error, and also to suggest a deep learning model that can be easily implemented with different dimensions of open-ended coaxial probe. Therefore, the problematic issues the of open-ended coaxial probe are investigated from an engineering perspective as well as illuminated through offering a new deep learning approach.

The current diagnostic approach for skin cancer is are digital dermoscopy and biopsy techniques. Present biopsy methods are costly and invasive.The open-ended coaxial probes can be employed as a low-cost non-destructive technology to diagnose skin cancer by utilizing the inherent dielectric property discrepancy between healthy and malignant skin tissues. However, the open-ended coaxial probes suffer from high error rates and tissue heterogeneity is a known factor that contributes to this error. The main contribution of this work is to designate the sensing depth of the open-ended coaxial probe in order to minimize the tissue heterogeneity related errors for skin cancer detection. The skin is the most sizable organ that covers the entire surface area of the body, and it mainly functions as a barrier against dehydration and microbial infection from the outside environment. Additionally, the skin type can change based on genetics, environment and nutrition. In the first part of the thesis, the sensing depth of the 2.2 mm-diameter open-ended coaxial probe was investigated using two double-layered configurations to mimic the tissue heterogeneity. This study employed a simple experimental protocol that can be easily adopted to other tissue types. It was concluded that the measured results can be affected by the material resident (layer formed between probe tip and skin tissue) within the first 170 – 260 microns of distance from the probe tip. Therefore, to obtain accurate dielectric property measurement results with the open-ended coaxial probe method, there is a need to establish a preparation protocol for the measurement of skin tissue. Otherwise, non-standardized skin tissues can confound the measurement results.

The second part of the thesis reports the sensing depth analysis of open-ended coaxial probe in order to eliminate errors caused by tissue heterogeneity for ex-vivo

experiments. By targeting the decrease in the measurement error, the tissue classification accuracy can be increased particularly for tissues with similar dielectric properties. Therefore, this approach can enable practical applications, such as microwave biopsy. The open-ended coaxial probes suffer from high error rates due to the contribution of tissue heterogeneity. Therefore, the sensing depth of the open-ended coaxial probe is analyzed to minimize the tissue heterogeneity related errors in real experiment process. To this end, sensing depth analysis was performed with double-layered sample configuration including ex vivo rat's tissue (breast and wet skin) and intervening liquids (olive oil and triton X-100) for 0.5 to 6 GHz frequency range. A simple experimental protocol that can be easily adopted to other types of tissues was established in this study. Sensing depth was determined by tracking five different measured dielectric property percent change values. It was concluded that a membrane layer (between 0.4-0.8 mm thickness) on the wet skin tissue and breast tissue will potentially affect the measurement results of dielectric property by 52%-84%.

The third part of the thesis aimed to specify the sensing depth of the open-ended coaxial probe for the employment of the appropriate probe dimension for any given measurement scenario. This approach can potentially minimize the tissue heterogeneity related errors for skin cancer detection. Towards this end, the sensing depth of three different probe aperture sizes were compared. Probes with 0.5, 0.9 and 2.2 mm-diameter were simulated with double-layered skin tissue and olive oil sample configuration. The experimental validation of the simulation was performed with the 2.2 mm-diameter probe with the double-layered configuration. The obtained results show that the sensing depth is proportional to the probe aperture and probes with smaller aperture can potentially aid in diminishing errors caused by the heterogeneity of the tissue and allow accurate dielectric property characterization of thin skin tissue layers. As an example, 5% increase in retrieved relative permittivities were obtained at 0.31, 0.56 and 0.71 mm thicknesses for the 0.5, 0.9 and 2.2 mm-diameter probes, respectively. Based on these results, we can state that using the 0.5 mm-diameter probe can provide more accurate results when a thin skin layer measurement is performed. However, any membrane or tissue fluid that may be present on the tissue surface during measurement with the 0.5 mm-diameter probe may affect the measurement result

unexpectedly. Therefore, measurement protocols should be established to prepare the measurement surface for tissues that consist of a multi-layered structure or that may have a membrane or any other layer on the measurement surface. Alternatively, tissue heterogeneity can be determined using probes with multiple aperture sizes.

In the forth and last part of the thesis, we propose a new technique for the determination of Debye parameters, from the reflection coefficient response of the open-ended coaxial probes. The method retrieves the Debye parameters using a deep learning model which is trained with numerically generated dataset. Unlike real data, using synthetically generated input and output data for training purposes provides representation of a wide variety of materials with rapid data generation. Furthermore, the proposed method provides design flexibility and can be applied to any desired probe with intended dimensions and material. Next, we experimentally tested the designed deep learning model with real measured reflection coefficients measured from five different standard liquids, four mixtures,and a gel-like material and also compared the results with the results in literature. The obtained mean percent relative error was ranging from 1.21 ± 0.06 to 10.89 ± 0.08. Our work also presents a large-scale statistical verification of the proposed dielectric property retrieval technique.

2.2 Literature Review

The dielectric properties of biological tissues across different frequency ranges have been widely examined by utilizing various measurement techniques within the last century [2, 3, 43, 50]. Since the 1980s, the open-ended coaxial probe has come into prominence due to its non-destructive nature and its application in vivo and ex vivo broadband measurements. [10, 51]. Furthermore, the dielectric properties were analyzed according to the physiological characteristics of biological tissues such as water content, healthy or malignant, and in vivo or ex vivo. In 1996, a large dielectric property measurements that include in vivo and ex vivo animal and human tissues was accomplished with three different methods [9, 52, 53]. The open-ended coaxial probe method is the preferred technique for the measurement of dielectric properties of biological tissues, thus, this technique has been improved in many different aspects such as error correction methods, probe design, procedure development.

Based on shape and size of the biological tissue, and the required frequency range of the research, the customization of probe with respect to these properties of the tissue is one of the most crucial points for the open-ended probe technique. Since the sensing volume is affected by the size of the probe, a small tissue sample requires a smaller probe for accurate measurements. There are several studies examining the different probe apertures. For example, in [46], the 2.1 mm probe with flange has been used to obtain dielectric properties of the tissue in vivo and ex vivo measurement between 0.1 to 10 GHz. In [9], two probes with different outer diameters of 10 mm and 2.9 mm were employed to measure dielectric properties from 100 Hz to 200 MHz and from 200 MHz to 20 GHz respectively. Another important study was conducted with the 2.2 mm probe in [52], where the dielectric property of in vivo malignant and healthy rat liver tissue was measured between 500 MHz and 6 GHz. By using off-the-shelf slim-form open-ended coaxial probe in [53], dielectric property measurement of freshly excised normal and malignant human skin has been performed from 0.5–50 GHz frequency range. In [54] the dielectric properties of rat skin tissues have been measured between 0.55–6 GHz frequency range with slim-form open-ended coaxial probes having 0.5 mm, 0.9 mm and 2.2 mm aperture diameters in order to detect skin cancer in a small area. Dielectric property measurement of breast tissue is complicated due to the structure of breast tissue, which is heterogeneous [55]. In [56] sensing volume of commercial dielectric probes have been investigated in order to correctly measure heterogeneous tissue type. Apart from the design and choice of probe size, there is also a modification in metal and filled fabrication. In order to reduce chemical reaction occurring between the probe and the electrolyte in the tissue, [46] plated the tips of inner and outer conductors of the probe with gold. Moreover, borosilicate glass-filled, stainless-steel have become appealing due to their bio-compatible features, and high-temperature sterilization advantages.

In the last decade, new medical devices and clinical applications have been started to be designed according to the dielectric properties of the biological tissues in order to find new diagnostic and therapeutic methods. According to recent studies, the development of new medical technologies based on dielectric properties of biological tissues is still a hot topic and necessary improvements have not been completed yet. Therefore, by taking advantage of the open-ended coaxial probe measurement

technique for this thesis work, we investigated the problems of this technique in terms of low measurement accuracy and repeatability. Furthermore, possible suggestions are made for improvements of the open-ended coaxial probe measurement technique.

2.3 Hypothesis

Current dielectric property retrieval methods generate low accuracy dielectric property measurements. A robust and applicable new methodology based on sensing depth of the open-ended coaxial probe is one approach that can add considerable contribution in dielectric property measurement available in literature. Furthermore, a new approach for deep learning algorithms has been introduced and design flexibility for different probe dimensions is achieved via this method. Finally, this research can lead to the development of a novel method for tissue anomalies diagnosis and a new perspective in hyperthermia, radiofrequency ablation, microwave ablation treatment. One of problems of our generation is to discover cancer treatment and to find early diagnosis methods. With this proposed thesis, the researcher will be able to pervade to this subject while applying their current experience in the field of bioelectromagnetics.

To this end the originality of the study can be summarized as follows:

1. In the first part of the thesis, we investigated the sensing depth of the 2.2 mm-diameter open-ended coaxial probe for skin cancer detection.
2. In the first part of the thesis, we have defined sensing depth of the probe based on three different percentage changes in the relative permittivities.
3. In the first part of the thesis, we determined the sensing depth of the probe for skin tissue by utilizing skin mimicking phantom and materials.
4. In the first part of the thesis, we described a simple measurement protocol to quantify the sensing depth of the open-ended coaxial probes.
5. In the second part of the thesis, we developed an experimental setup to explore how sensing depth can effect the results during ex-vivo experiments.
6. In the second part of the thesis, we measured the dielectric property of rat's tumor, breast, skin, white adipose tissues.

7. In the second part of the thesis, we defined the sensing depth of the probe for rat's breast and skin tissues with five different percentage changes in relative permittivities and conductivities.

8. In the both first and second part of thesis, we developed an approach to acquire dielectric property.

9. In the third part of the thesis, we defined the sensing depth of the open-ended coaxial probe with small radii to enable selection of appropriate probes during dielectric property characterization of highly heterogeneous, skin-like, tissues consisting of multiple thin layers.

10. In the third part of the thesis, we established a definition for sensing depth via examination of the three different percent change thresholds in retrieved/measured dielectric property for different probe dimensions.

11. In the third part of the thesis, we investigated the significance of tissue layers located immediately at the probe aperture during sensing characterization eg. how thin and high dielectric property contrast layers positioned on top of the tissue effect the probe sensing depth.

12. In the forth part of the thesis, we design a deep neural network, which can retrieve Debye parameters from reflection coefficients.

13. In the forth part of the thesis, we synthetically generated very large dataset to conveniently train the deep learning model in a short time.

14. In the third part of the thesis, we theoretically modelled the open-ended coaxial probe and proposed an approach that offers the opportunity easily work with any desired probe dimensions, and any data fitting model such as Cole-Cole, Debye or multipole Debye.

15. In the third part of the thesis, we tested the designed model with reflection coefficients obtained from CST and ADS simulations to retrieve Debye parameters.

16. In the third part of the thesis, we experimentally tested the the designed model with the reflection coefficients obtained from five different standard liquids, four mixtures, and a gel-like material.

17. In the third part of the thesis, we statistically verified the designed model with both the synthetically generated and measured data.

At researcher level, the impact of this thesis is to gain new skills and perspective in electromagnetics. Additionally, it also enabled the transfer of innovation based thinking and planning capabilities to the researcher. Other technical skills such as simulation and experimental validation of open-ended probe methods and classification techniques were also acquired. These technical skills can be applied to other research projects and currently its been applied on classification of kidney stone, detection of skin cancer. Furthermore, other technical skills gained such as experience on the animal experiment procedures and ethical approvals for such experiments will ultimately help the researcher on future bioelectromagnetics research. The long-term impact of the thesis is expanding the life quality and life span through development of microwave sensors for detection of biological tissue anomalies based on microwave dielectric properties discrepancy.

This work will lay out the foundations for a novel diagnostic technology that can enable low-cost biopsy procedures and decrease cancer recurrence rates after cancer resection surgeries. Societal impact of these two devices are (1) enabling low-cost biopsies, (2) decrease cancer recurrence rates.

3. TOWARDS NON-INVASIVE DIAGNOSIS OF SKIN CANCER: SENSING DEPTH INVESTIGATION OF OPEN-ENDED COAXIAL PROBES [1]

Dielectric properties of biological tissues are traditionally measured with open-ended coaxial probes. Despite being commercially available for laboratory use, the technique suffers from high measurement error. This prevents the practical applications of the open-ended coaxial probes. One such application is the utilization of the technique for skin cancer detection. To enable a diagnostic tool, there is a need to address the error sources. Among others, tissue heterogeneity is a major contributor to measurement error. The effect of tissue heterogeneity on measurement accuracy can be decreased by quantifying the probe sensing depth. To this end, this work (1) investigates the sensing depth of the 2.2 mm-diameter open-ended coaxial probe for skin mimicking material and (2) offers a simple experimental setup and protocol for sensing depth characterization of open-ended coaxial probes. The sensing depth characterized through simulation and experiments using two double-layered configurations composed to mimic the skin tissue heterogeneity. Three thresholds in percent increase of dielectric property measurements were chosen to determine the sensing depth. Based on the experiment results, it was concluded that the sensing depth was effected by the dielectric property contrast between the layers. That is, high contrast results in rapid change whereas low contrast results in a slower change in measured dielectric properties. It was also concluded that the sensing depth was independent of frequency between 0.5 to 6 GHz and was mostly determined by the material located immediately at the aperture of the probe.

3.1 Introduction

Over the past half-century, researchers showed a great interest in quantifying the microwave dielectric properties of biological tissues. This effort paved the way for the development of microwave diagnostic and therapeutic technologies [2–4, 6,

[1] This chapter is based on the paper "Aydinalp, C., Joof, S., Yilmaz, T. 2021. Towards Non-Invasive Diagnosis of Skin Cancer: Sensing Depth Investigation of Open-Ended Coaxial Probes, Sensors, 21(4), 1319."

50]. Dielectric properties of biological tissues are pivotal design parameters for the development of such devices [9, 51, 57, 58]. Among other dielectric property measurement techniques, open-ended coaxial probe technique has been a widely preferred data collection method due to several advantages including non-destructive measurement features, broadband measurement capabilities, and flexible sample requirements [22,39,59,60]. Therefore, the technique is widely utilized to quantify the in vivo and ex vivo dielectric properties of different biological materials. For example, in [9], open-ended coaxial probe technique was utilized to measure dielectric properties of excised animal tissue, human autopsy materials, and in vivo dielectric properties of human skin, tongue tissue between 10 Hz and 20 GHz. This study reported a comprehensive data reservoir of biological tissue dielectric properties. In another study, ex vivo dielectric properties of normal, benign, and malignant breast tissues were analyzed between 0.5 to 20 GHz [39, 61]. More recently, practical applications of open-ended coaxial probe technique was envisioned one such application is the utilization of the technique as a biopsy device [48, 52]. Even though open-ended coaxial probe technique has a number of advantages, the technique suffers from high error rates that prevent the launch of the technique to clinical practice as a medical device. High error rates can stem from equipment or tissue related variability. Equipment related errors can result from the equipment of choice, measurement uncertainties, and calibration [42]. Tissue related errors are caused by temperature discrepancies, probe-sample contact, probe contact pressure, in vivo versus ex vivo experiments, sample handling procedure, tissue sample properties, and tissue heterogeneity. Reported in vivo tissue and phantom dielectric property comparisons show that the sample heterogeneity has a large effect on tissue-related errors [48]. To mitigate the tissue-related errors, there is a need to define the relationship between the sample and probe sensing depth.

Several studies were presented in the literature attempting to characterize the sensing depth of the open-ended coaxial probes. In [62], two probes with 18 mm and 21 mm aperture diameters were used to analyze the probe aperture dependent effective penetration depth for heterogeneous tissue samples. In another study, the sensing volume of two open-ended coaxial probes with 2.2 mm and 3.58 mm aperture diameters were examined for measurement of breast tissue dielectric properties [63].

In [56], sensing the volume of open-ended coaxial probe with 2.2 mm-diameter was investigated by using double-layered configuration composed of liquid and Teflon to represent the heterogeneous tissue composition. In [64], sensing depth of open-ended coaxial probe with 2.2 mm aperture diameter was investigated by performing experiments with six double-layered configurations based on analysis of five different sensing depth definitions. These studies used different terminologies such as effective penetration depth, sensing volume, histology region, sensing depth to describe the relationship between sample heterogeneity and measured dielectric properties with open-ended coaxial probes [56, 62–65]. In [63], sensing volume was explained as the smallest distance between the probe and boundary (beaker, stand and air) for which the real (ε') and imaginary (ε'') parts of the complex permittivity errors remain below 10%. In [56], sensing volume was described as the thickness of intervening liquid when the measured dielectric properties reached 50 and 90%. For a double-layered configuration, histology region or depth was described as the distance where the contribution of the second layer's dielectric properties to the measured dielectric properties of the first layer becomes undetectable [64]. Reported studies in [56,62–64] indicate that the definition of sensing depth varies based on measurement sample, probe aperture size and the chosen measured dielectric property threshold (variation of dielectric property as a percentage). While these analyses are important for understanding the relationship between sensing depth and dielectric properties of heterogeneous tissues, these studies must be expanded by including specific tissue types to realize the practical applications of open-ended coaxial probes. Further, there is a need to establish a robust and replicable measurement protocol to quantify the sensing depth. To this end, the goal of this work is to investigate the sensing depth of a commercially available open-ended coaxial probe with 2.2 mm aperture diameter for skin cancer detection in order to,

- define the sensing depth of the probe for skin tissue by utilizing skin mimicking materials,
- establish a simple measurement protocol to quantify the sensing depth of open-ended coaxial probes.

This work attempts to minimize the potential measurement errors to enable an open-ended coaxial probe-based skin cancer detection device. To do so, two double-layered sample configurations were prepared to represent the heterogeneous tissues. Considering that many different definitions were used to describe this measurement concept, we used the term "sensing depth" to define the measurement sensitivity; that is, the intervening liquid thickness where the measured dielectric properties changes by 5% of the pure liquids' dielectric properties. In this study, we also chose three thresholds (reflecting the percent change) for sensing depth measurement. The sensing depth of open-ended coaxial probe with 2.2 mm aperture diameter (Keysight Technologies, Santa Rose, CA, USA) was investigated utilizing the heterogeneous double-layered samples. The remainder of this paper is organized as follows: Section 3.2, materials and methods, simple and easily replicable measurement setup and protocol are explained in detail. In Section 3.2 simulation configurations are described. Section 3.3 shows results obtained from both experiments and simulations. In Section 3.4, obtained results are discussed in detail.

3.2 Materials and Methods

In the following section, the details of dielectric property measurements and simulations are explained. Experiment setup, prepared skin mimicking phantom material, double-layered sample arrangements and measurement protocol along with simulation configurations are given.

3.2.1 Experiment setup

Dielectric property measurement setup consisted an Agilent FieldFox N9923A 6 GHz RF Vector Network Analyzer (VNA) (Santa Clara, CA, USA), an Agilent dielectric slim form probe with 2.2 mm aperture diameter, Agilent 85070E dielectric property measurement software (Santa Clara, CA, USA), an external computer, an adjustable stand, and a digital caliper. The experiment setup is shown in Figure 3.1. Open-ended coaxial probe with 2.2 mm aperture is frequently preferred for dielectric property measurements of biological tissues and high permittivity, high loss liquid or gel-like materials; therefore, the probe was selected for this work [22, 52].

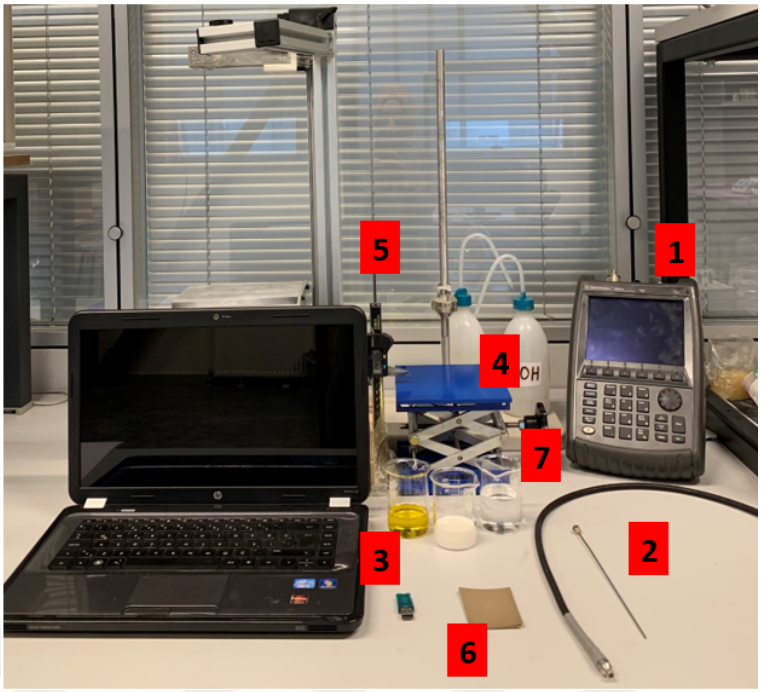

Figure 3.1 : Experimental setup: (1) Agilent FieldFox N9923A 6 GHz RF Vector Network Analyzer (VNA), (2) Agilent N1501A Dielectric Slim Form Probe, (3) Agilent 85070E software, (4) an adjustable stand, (5) a digital caliper (6) conductive textile and (7) pure material samples (olive oil, skin phantom and triton X-100).

The (VNA) was used to collect the S parameter response between 0.5 and 6 GHz with 55 MHz increments. This frequency range was chosen based on the limitation of the VNA and also many biological tissue studies were performed in this frequency range. Agilent 85070E software was installed on the external computer for dielectric property calculation from the measured S parameter response of the probe. The calibration process was carried out according to the software instructions: open circuit (the probe tip was left in the open air), short circuit (the probe tip was terminated with a conductive textile), a broadband load (the probe tip was immersed in distilled water with known temperature). In order to eliminate temperature drift errors caused by thermal expansion characteristics, the experiment setup was turned on 4 h prior to measurements. Mitutoyo absolute digimatic caliper 0–150 mm with 0.01 mm digital step size was used to measure the probe tip distance from layers.

3.2.2 Sample configuration

Sensing depth of 2.2 mm-diameter open-ended coaxial probe was analyzed by preparing two different double-layered sample configurations; that is, skin mimicking

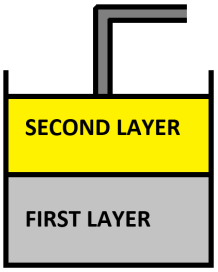

Figure 3.2 : Diagram of the double-layered configuration consisting of skin mimicking phantom as the first layer and olive oil or triton X-100 as the second layer.

phantom-olive oil and skin mimicking phantom-triton X-100 as shown in Figure 3.2. Although the prepared samples were heterogeneous, each layer was individually homogeneous. The first layer (skin mimicking phantom) was placed at the bottom of the configuration while the second layer (olive oil or triton X-100) was at the top of the configuration. Note that the composed phantoms are chemical gels and once jellified it can not be liquified again. Therefore, we do not expect an interaction, chemical or otherwise, between the liquids and the phantom. Throughout the experiments, the samples were inspected by eye to ensure that the second layer was visibly clear.

The details of the skin mimicking phantom recipe and preparation along with a comparison to skin tissue dielectric properties were given in [66]. The homogeneity of the phantom was evaluated by measuring at seven different depths from the surface to the bottom of a cylindrical shaped phantom. The phantom dimensions were 65 by 65 mm in diameter and height, respectively. At each depth, five different positions were measured. In total, the standard deviation from the mean of the measurement results taken from 35 different points on the skin-mimicking phantom was found to be 0.428 at 0.5 GHz, which indicated that the phantom was homogeneous enough to be utilized as the first layer. For the double-layered configurations; first, 15 mL of liquid phantom was solidified in a beaker then the desired liquid was added as the second layer. Prepared double-layered configuration samples are shown in Figure 3.3. Measured dielectric properties of each layer at 0.5 and 4.02 GHz frequency points are listed in Table 3.1.

3.2.3 Measurement protocol for sensing depth characterization

The experimental procedure utilized in order to investigate the sensing depth of the 2.2 mm open-ended coaxial probe, shown in Figure 3.4, is explained as follows :

Table 3.1 : Relative permittivity and conductivity measurements of each layer in double-layered configurations at 0.5 GHz and 4 GHz.

Sample	Relative Permittivity		Conductivity (S/m)	
	0.5 GHz	4.02 GHz	0.5 GHz	4.02 GHz
Skin Phantom	38.26	32.89	0.98	2.30
Olive Oil	2.56	2.26	0.02	0.04
Triton X-100	5.86	3.85	0.04	0.21

(a) **(b)**

Figure 3.3 : Double-layered configurations and part of the experiment setup for the measurement of layer thickness and step size: (a) skin phantom-olive oil (left) and skin phantom-triton X-100 (right), (b) adjustable stand and digital caliper for thickness measurements.

- Figure 3.4 Step 1
  - The probe was placed in a fixed position and the same position was maintained throughout the measurement procedure in order to reduce the error due to cable movement.
  - The first layer was placed on the adjustable stand platform and slowly lifted towards the probe tip.
  - When the first layer's surface reached the probe tip, the caliper reading was recorded as the reference distance value for the second layer.

- Figure 3.4 Step 2
  - The adjustable stand was lowered in order to add the second layer.
  - Without changing the position of the sample, the liquid second layer was added using a Pasteur pipette.
  - Similar to step 1, when the top surface of the liquid second layer reached the tip of the probe, the value displayed on the caliper was recorded as the

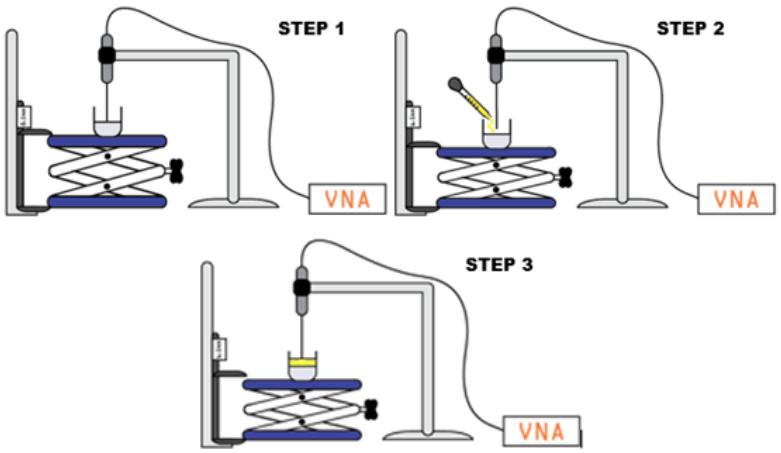

Figure 3.4 : The process of the dielectric property measurement for sensing depth analysis.

second reference distance value. Note that the difference between the two reference points gives the thickness of the second layer and the measurement step size was determined accordingly. The knowledge of the first reference point eliminates the changes in measured distance due to probe pressure to gel-like the first layer. This simple approach prevents a potential misleading sensing depth measurement.

- Figure 3.4 step 3
  - The first dielectric property measurement was taken when the probe tip was touching the top surface of the second layer; that is, the second reference point.
  - Next, the double-layered sample was gradually lifted with the adjustable stand allowing the probe to immerse into the second liquid layer. The dielectric property measurement was collected for each probe position at different depths in the liquid second layer.
  - Experiments were finalized when the probe tip reached the top surface of the first layer; that is, the first reference point.

3.2.4 Simulation configuration for sensing depth characterization

Open-ended coaxial probe and two different double-layered sample configurations were simulated with Ansys High-Frequency Structure Simulator (HFSS), 3D electromagnetic (EM) simulation software as shown in Figure 3.5. The commercially available Agilent's 2.2 mm probe datasheet, provides only the outer diameter of the

probe. This probe was replicated using the same outer diameter. Teflon (ε_r = 2.1) is used as the dielectric between the inner and outer conductor. For a coaxial probe with an outer diameter of 2.2 mm and Teflon as the dielectric material, the diameter of the inner conductor was calculated as 0.657 mm for 50 Ω impedance matching. Two different double-layer configurations were configured by assigning skin tissue for the first layer and olive oil or triton X-100 for the second layer. The simulations were performed in the frequency range of 0.5 to 20 GHz with 0.25 GHz increments by selecting various top layer thicknesses (d_2) with three different ranges: 0.01–1 mm with 0.05 mm increments, 1–3 mm with 0.2 mm increments and 3–5 mm with 1 mm increments. The main reason for determining three different ranges was to reduce the simulation time and to be able to work with small increments in the range where the relative permittivity alteration was highest. Note that the sensing depth is determined based on the percent change in relative permittivity. Therefore, it is important to collect probe response in smaller distances when the measured dielectric property change could be significant. To retrieve complex dielectric properties from simulated S parameter responses, an in-house algorithm was used. Validation of the in-house algorithm was performed by comparing the literature, simulation, and experiment results for skin tissue that are listed in Table 3.2. For the simulation, the Debye parameters ε_∞, ε_s and τ were selected as 4, 42 and 6.9 ps,respectively [67]. Please note that the dielectric properties used in the simulation were obtained from [67] and literature values used for comparison were obtained from [9]. Therefore, conductivity discrepancy in Table 3.2 represents the discrepancy between the sources in the literature. Nevertheless, the sensing depth characterization is traditionally performed with relative permittivity values due to higher measurement uncertainty of conductivity. Thus, the difference between simulation and literature results for the conductivity in this work was omitted. Broadband validation of the in-house algorithm with various materials is given in Section 3.3.1.2.

Table 3.2 : Comparison of the literature data, simulation, and experiment results for skin mimicking phantom at 2 GHz.

Property	Literature [9]	Simulation [67]	Experiment
Relative Permittivity	43.54	41.72	37.04
Conductivity (S/m)	1.33	0.37	1.49

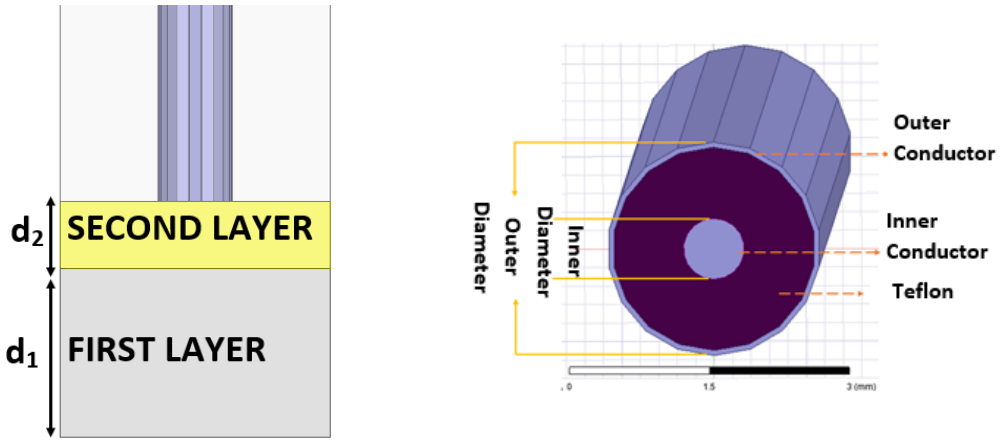

(a) **(b)**

Figure 3.5 : Double-layered simulation configuration and 2.2 mm-diameter probe design: (a) first layer represents the skin tissue with d_1 thickness and the second layer represents the liquid (olive oil or triton X-100) with d_2 thickness. (b) Simulated open-ended coaxial probe with 2.2 mm outer diameter and 0.657 mm inner diameter.

3.2.5 Sensing depth determination

Reported studies in the literature are analyzed in this section to determine the sensing depth measurement procedure that will be adopted in this work. Details of the two previously reported studies are listed in Table 3.3 [56, 64]. Both studies employed the commercially available Agilent slim form dielectric probe with 2.2 mm aperture diameter.

In the literature, special experiment setups were designed and used to collect the dielectric property data for sensing depth analysis of the 2.2 mm-diameter probe with double-layered sample configurations. In [56], the double-layered configuration was comprised of Teflon and water for the first and the second layer, respectively. The sensing depth of the probe was determined based on the percentage of the relative permittivity change. The sensing depth for 50% relative permittivity change was calculated as 0.2 mm; that is, the distance of probe tip from the top of the first layer. Please note that 50% relative permittivity change indicates measured relative permittivity was equal to 50% of the second layer's (water) relative permittivity. Similarly, the sensing depth for 90% relative permittivity change was measured at 0.5 mm. Likewise, this sensing depth indicates measured relative permittivity reached to 90% of the second layer relative permittivity. In [64], the distance (the range

1.2–3.65 mm) was calculated based on the flattening of the change in measured dielectric properties. Both reported studies collected the measurements by lowering the samples; thus, started collecting dielectric property data from the first layer. In this work, the sample was lifted towards the probe; therefore, data collection starts from the second layer.

In this work, the sensing depth determination techniques reported by the studies given in Table 3.3 are utilized. In accordance with the literature, 5, 20 and 80% change in measured relative permittivity rather than the change in measured conductivity due to higher measurement uncertainty reported for conductivity [64]. The reported error of the commercial systems is 5% [68]. To analyze the sensing depth findings within the reported error range we use 5% as the first threshold for sensing depth analysis. The effective penetration depth for 2.2 mm aperture probe was defined as 20% [56]. Therefore, in this study, we selected the 20% as the second threshold for sensing depth analysis. Similarly, in the literature, a complimentary point was chosen to analyze the sensing dept one example is the 10 and 90% change in measured dielectric properties. Therefore, 80% change was chosen as the third threshold complementary to 20%. Obtained results are given in detail in Section 3.3.

3.3 Results

This section presents the sensing depth analysis performed on relative permittivity obtained from the simulations and measurements. Axial electric field magnitude obtained from simulations using different configurations are shown in this section. Furthermore, the validation of in-house algorithm is demonstrated for pure materials (triton X-100, olive oil) and skin tissue. Note that these materials were used for double-layered configurations. Sensing depth analysis of 2.2 mm-diameter probe from simulation results using double-layered configurations were performed and three probe positions were designated based on the previously defined percent thresholds. Various frequency points were also considered for sensing depth analysis. In the second part of this section, the experiment results based on probe positions are given. Additionally, sensing depth obtained from two different double-layered configurations are compared to analyze the role of the relative permittivity of the second layer. Lastly,

Table 3.3 : Reported sensing depth analysis of open-ended coaxial probe with 2.2 mm aperture diameter utilizing double-layered configuration.

Definition	First Layer	Second Layer	Probe Aperture	Distance	
Sensing volume [56]	Teflon block (ε_r = 2)	water	2.2 mm	50% 0.2 mm ⋆	90% 0.5 mm ⋆
		0.9% clinical saline			
Histology depth [64]	Rubber A (ε_r = 7 at 5 GHz)	0.9% saline	2.2 mm	1.20 to 3.65 mm ⋆⋆	
	Rubber B (ε_r = 52 at 5 GHz)				
	Rubber A (ε_r = 7 at 5 GHz)	Fat (ε_r = 2.5 at 5 GHz)			
	Rubber B (ε_r = 52 at 5 GHz)				
	Porcine Muscle (ε_r = 46 at 5 GHz)				
	Porcine Fat (ε_r = 11 at 5 GHz)				

⋆ The distance where the measured relative permittivity reflects the 50% and 90% of the second layer relative permittivity. ⋆ ⋆ The distance where the measured relative permittivity fully reflects the second layer.

similar to simulations, three positions were determined to specify the sensing depth for experiment results.

3.3.1 Simulation results

3.3.1.1 Electric field distribution

The axial magnitude of the electric field at 2 GHz is illustrated in Figure 3.6a–d when the probe tip is terminated with only skin, only olive oil and two skin–olive oil double-layered configurations. The double-layered configurations include 0.3 and 3 mm olive oil thicknesses. The electric field of these configurations are given directly around the probe tip to precisely demonstrate the field distribution closest to the probe. From the figures, it can be seen that the electric field of the single-layer

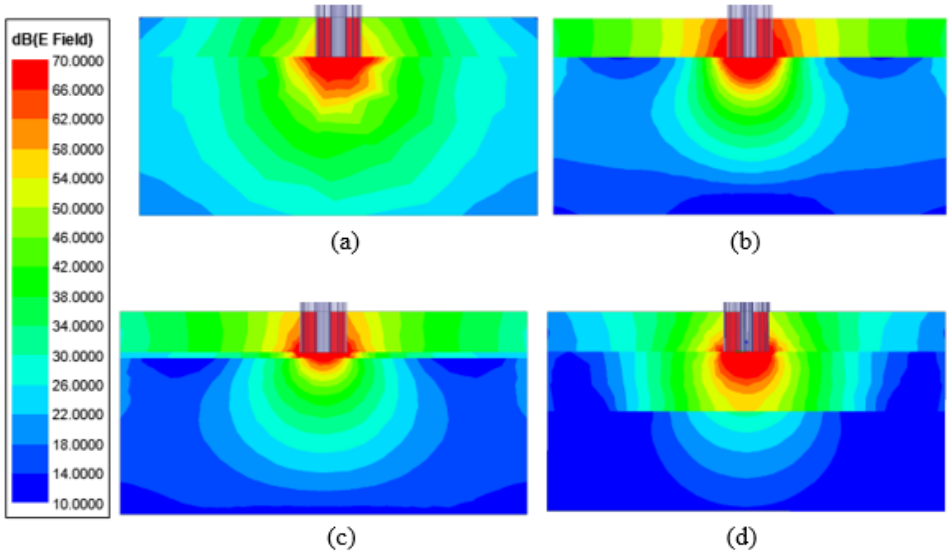

Figure 3.6 : Electric field strength in single layer configurations (a) olive oil, (b) skin tissue, and double-layered configurations (c) olive oil with 0.3 mm thickness, (d) olive oil with 3 mm thickness.

configurations are different from the double-layered configurations. The electric field was approximately 70 dB around all probe tips, and the electric field magnitude difference between the furthest point and near the probe tip was approximately 60 dB. As seen in Figure 3.6c, when olive oil thickness was equal to 0.3 mm, the electric field on both layers were approximately 70 dB. When olive oil thickness was selected as 3 mm, the electric field on the skin layer decreased to approximately 30 dB.

3.3.1.2 In-house algorithm validation

Dielectric properties are not directly measurable quantities and in the open-ended coaxial probe technique, these properties are derived from the admittance model [69]. The admittance model relates the ratio of the material's admittance ($Y(\varepsilon)$) and probe's admittance ($Y(0)$) to the material dielectric properties via an integral equation. The admittance ratio is calculated from the probe's reflection coefficient (Γ) which is obtained through the measured S parameter response of the probe when terminated with known materials, so-called calibration, and with the Material Under Test (MUT) as shown in equation (3.1).

$$\frac{(Y(\varepsilon))}{(Y(0))} = \frac{(1-\Gamma)}{(1+\Gamma)} \tag{3.1}$$

Based on the admittance model, the in-house algorithm adopts the Gauss–Newton iterative algorithm with Tikhonov regularization to solve the integral equation.

One important aspect of the in-house model is, unlike traditional approaches, the algorithm derives the mathematical model parameters of the MUT dielectric properties instead of solving the admittance model for each frequency. For example, parameters of Debye model or Cole–Cole model. The algorithm solves the admittance model numerically while minimizing the error between the numerical solution (Y') and measured admittance response (Y) as shown below in equation (3.2):

$$\begin{aligned} err &= abs(Y - Y') \\ min &\Rightarrow err \end{aligned} \tag{3.2}$$

When the solution converges the measured values, the algorithm returns the parameters of the mathematical model representing the complex dielectric properties of the MUT. Note that the input of the algorithm constitutes the simulated or measured S parameter response of the probe with known materials and with MUT.

The proposed in-house algorithm was verified by retrieving the dielectric properties of materials employed in this work namely olive oil, triton X-100 and skin tissue. The following steps were followed for verification, (1) to perform the simulation of the pure materials (skin phantom, triton X-100 and olive oil), the Debye parameters from literature [67, 70, 71] were given to the simulation, (2) the obtained properties were entered to the simulation program and the S parameter responses of the open-ended coaxial probe were obtained, (3) the simulation results were fed to the in-house algorithm to retrieve a new set of Debye parameters, (4) dielectric properties were calculated by inserting the desired frequency range to the Debye parameters obtained from the in-house algorithm, (5) literature dielectric properties were calculated from the Debye parameters given in [67, 70, 71] and compared to the retrieved dielectric properties. The comparison of the dielectric properties obtained from the literature [67, 70, 71] and the in-house algorithm are given in Figure 3.7. From the figure, it can be seen that the calculated dielectric properties from the Debye parameters retrieved via an in-house algorithm provide good accuracy. Furthermore, the maximum discrepancy between the obtained dielectric properties from the literature data and retrieved dielectric properties from the in-house algorithm at 0.5–6 GHz frequency range are listed in Table 3.4. The discrepancy was calculated based on absolute values over 0.5–6 GHz frequency range.

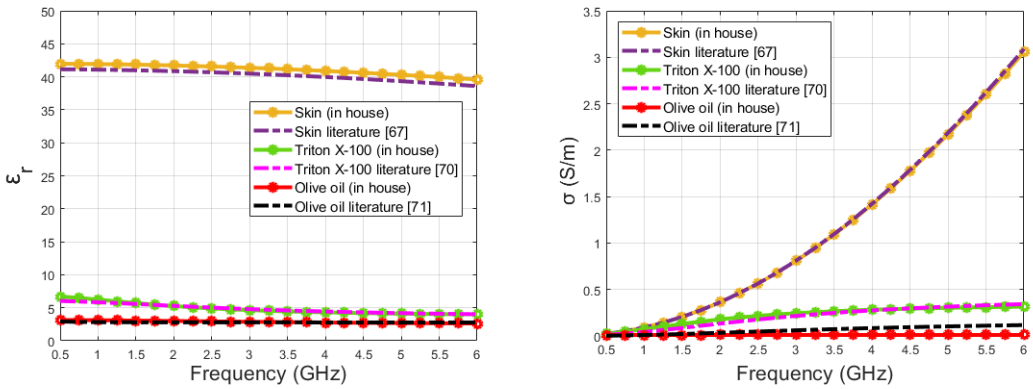

(a) **(b)**

Figure 3.7 : Comparison of pure material (skin, triton X-100 and olive oil) dielectric properties (a) relative permittivity and (b) conductivity calculated from Debye parameters obtained from the literature and retrieved from the in-house algorithm.

Table 3.4 : Maximum dielectric property discrepancy between retrieved and Debye model for pure materials (skin, triton X-100 and olive oil) used for double-layered configurations in simulations.

Materials	Discrepancy for ε_r	Frequency (GHz)	Discrepancy for σ (S/m)	Frequency (GHz)
Skin [67]	1.00	6	0.31	6
Triton X-100 [70]	0.68	0.5	0.05	2
Olive oil [71]	0.29	1	0.11	6

3.3.1.3 Sensing depth analysis: Simulation results

In order to analyze the sensing depth of the probe, we selected 5 frequency points between 0.5 and 20 GHz. For analysis purposes, we specified three thresholds for retrieved relative permittivity percent increases as described in Section 3.2.5. In Figure 3.8, the change in the dielectric property of the skin–triton X-100 configurations is demonstrated for 0.5, 2, 4, 10 and 20 GHz frequency points against probe distance from the surface of the first layer; that is, the first reference point.

Although the sensing depth was analyzed from 0 to 5 mm probe distance, 0 to 1.2 mm probe distance from the first layer is given in Figure 3.8 for precise graphical representation. In Table 3.5, increments of 5, 20 and 80% in measured relative permittivity values and corresponding distances at five frequency points are listed. As

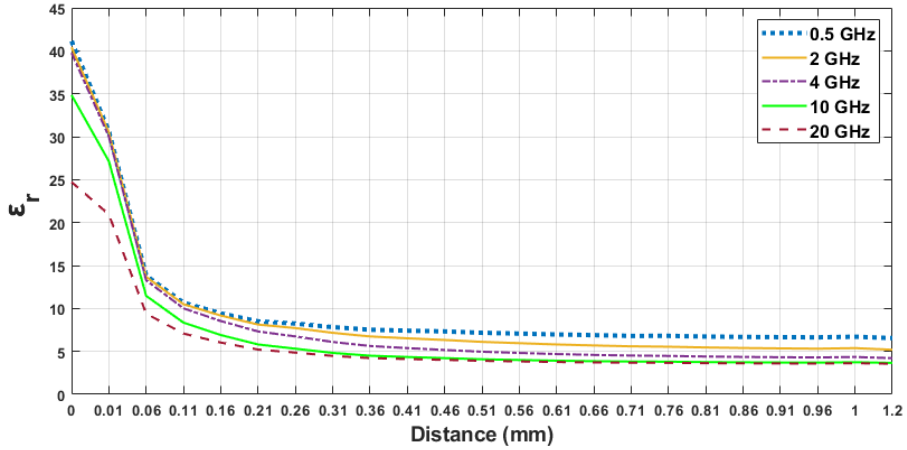

(a)

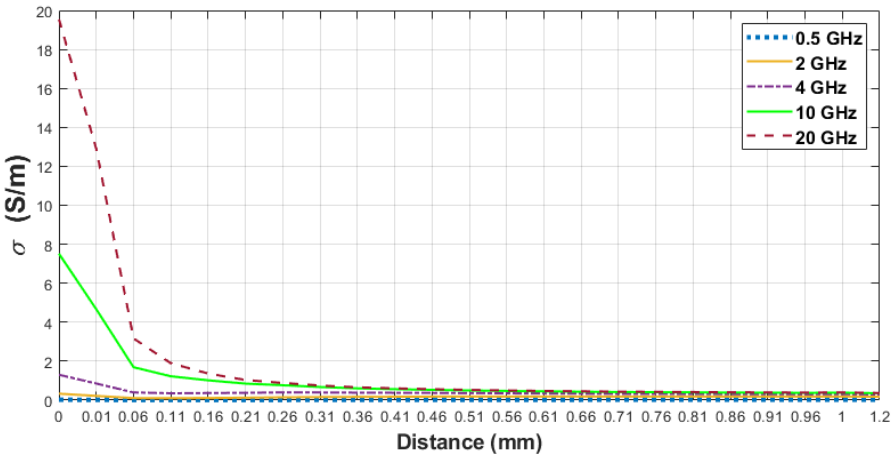

(b)

Figure 3.8 : Retrieved dielectric properties of the double-layered skin–triton X-100 configuration: (a) relative permittivity and (b) conductivity as a function of probe's distance from first layer at 0.5, 2, 4, 10 and 20 GHz.

seen in Table 3.5, the relative permittivity of triton X-100 increased by 5% between 0.76 and 1.2 mm at five frequency points. As the probe tip approached the first layer, the measured relative permittivity increased by 20% between 0.36 and 0.56 mm probe distances. Between 0.14 and 0.24 mm distances the relative permittivity of the first layer was dominant in double-layered measurement and the retrieved relative permittivity increased by 80% within this region.

The above-explained simulation design was also performed for skin–olive oil double-layered configuration, where the second layer had lower relative permittivity and conductivity in comparison to skin–triton X-100 configuration. The relative permittivity and conductivity alteration of skin–olive oil configuration are demonstrated

in Figure 3.9a,b, respectively at 0.5, 2, 4, 10 and 20 GHz frequency points. As listed in Table 3.6, the results obtained are 0.66–1 mm, 0.36–0.86 mm, 0.16–0.36 mm sample thicknesses (distance from the first layer) for 5%, 20%, 80% increase in retrieved relative permittivity, respectively. Figure 3.10 demonstrates the comparison of double-layered configurations' dielectric property alterations as a function of probe distance from the first layer (skin) at 4 GHz frequency. In [64], the sensing depth was evaluated in terms of the materials used for double-layered configuration. By comparing the analysis performed in [64] to our results, it can be concluded that the pace of change in retrieved dielectric properties is dependent on the dielectric property contrast between the two layers.

As seen in Figure 3.10, the change in dielectric properties was gradual for the lower contrast scenario. According to the results given in Tables 3.5 and 3.6 at 2 GHz, the transition from 5 to 80% increase was required more distance for skin–triton X-100 configuration, which verifies the previous finding indicating that sensing depth is dependent on the sample dielectric properties [64]. A more detailed interpretation of sensing depth is given in the following section.

Table 3.5 : Distances at the specified thresholds for simulated skin–triton X-100 configuration at 0.5, 2, 4, 10 and 20 GHz frequency points.

Frequency	Distance (mm) for 5% Increase	Distance (mm) for 20% Increase	Distance (mm) for 80% Increase
0.5	1.00	0.36	0.24
2	1.20	0.56	0.17
4	0.96	0.56	0.21
10	0.76	0.41	0.14
20	0.76	0.36	0.15

3.3.1.4 Sensing depth analysis: Experiment results

In order to analyze the sensing depth in detail, the dielectric property measurements were taken by manually adjusting the distance between the probe and the first layer. Measured relative permittivity change with respect to the probe position between 0.5 to 6 GHz is given in Figure 3.11. In the figure, d_1 indicates the value assigned to the point where the probe tip is fully in contact with the first layer (first reference point)

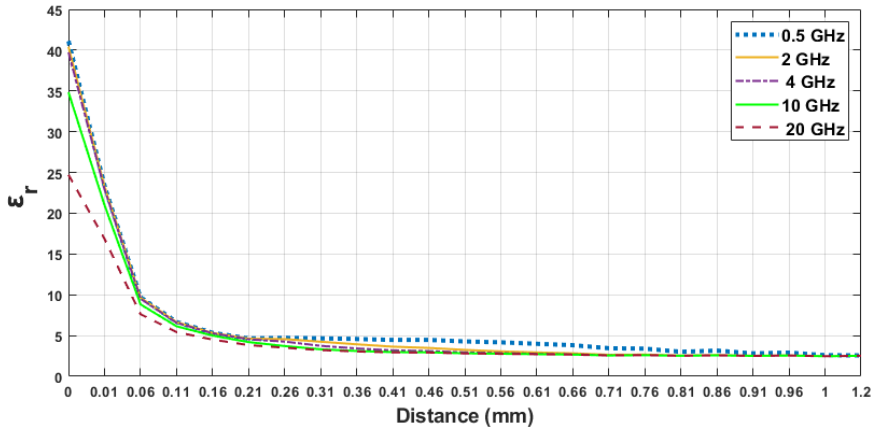

(a)

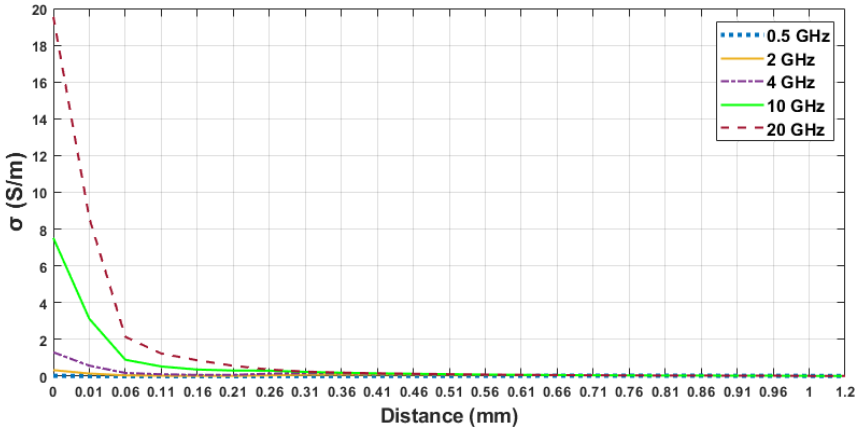

(b)

Figure 3.9 : Retrieved dielectric properties of the double-layered skin–olive oil configuration: (a) relative permittivity and (b) conductivity as a function of probe's distance from first layer at 0.5, 2, 4, 10 and 20 GHz.

and d_{32} indicates the value assigned to the position where the probe tip is in contact with the second layer (second reference point).

The distances from d_1 to d_8 were 0, 0.03, 0.06, 0.1, 0.15, 0.18, 0.22 and 0.27 mm. At these distances, the dielectric property measurements were similar to single-layer skin phantom configuration, since the thickness of olive oil at the tip of the probe were relatively small. Measured dielectric properties of double-layered configuration varied drastically at d_9 (0.28 mm) and d_{10} (0.32 mm) distances. Even though there is a drastic change between these two points, the measured relative permittivities were still affected by the contribution of the first layer. The measured relative permittivities between 0.38 mm (d_{11}) and 0.49 mm(d_{14}) probe distance varied from 6.14 and 3.84.

Table 3.6 : Distances at the specified thresholds for simulated skin–olive oil configuration at 0.5, 2, 4, 10 and 20 GHz frequency points.

Frequency	Distance (mm) for 5% Increase	Distance (mm) for 20% Increase	Distance (mm) for 80% Increase
0.5	1	0.86	0.36
2	0.76	0.56	0.26
4	0.71	0.46	0.21
10	0.66	0.41	0.21
20	0.66	0.36	0.16

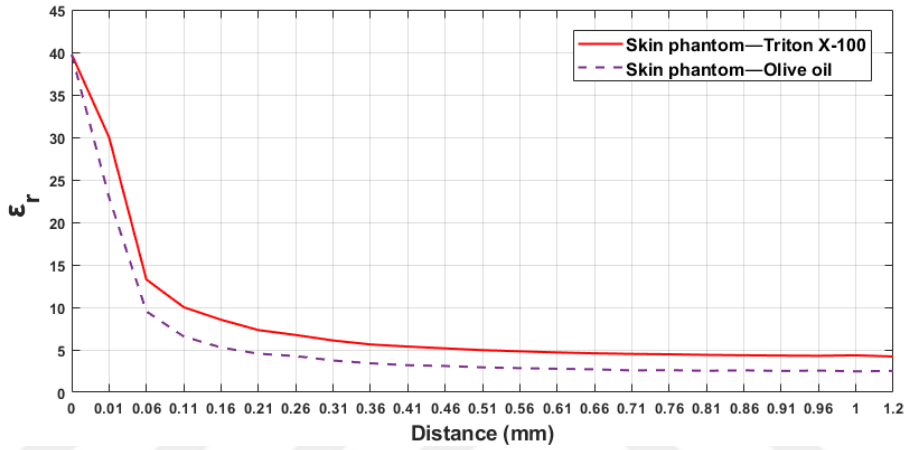

(a)

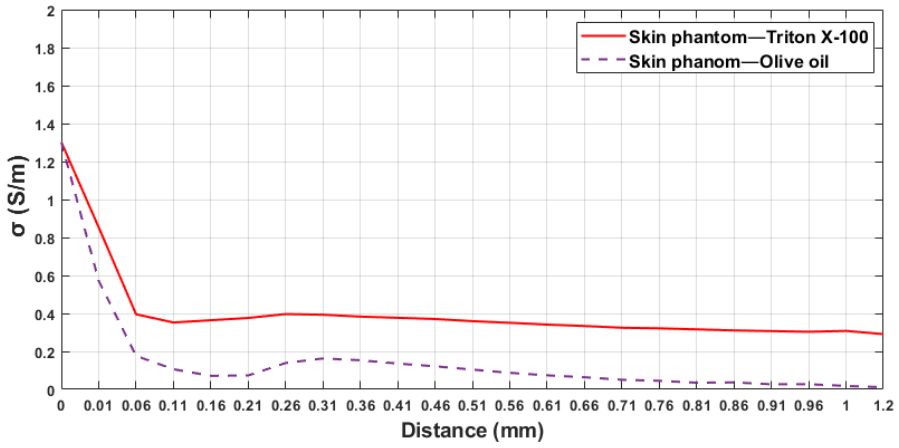

(b)

Figure 3.10 : Skin–triton X-100 and skin–olive oil simulated dielectric properties: (a) relative permittivity and (b) conductivity as a function of probe's distance from first layer at 4 GHz frequency.

As seen in Figure 3.11, smaller dielectric property values are obtained from d_{15} to d_{32}. In Figure 3.12, dielectric property changes of these distances for the skin

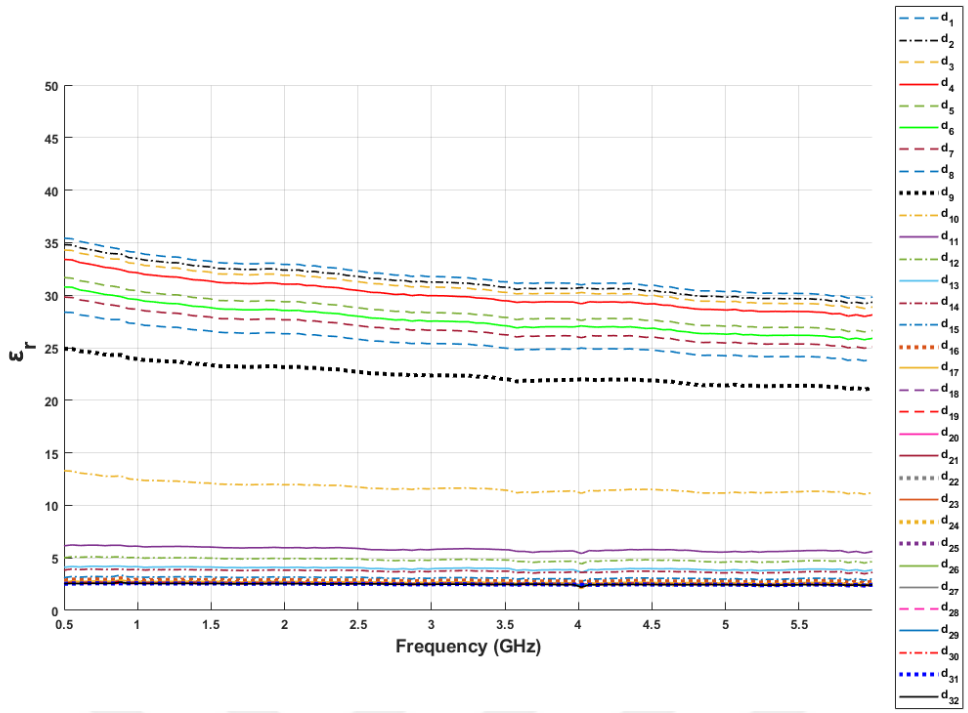

Figure 3.11 : Relative permittivity of skin–olive oil as a function of frequency at various distances between the probe tip and first layer. The distances are expressed as d_1 to d_{32}. In d_1 position indicates that the skin phantom layer was in full contact with the probe tip.

Table 3.7 : Specified three levels for measured relative permittivity of skin–triton X-100 and skin–olive oil configurations at 0.5, 1, 2.04, 4.02 and 6 GHz frequency points.

Materials	**Distance (mm) for 5% Increase**	**Distance (mm) for 20% Increase**	**Distance (mm) for 80% Increase**
Skin–Triton X-100	0.87	0.58–0.66	0.36–0.42
Skin–Olive oil	0.81	0.6	0.42

phantom-olive oil configuration are shown in detail by plotting relative permittivity and conductivity versus the distance between the probe tip and the first layer at four different frequency values. Although the thickness of the second layer was 6 mm, the graphs were plotted until 1.32 mm thickness to clearly show the distance axes. Additionally, the sensing depth with three percentage values was analyzed at different frequency points as shown in Figure 3.13. The sensing depths for previously designated percent change thresholds are given in Table 3.7 at 0.5, 2.04, 4.02 and 6 GHz frequency points. Note that all percent increases were calculated with respect to dielectric properties of the second layer both in measurements and simulations.

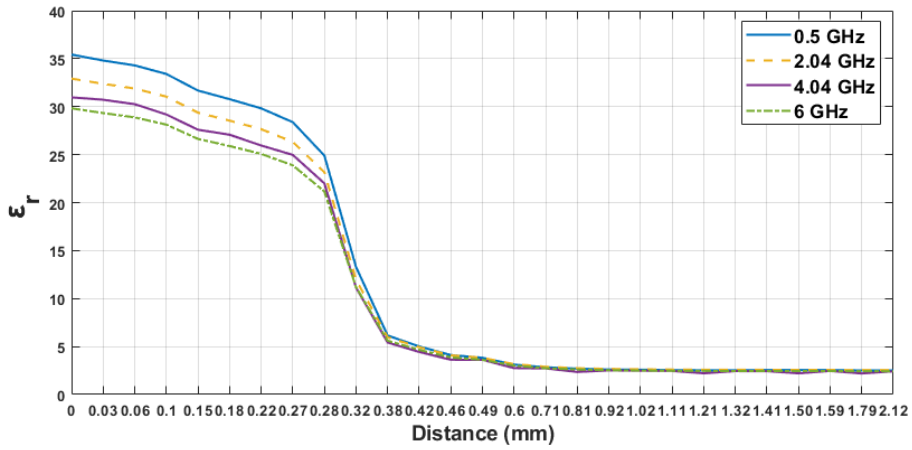

(a)

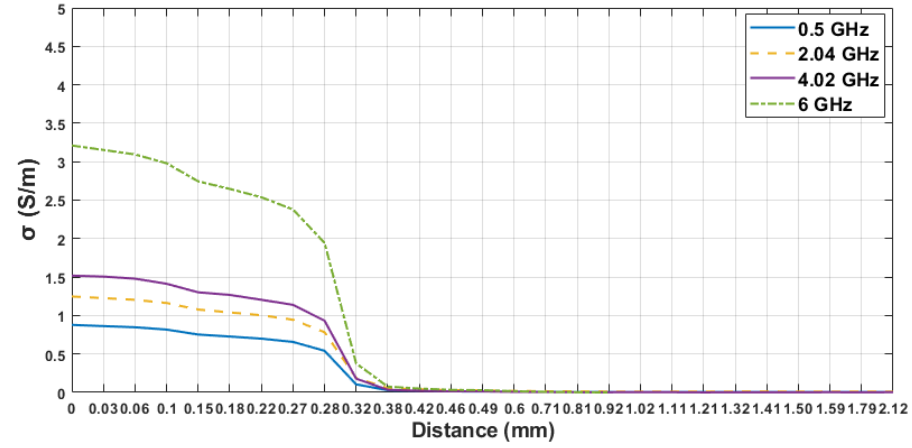

(b)

Figure 3.12 : Skin–olive oil dielectric properties as a function of probe distance from the first layer at 0.5, 2.04, 4.02 and 6 GHz frequency points: (a) relative permittivity and (b) conductivity.

Figure 3.14 represents the dielectric property of skin–olive oil configuration as a function of probe tip distance from the surface of the first layer (first reference point) at 2 GHz. If the change in the dielectric property was linear, we would have obtained a decreasing linear line, which is shown in Figure 3.14, obtained by using two points from the measured results. Based on our measurement results, when the distance between the probe tip and the first layer was 0.28 mm, the measured dielectric property change was 20% below the expected value according to the linear line. A similar percentage difference was, also, recorded between the measured and expected value in [62]. The difference between the previous study and this work is at 0.28 mm reported measured dielectric properties were close to the second layer (water ε_r = 78.8) in [62]

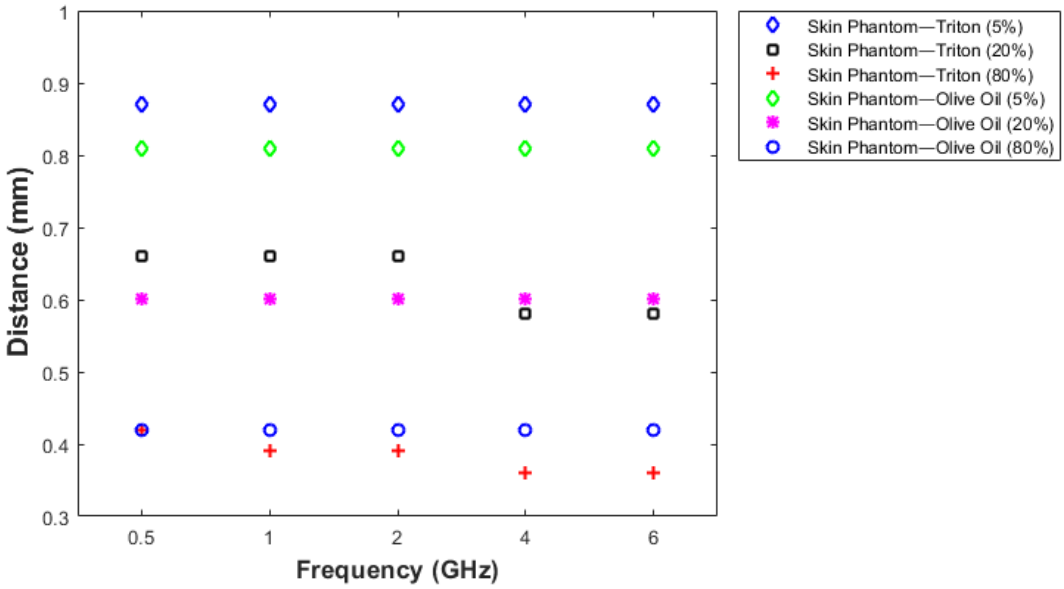

Figure 3.13 : Skin–triton X-100 and skin–olive oil 5, 20 and 80% increase in relative permittivities at 0.5, 1, 2,4 and 6 GHz frequency points.

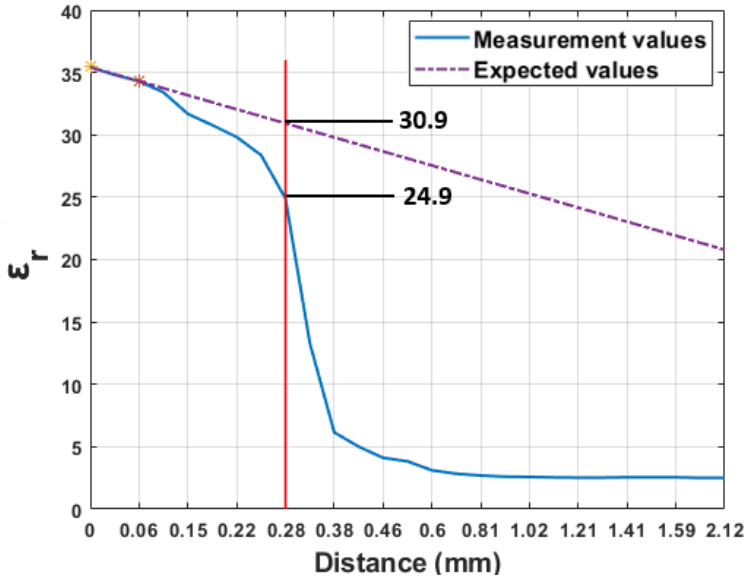

Figure 3.14 : The analysis of relative permittivity changes according to 20% difference between expected and obtained values at 2.04 GHz frequency point for skin–olive oil configuration.

and it is close to the first layer (skin mimicking material $\varepsilon_r = 37.4$) in this work. From the obtained results we can state that the medium with a high dielectric property in the close proximity of the probe tip has more impact on the measurements.

3.4 Discussion

Several studies on sensing depth analysis of the coaxial probe have been presented in the literature to overcome tissue and equipment related errors. In this work, application-specific investigation of sensing depth is presented to minimize the dielectric property characterization error for diagnostic purposes. To this end, we characterized a homogeneous skin mimicking phantom for the detection of skin anomalies. A commercially available 2.2 mm aperture diameter probe was used. Double-layered material was prepared by pouring liquid triton X-100 (ε_r = 5.86) and olive oil (ε_r = 2.56) layers on top of the skin mimicking phantom (ε_r = 38.26). Skin–olive oil configuration and the skin–triton X-100 configuration represents high and low dielectric contrast between the layers, respectively. Dielectric properties were collected by gradually lifting the sample towards the tip of the probe. 5 to 80% change in a dielectric property of the triton X-100 layer occurred when the distance between the probe tip and skin phantom top surface was within 1.2–0.17 mm range. A similar percentage change in the dielectric property of the olive oil occurred within 0.81–0.26 mm range for skin–olive oil configuration. From our results, we concluded that the rate of change in measured relative permittivity is approximately 50% faster when there is a high dielectric contrast between the layers. Additionally, the impact of the contrast between two layers can be characterized as: (1) if a large contrast exists between two layers, rapid change in dielectric property measurement is observed, and (2) gradual change in dielectric property is observed if there is a small contrast between two layers.

External factors such as dust, humidity or genetic pre-disposition can cause the formation of a layer above the skin. We investigated the effects of such a layer on the measured dielectric properties of skin tissue by considering the percentage change in measured relative permittivity of a double-layered configuration. This was represented by skin mimicking material and triton X-100 or olive oil in this study. Even though the layer created above the skin by explained factors can be very thin, our study suggests that it will highly affect the dielectric property measurement.

In practice, it is recommended to choose a minimum sample thickness of 5 mm when using the open-ended coaxial probe [68]. Based on our results, we concluded that

the surface of the sample under test has more influence on the dielectric property measurements than the size of the sample. For instance, when the thickness of the intervening liquid was 0.28 mm in [62], the measured relative permittivity was 60.6 for Teflon–water double-layered configuration. We obtained a relative permittivity of 24.9 for skin–olive oil configuration at the same distance. The study of sensing depth in [63] was based on 10% error threshold for a dielectric property measurement of ethanol, methanol and water. 10% change in (ε') and (ε'') was observed within 0.75–1.5mm. In [64], the histology region was reported as 1.20–3.65 mm thickness. In this work, 5% increase in the dielectric property of liquid layers (triton X-100 ε_r=5.86 and olive oil ε_r=2.56) was observed within 0.81–0.87 mm the thickness. This work reports a minimum required thickness of 0.81 mm. These results confirm that the material located immediately at the tip of the probe significantly affects the measured dielectric properties.

In [56], when the thickness of the intervening liquid was 0.2 mm, the measured dielectric property reached 50% of liquid's dielectric property for Teflon–water double-layered configuration. In this work, at 0.22 mm thickness, the measured relative permittivity was 30.7 which is 10 times higher than the dielectric property of intervening liquid. The discrepancy between our results and the previous work can be attributed to the dielectric properties of the materials chosen for each study. In [56], the dielectric property of the intervening liquid was higher than the value of the solid layer; however, in this work, a reverse configuration was employed. Due to the difference in configuration, the dielectric properties of the intervening liquid in [56] was dominant; in contrast, the dielectric property of a solid layer was dominant in our measurement results.

3.5 Conclusions

Knowledge of biological tissue dielectric properties is of paramount importance in the design of microwave medical devices. Therefore, there is a need to accurately characterize the dielectric properties of biological tissues. Tissue heterogeneity is known to be one of the major causes of erroneous dielectric property measurements. Therefore, an accurate and specified definition of sensing depth can contribute towards minimizing the error in the characterization of dielectric properties. To this end, this

work investigates the sensing depth of 2.2 mm-diameter open-ended coaxial probe for skin cancer detection. While measuring in-vivo dielectric properties of the skin tissue it must be noted that the skin is composed of layers; therefore, it is heterogeneous and the sensing depth of the probe must be defined for accurate determination of potential abnormalities such as early-stage moles that can potentially be malignant and curable when diagnosed early. In this study, simulations and experiments were performed for sensing depth analysis with double-layered configuration samples. Unlike previously reported studies, the experiments consisted of a simple measurement setup without forming a special experiment setup tank. The double-layered samples included a skin mimicking phantom as a first layer and liquids with low dielectric properties; that is, olive oil and triton X-100, were added as second layers. The thickness of each layer was calculated before dielectric properties were measured in order to calculate the measurement step size and a reference level was set to eliminate probe pressure-related errors. Liquids with low dielectric properties provide substantial insight for a potential change in measured dielectric properties since the liquids mimic the effect of the keratin layer which covers the top of the skin tissue. Three percent thresholds in relative permittivity changes 5, 20, and 80% were tracked to define the sensing depth at multiple frequencies. Both in the simulation and experiment results, at 2 GHz 5%, 20% and 80% increase in dielectric properties of olive oil and triton X-100 was observed when the probe tip distances are 0.66–1.2 mm, 0.36–0.86 mm and 0.14–0.42 mm, respectively, from the first layer (first reference point; that is, the top surface of skin phantom). Based on the results, we can state that a membrane layer or keratin layer on the skin tissue will potentially affect the measurement dielectric property results by 80%. These findings also suggest that the layer that is in immediate contact with the probe tip will have the most significant effect on dielectric property measurements.

4. TOWARDS ACCURATE MICROWAVE CHARACTERIZATION OF TISSUES: SENSING DEPTH ANALYSIS OF OPEN-ENDED COAXIAL PROBES WITH EX VIVO RAT BREAST AND SKIN TISSUES [1]

Dielectric properties of biological materials are commonly characterized with open-ended coaxial probes due to the broadband and non-destructive measurement capabilities. Recently, potential diagnostics applications of the technique have been investigated. Although the technique can successfully classify the tissues with different dielectric properties, the classification accuracy can be improved for tissues with similar dielectric properties. Increase in classification accuracy can be achieved by addressing the error sources. One well-known error source contributing to low measurement accuracy is tissue heterogeneity. To mitigate this error source, there is a need define the probe sensing depth. Such knowledge can enable application-specific probe selection or design. The sensing depth can also be used as an input to the classification algorithms which can potentially improve the tissue classification accuracy. Towards this goal, this work investigates the sensing depth of a commercially available 2.2 mm aperture diameter probe with double-layered configurations using ex vivo rat breast and skin tissues. It was concluded that the dielectric property contrast between the heterogeneous tissue components has an effect on the sensing depth. Also, a membrane layer (between 0.4–0.8 mm thickness) on the rat wet skin tissue and breast tissue will potentially affect the dielectric property measurement results by 52% to 84%.

4.1 Introduction

Interaction of electromagnetic fields with biological tissues has been a research topic for almost a century partly due to ever increasing pervasiveness of such signals in the environment [1, 5, 72]. Dielectric properties govern the interaction between the biological tissue and the electromagnetic waves; therefore, the accurate knowledge of

[1]This chapter is based on the paper "Aydinalp, C., Joof, S., Yilmaz, T. 2021. Towards Accurate Microwave Characterization of Tissues: Sensing Depth Analysis of Open-Ended Coaxial Probes with Ex Vivo Rat Breast and Skin Tissues, Diagnostics, 11(2), 338."

dielectric properties is crucial for modeling of electromagnetic wave and biological tissue interaction. Open-ended coaxial probes have been widely used for dielectric property characterization of biological tissues [8–10]. Due to the potential applications of electromagnetics in breast cancer research such as microwave breast imaging and breast cancer hyperthermia, the dielectric properties of breast tissue have been a research interest. In [61], the dielectric properties of normal, malignant and benign breast tissues were reported from 0.5 to 20 GHz using the open-ended coaxial probe technique. Measurements carried out with ex vivo human breast tissues from 0.5 to 50 GHz were reported in [60]. These studies formed the dielectric property database for the microwave breast cancer research on imaging and hyperthermia applications. Recently, in vivo rat breast tissue dielectric properties have been explored to unveil other diagnostic applications such as potential use of open-ended coaxial probes for biopsy purposes [22]. It should be noted that the emerging diagnostic applications of the technique have also revealed the need to measure the experiment animal breast tissue dielectric properties. Although promising results for categorizing the high dielectric property difference tissues were obtained [52, 53, 60, 61, 73], there is still a need to improve the classification accuracy for tissues with low dielectric property difference. The technique is known to suffer from high measurement error and low measurement repeatability. The error can stem from the tissue heterogeneity or equipment degradation [42]. Equipment related errors are mitigated by improving the calibration methods. However, it was shown that the large error margins tend to mostly emanate from tissue heterogeneity [48]. To realize practical applications of the probe, there is a need to investigate the probe sensing depth where the sensing depth can either be used to choose the probe type or it can be used as an input for machine or deep learning algorithms for accurate characterization of the tissue under investigation.

Several studies have been reported on the open-ended coaxial probe sensing depth definition to overcome the tissue heterogeneity related errors. These studies used different terminologies such as effective penetration depth, sensing volume, histology region and corresponding definitions for the used terminologies [56, 62–64]. For example, in [63], sensing volume of open-ended coaxial probe with 2.2 mm aperture diameter was investigated using pure alcohols and de-ionized water. Required sample thickness for 2.2 mm probe was determined as 1.5 mm for the samples. Similarly,

in [56], sensing volume of 2.2 mm aperture diameter probe was determined as 200 to 400 microns where the tissue heterogeneity was modeled using double-layered Teflon and de-ionized water configuration. In [62], the effective penetration depth characterized using previously introduced Teflon and de-ionized water configuration was used to measure the penetration depth with 2.2 mm aperture diameter open-ended coaxial probe. The definition used for the reported experiment in [62] was 20% change in measured permittivity values and the penetration depth was given as 0.28 mm. The percent change was determined through a linearly extrapolated line. In another study [64], the histology region was defined as the depth at which the measured results can reflect the changes in the tissue sample. When determining the changes, the measurement uncertainty was considered. The analysis in the reported work was carried out with six different sample configurations, two of which included ex vivo porcine tissue. Determined histology region for the 2.2 mm aperture probe was varied from 1.20 to 3.65 mm based on the frequency and the material under test.

Although the reported studies give valuable insights, the sensing depth of the probe with low dielectric property difference samples have not been explored. Mostly high dielectric property difference scenarios, such as Teflon and de-ionized water or muscle and fat were used for heterogeneity representation. However, the heterogeneity can have varying dielectric property discrepancies in a realistic setting. One example is the difference between breast benign and malignant tumor tissues reported as 10% [61]. Therefore, this study explores open-ended coaxial probe sensing depth with samples with varying heterogeneity in an attempt to understand the effect of dielectric property difference on sensing depth. The heterogeneity was represented by using double-layered configurations composed with ex vivo rat breast tissue and oil also ex vivo rat skin tissue and triton X-100. Rat tissues were chosen due to common use of rat models for as experiment animals [74]. The experiments were conducted using commercially available and widely used 2.2 mm slim form open-ended coaxial probe. Unlike previously introduced specialized measurement tanks, a simple measurement setting was used. Sensing depth was determined by tracking five different measured dielectric property percent change values.

Remainder of this paper is arranged as follows: Section 4.2, background is given. In Section 4.3, materials and methods including experiment setup, sample configuration

and measurement protocol are explained in detail. Section 4.4 presents results obtained from the experiments. In Section 4.5, findings are discussed in detail.

4.2 Background: Rat Tissue Characteristics

The skin is the most sizable organ, since it covers the entire surface area of the body. It mainly functions as a barrier against dehydration and microbial infection from the outside environment. The skin is comprised of various tissue types: (1) epidermis (epithelial cells), (2) dermis (collagen, fibroblasts, mast cells, nerves, blood vessels), (3) hypodermis (white adipose tissue), (4) panniculus carnosus muscle, and (5) adventitia (subcutaneous tissue) [74].

1. The epidermis contains one or two cell layers of cornified stratified squamous epithelium [75].

2. The dermis is a connective tissue that takes place beneath the epidermis and serves as a support with many blood vessels, lymphatic vessels and nerve fibers. Moreover, the hair follicles with their attendant sebaceous glands and the sweat glands are in the dermis [75].

3. The hypodermis is a layer of white adipose tissue (white fat) under the dermis. Adipose tissue is formed of adipocytes which are circular cells containing fat vacuoles. The hypodermal thickness is an important factor that shows the nutritional condition of the animal.

4. The panniculus carnosus is a skeletal muscle and can be described as the boundary between the dermal layers and the underlying adventia.

5. Subcutaneous tissue is a non-uniform collagenous tissue beneath the panniculus carnosus and contains fibroblasts, nerves, and blood vessels. It connects the skin to the skeletal muscle and provides the necessary elasticity and movements for the skin.

This intricate organ constitutes various adnexal structures such as modified sebaceous glands, eccrine and apocrine sweat glands. For instance, the mammary glands are a modified form of apocrine sweat gland. Since the mammary glands are formed from

the epidermal precursors that develop downward during prenatal development, they are considered to be cutaneous adnexa.

Nipples are in the abdominal region as 6 pairs following lines that curve towards the midline. Generally, they are 2 mm in length; however, they grow to around 4 mm during lactation period [75]. Beneath the rat's pelt, the mammary glands are placed within subcutaneous fat pads that can be divided into six mammary complexes: three pairs in the thoracic region and three pairs in the inguinal region as shown in Figure 4.1 [75]. They are branched tubular organs formed of one or two epithelial cell layers and are responsive to the hormonal and local epigenetic changes (adolescence, pregnancy, lactation, and senescence) [74]. It is essential to emphasize when the extensive rat mammary fat pads are completely developed, they extend from the inguinal area and base of the tail to the salivary gland region of the neck and around to the dorsum [74].

Dielectric property measurements of breast tissue, white adipose tissue, wet skin tissue and tumor tissue were performed to analyze the interior part of the pelt which has an intricate structure. The experiment was carried out with two female Sprague-Dawley rats obtained from Bogazici University, Center for Life Sciences and Technologies. To facilitate the forming of breast tumors, one animal (47 days old) was subjected to a single dose of carcinogenic solution that was prepared by dissolving 20 mg/kg 7,12-Dimethylbenz(a)anthracene (DMBA) in 1 mL olive oil in an ultrasound bath. Twenty-four hours prior to the application, the animal was prevented from accessing the food dispenser. The carcinogenic solution was applied via oral gavage and the animal was given a two-day rest period. The peritoneal area was checked for tumor formation by hand weekly. The resting conditions for the animals throughout the experiment were set as a 12 h light/dark cycle and free access to standard pellet food as well as tap water. The other animal was selected to be the control and was given a dummy solution of 1 mL olive oil via oral gavage, under the same conditions. Weight of the control and experiment animal during the experiments were 285 g and 230 g, respectively. Also, during the experiments, the ages of the control and experiment animal were 359 and 261 days old, respectively.

The animals were given an intraperitoneal injection for anesthesia composed by mixing 80 mg kg^{-1} ketamine and 10 mg kg^{-1} xylazine. After the animal completely

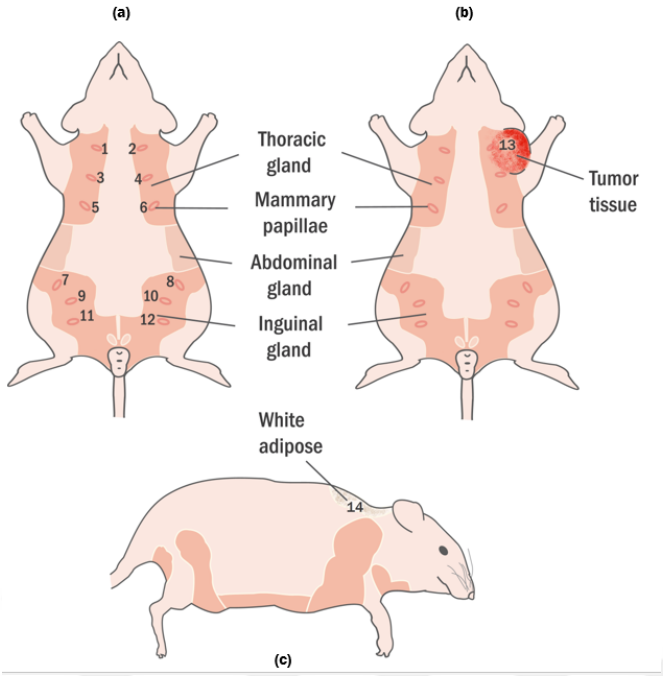

Figure 4.1 : Healthy and tumor-bearing rats have been demonstrated. (**a**) Healthy rats are shown in the frontal plane with marked 12 nipples. The locations of the nipples are in the region of thoracic and inguinal. (**b**) The rat with tumor is shown in the frontal plane and tumor was marked with 13. The tumor according to the mammary tissues was formed around the 2nd and 4th tissue. (c) The healthy rat was shown in the sagittal plane. The white adipose, located on the nape, is marked 14.

fell unconscious, peritoneal skin was incised, and dielectric measurement data was collected. The tumor was located between the second and fourth breast tissues as indicated with 13 in Figure 4.1b. The tumor had an elliptical shape and dimensions were 25.22 mm, 14.65 mm 4.4 mm for width, height and depth, respectively. Dielectric properties of thebreast tissues, wet skin from the abdomen and white adipose tissue from the nape as indicated with 14 in Figure 4.1c were measured on the control animal. Five dielectric property measurements were taken from each measurement point for every sample as shown in Fig. 4.2. The median value of five measurements was selected to represent dielectric property. The average temperature of the samples was 29.5 $\pm$ 1.5 °C. When the measurement process was completed, the animals were immediately euthanized. The tumor was resected for pathological analysis and the breast tissues was removed as a bloc with skin attached for sensing depth analysis.

The experiments were conducted in accordance with the ethical regulations approved by Bogazici University Animal Local Ethics committee. In vivo relative permittivity and conductivity measurement results ofbreast, wet skin, white adipose and tumor

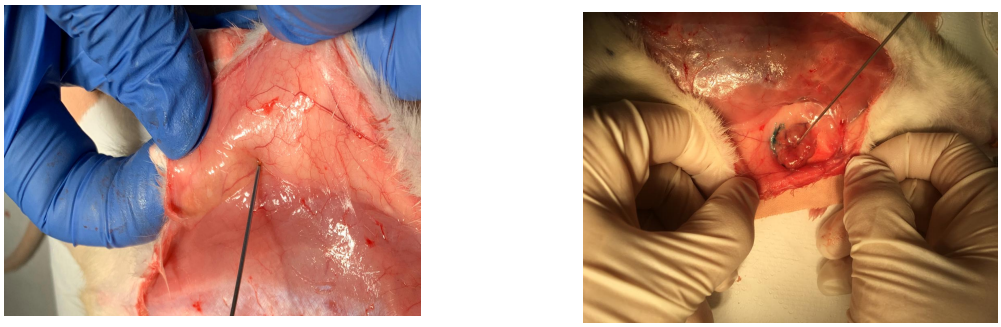

(a) **(b)**

Figure 4.2 : In vivo dielectric property measurements: (a) Measurement collected from the healthy breast tissue and (b) measurement of the malignant breast tumor tissue.

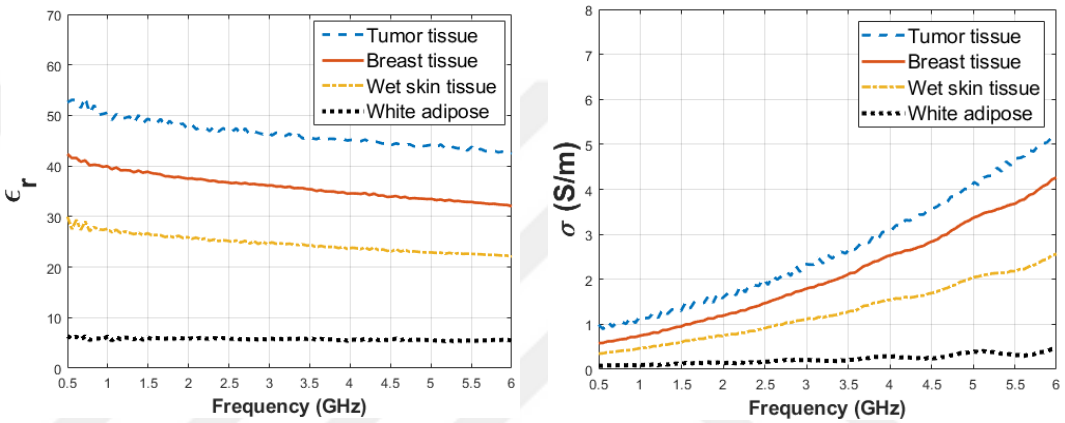

(a) **(b)**

Figure 4.3 : Median dielectric property measurement results between 0.5 and 6 GHz collected from various rat tissues including tumor, breast, skin, white adipose tissues: (a) relative permittivity and (b) conductivity.

Table 4.1 : Maximum standard deviation (SD) from the mean of five measurements for rat tissues (tumor, breast, wet skin and white adipose) over the frequency range of 0.5–6 GHz.

Tissue Types	**Relative Permittivity**		**Conductivity (S/m)**	
	SD	**Freq. (GHz)**	**SD**	**Freq. (GHz)**
Tumor Tissue	0.68	0.72	0.04	5.73
Breast Tissue	3.23	0.5	0.34	6
Wet Skin Tissue	3.16	0.5	0.40	6
White Adipose	0.64	4.46	0.02	5.95

tissues are given in 4.3a and b, respectively. The standard deviation from the mean of five measurements for each tissue sample was calculated in the frequency range of 0.5–6 GHz with 101 points. The maximum standard deviation of dielectric property

was listed in Table 4.1 for each tissue sample along with corresponding frequency point.

4.3 Materials and Methods

In the following section, the details of experiment setup, preparation of two double-layered sample configurations and applied dielectric property measurement protocol in detail are explained.

4.3.1 Experiment setup

The experiment setup is composed of an Agilent FieldFox N9923A 6 GHz RF Vector Network Analyzer (VNA) (Santa Clara, CA, USA), Agilent Dielectric Slim Form open-ended coaxial probe (2.2 mm aperture diameter) (Santa Clara, CA, USA), Agilent 85070E dielectric property measurement software (Santa Clara, CA, USA), external computer, an adjustable stand, a digital caliper and two double-layered configuration samples. The setup is shown in Figure 4.4 and the function of each equipment is marked with 1 to 4 given in the figure:

1. The function of the VNA was to retrieve the S parameter responses from the probe. To eliminate temperature drift errors caused by device and cable connections, the VNA was turned on four hours prior to measurements. The frequency range was set from 0.5 to 6 GHz with 55 MHz increments which is a sufficient range for the biological tissue studies.

2. The 2.2 mm-diameter open-ended coaxial probe was used in this experiment. It is a widely preferred dielectric property measurement tool due to its wideband properties and non-destructive measurement features [22,53,56,64]. Additionally, the position of the probe was fixed and remained in the same position during the entire experiment to avoid errors caused by cable movement.

3. Agilent 85070E software was used to calculate the complex permittivity from the retrieved S parameters. The software requires guided “three standards” calibration steps in the order of open circuit, short circuit and a broadband load. In our case, the probe tip was terminated with open air, a conductive textile and distilled water with known temperature, respectively.

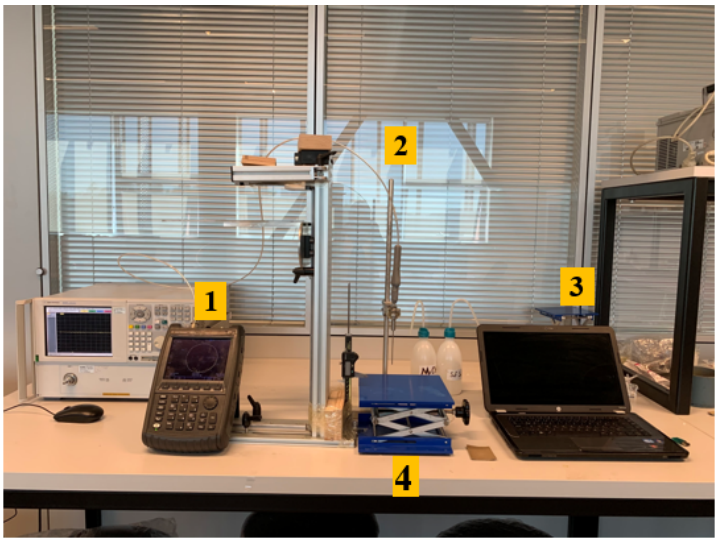

Figure 4.4 : Experimental setup includes (1) Agilent FieldFox N9923A 6GHz RF Vector Network Analyzer (VNA), (2) Agilent Dielectric Slim Form open-ended coaxial probe, (3) Agilent 85070E software, external computer, (4) an adjustable stand and a digital caliper.

4. The sample location was defined via an adjustable stand and a caliper. The top plate of the adjustable stand was a stainless steel structure and the thickness of plate was 12 mm. The adjustable stand was used to move the sample up and down while the caliper measures the position of the stand during the experiment. The probe tip distance from layers was measured via Mitutoyo absolute digimatic caliper 0–150 mm with 0.01 mm digital step size.

System validation was performed with three known materials: ethanol (ε_r = 8.73 and σ = 0.86 S/m at 2 GHz), methanol (ε_r = 26.86 and σ = 1.38 S/m at 2 GHz) and Dimethyl Sulfoxide (DMSO) (ε_r = 44.23 and σ = 1.02 S/m at 2 GHz). The measurements were taken when the average temperature of materials was 28.3 $\pm$ 0.2 °C. The measurement results were compared with calculated dielectric properties based on the Debye parameters from literature [76–78]. The temperatures of the materials were 29.5 °C in the literature. The measured and calculated dielectric properties are shown in Figure 4.5. Also, maximum difference between measured and calculated dielectric properties from the Debye parameters given in the literature are listed in Table 4.2 at the corresponding frequency points.

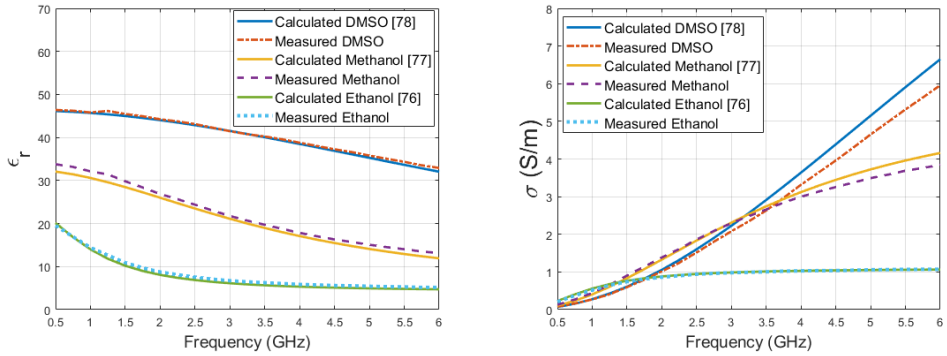

(a) **(b)**

Figure 4.5 : Comparison of known materials (ethanol, methanol and DMSO) dielectric properties calculated from Debye parameters obtained from the literature and measured by the experiment setup: (a) relative permittivity and (b) conductivity.

Table 4.2 : Maximum dielectric property difference between measurements and Debye model calculation for known materials (ethanol, methanol and DMSO) used for system validation.

Materials	Diff. for ε_r	Freq. (GHz)	Diff. for σ (S/m)	Freq. (GHz)
Ethanol [76]	0.8	1	0.04	1.25
Methanol [77]	1.8	1.25	0.31	6
DMSO [78]	0.9	6	0.69	6

4.3.2 Sample configuration

The prepared two double-layered configurations consisted of rat breast and skin tissues as the first layer and triton X-100 and olive oil as the second layer. The first sample configuration included rat breast tissue and olive oil. The second sample configuration was composed of rat wet skin tissue and triton X-100. The liquids used to form the second layer are shown in Figure 4.6a (from left to right: olive oil and Triton X-100). The tissues were removed from 359 days old, 285 g Sprague-Dawley rat. The thickness of the rat tissue was 2.5 mm, and each sample was resected approximately with 3.5 cm-diameter. The measurements were performed within 1 h following the excision of rat tissues. A sample of the double-layered configuration composed of rat breast tissue-olive oil is given in Figure 4.6b.

(a) **(b)**

Figure 4.6 : Sample configuration: (a) olive oil (left) and Triton X-100 (right) were used as second layer liquids and () double-layered configuration with rat breast tissue and olive oil.

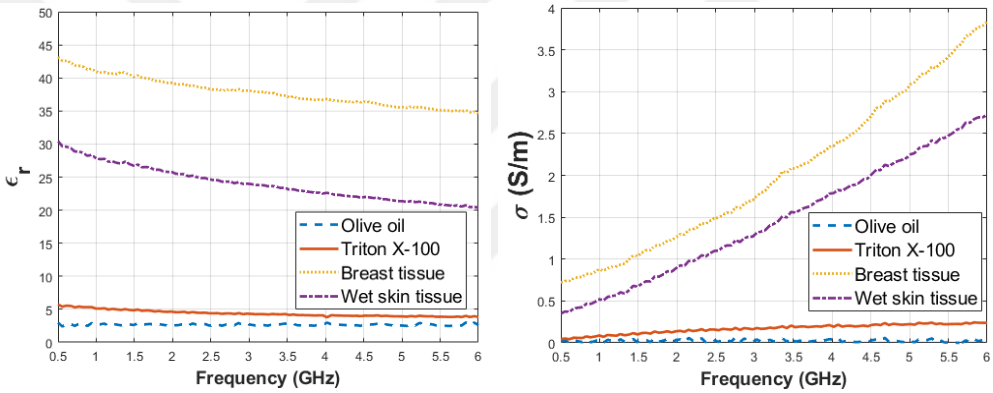

(a) **(b)**

Figure 4.7 : Median of dielectric properties obtained from pure materials olive oil, Triton X-100 and ex vivo rat tissues: (a) Relative permittivity and (b) conductivity.

Before starting the experiment, dielectric property measurement was performed for pure materials; that is, triton X-100 and olive oil. Also, dielectric property measurements were collected from ex vivo rat tissues. Five measurements were taken for every sample and median of the measurement results are given in Figure 4.7a,b for relative permittivity and conductivity , respectively. The average temperature of pure materials was 27.5 ± 0.5 °C. The standard deviation from the mean of five measurements for pure materials (olive oil, triton X-100, ex vivo breast and wet skin tissues) was calculated in the frequency range of 0.5–6 GHz with 101 points. The

Table 4.3 : Maximum standard deviation (SD) of five measurements over the frequency range of 0.5–6 GHz for pure materials (olive oil, triton X-100, breast and wet skin).

Tissue Types	Relative Permittivity		Conductivity (S/m)	
	SD	Freq. (GHz)	SD	Freq. (GHz)
Olive oil	0.13	4.02	0.02	3.59
Triton X-100	0.07	0.88	0.01	3.59
Breast tissue	1.13	5.84	0.2	5.73
Wet skin tissue	1.97	6	0.3	6

maximum standard deviations of dielectric properties are listed in Table 4.3 for each pure material at corresponding frequency points.

4.3.3 Measurement protocol

The applied measurement protocol for sensing depth characterization of the 2.2 mm open-ended coaxial probe shown in Figure 4.8. To eliminate potential error due to calibration degeneration, the open-ended coaxial probe, the probe holder, VNA, adjustable stand and caliper were placed in a fixed position and the same position was maintained during the measurement process. The distance between the probe tip and sample was adjusted by moving the adjustable stand; that is, the sample under test. Since a special measurement tank was not employed to simplify the measurement procedure, the sample movement was tracked by measuring the adjustable stand height. To do so, the caliper jaw was firmly attached to adjustable stand as shown in Figure 4.8. The protocol is described as follows:

- Steps in Figure 4.8(1)
  - The first layer (rat tissues) was laid flat at the bottom of a glass beaker. Please note that the tissues were fixed at the bottom of beakers by using a double-sided tape.
  - The beaker was placed on the platform of the adjustable stand and slowly moved towards the probe tip.
  - While the adjustable stand was moving towards the probe tip, the change in the S parameter response from the VNA was monitored. When a response significantly different from the open air; that is, S parameter

response of the probe converging to that when the probe was terminated with the tissue, was observed, it was confirmed that the first layer was touching to the probe tip. At this point, the measured value on the caliper was recorded as X_1 position. Please note that a dielectric property measurement was not performed at this step of the protocol to prevent any potential damage to tissue surface due to pressure.

  - The information of X_1 position reduces misleading sensing depth measurements caused by the probe pressure to the rat tissues.

- Steps in Figure 4.8(2)

  - The adjustable stand was moved down to place the second layer liquid.
  - Without shifting the location of the sample, the liquids (Triton X-100 or olive oil) were gently added with a Pasteur pipette .
  - Next, the double-layered sample was moved towards the probe tip.
  - When the surface of the second layer was in full contact with the tip of the probe, the measured value on the caliper was recorded as X_2 position.
  - The difference between X_1 and X_2 positions provides the distance "D" which is the distance from the probe tip to the surface of the first layer.
  - Knowledge of the distance D allows us to determine the increment size of the adjustable stand movement.

- Steps in Figure 4.8(3)

  - The double-layered sample was gradually moved up allowing the probe to immerse into the second layer. The dielectric properties were measured in each position (X_n) at different depths (D_n).
  - The measurements were concluded when the probe tip arrived at the X_1 position, which is the surface of rat tissues.

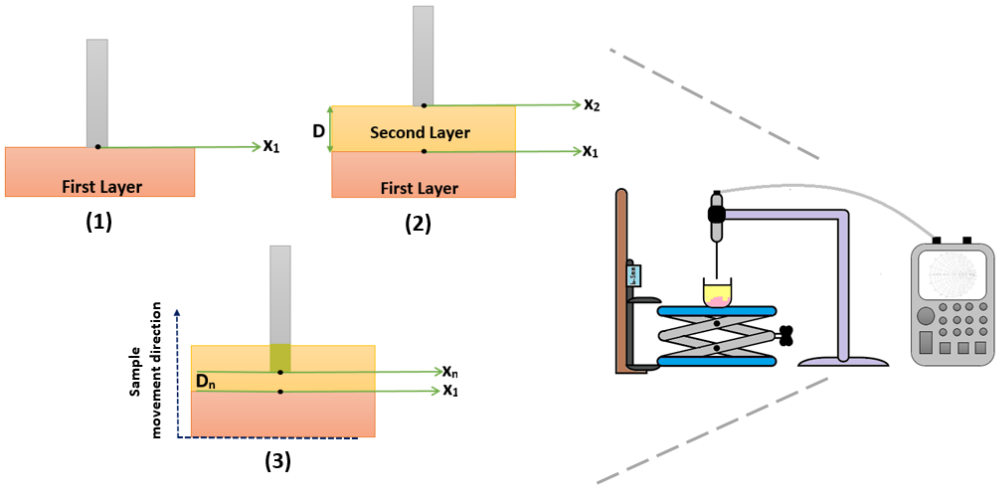

Figure 4.8 : Measurement protocol for analyzing sensing depth with double-layered sample configuration. (1) X_1 position was determined based on the thickness of the first layer. (2) X_2 position was determined based on the probe tip distance from the first layer (D) was calculated ($X_2 - X_1$). (3) Double-layered sample configuration was gradually moved up to analyze the dielectric property change and sensing depth of the probe.

4.4 Results

This section demonstrates the sensing depth analysis of the 2.2 mm-diameter open-ended coaxial probe based on the dielectric properties acquired from the two different double-layered configurations. The analysis was conducted by selecting five frequency points. The percent change in the measured dielectric properties of the double-layered configurations were analyzed at each frequency point with respect to the probe tip distance from the first layer (D_n).

4.4.1 Sensing depth analysis: Rat breast tissue-olive oil configuration

The relative permittivity and conductivity of pure materials (rat breast tissue and olive oil) used for this scenario are listed in Table 4.4. Moreover, the change in measured dielectric properties of the rat's breast tissue-olive oil configuration is plotted in Figure 4.9 for the selected five frequency points, 0.5, 1.05, 2.04, 3.03 and 6 GHz, against probe distance from the surface of the rat breast tissue. When the distance on the graphs is equal to zero, it refers to the probe tip touching on the rat breast tissue and the obtained values are compatible with the pure material dielectric properties. In Figure 4.9b, for distances smaller than 0.17 mm the dominant material is rat breast tissue

Table 4.4 : The relative permittivity and conductivity of pure materials (rat breast tissue and olive oil) at five frequency points.

Frequency (GHz)	**Relative Permittivity**		**Conductivity (S/m)**	
	Rat breast tissue	Olive oil	Rat breast tissue	Olive oil
0.5	43.2	2.59	0.72	0.0103
1.05	40.8	2.53	0.86	0.0055
2.04	39.1	2.45	1.30	0.0162
3.03	38.0	2.50	1.76	0.0170
6	34.7	2.45	3.83	0.0094

and the largest conductivity measured for the largest frequency. Around 0.17 mm the dominant material starts to become olive oil. Since the olive oil conductivity is very small, the system uncertainties start to be evident and same frequency-conductivity trend becomes less apparent. Furthermore, the relative permittivity and conductivity of the olive oil were very low ($\varepsilon_r = 2.45$ and $\sigma = 0.0162$ S/m at 2.04 GHz) and the reported error of the commercial systems is 5% [68]. In Figure 4.9, the results were shown with polylines due to the dielectric property of selected materials, system error and small incremental steps (approximately 0.02 mm). For analysis purposes, we investigated the dielectric property alteration of the double-layered configuration with respect to five percent change points: 5%, 10%, 20%, 80% and 90%. First, the increase in the relative permittivity and conductivity of olive oil with respect to pure olive oil measurement was examined based on these percentage values. Second, the decrease in relative permittivity and conductivity of breast tissue with respect to breast tissue measurement was analyzed based on same percentage changes. These percentage values were selected according to sensing depth analysis in the following literature. The dielectric permittivity of intervening liquid was small in our experiments, therefore we selected 5% changes according to the defined histology region with system uncertainty in [64]. 10% changes in dielectric property of alcohol samples was also determined as an accepted threshold for sensing depth of 2.2 mm-diameter probe [63]. The effective penetration depth was described as a 20% difference between expected and measured dielectric property in [62]. Approximately 90% of dielectric property for the intervening liquid was pointed out for sensing depth analysis of 2.2 mm-diameter probe [56]. 80% and 90% changes were also selected as complementary to 20% and 10% changes, respectively.

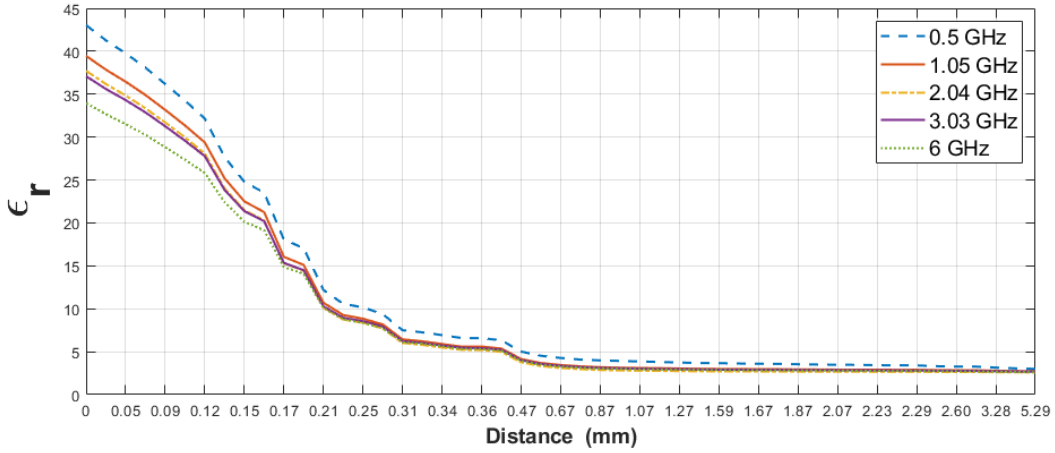

(a)

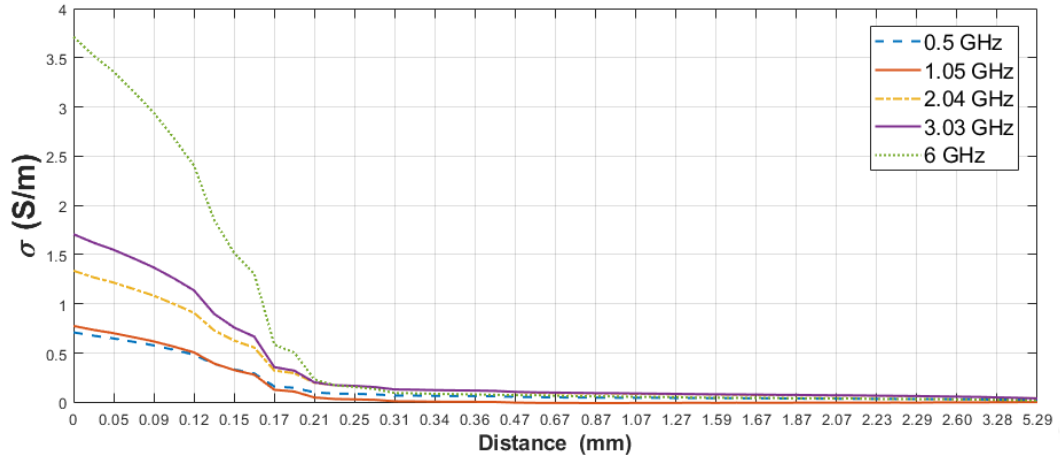

(b)

Figure 4.9 : Measured dielectric properties of the double-layered rat breast tissue-olive oil configuration: (a)Relative permittivity, (b)conductivity as a function of probe tip distance from first layer (D_n) at 0.5, 1.05, 2.04, 3.03 and 6 GHz frequencies.

The aim here is to find the distances where 5%, 10%, 20%, 80% and 90% change in the dielectric property of pure materials (olive oil and rat breast tissue) are observed. Since the dielectric properties of the pure materials are known, as shown in Table 4.4, the percentage changes mentioned above can be mathematically computed. On the other hand, the measured dielectric properties obtained from the distances (D_n) may not correspond to the expected percentage change. Therefore, an error margin is defined such that if the measured dielectric property from a certain distance (D_n) varies within 1% of the expected percentage change, then that distance is accepted as the distance where the expected percentage change occurs. Otherwise, if the measured dielectric property is larger or smaller than 1% of the expected percentage change,

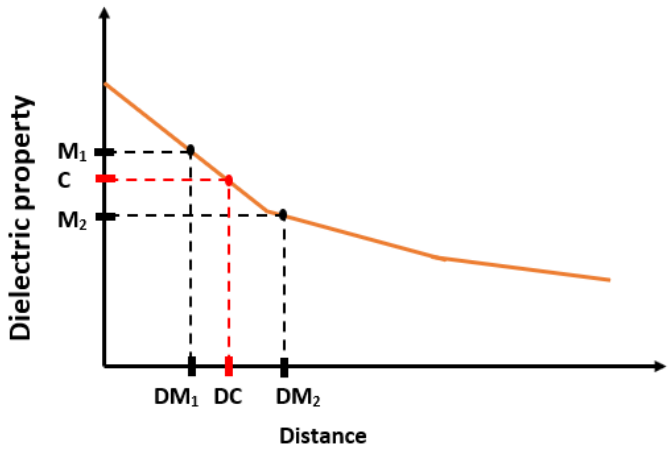

Figure 4.10 : The distance (DC) was estimated for calculated dielectric property (C) based on percentage change using measured consecutive dielectric properties (M_1 and M_2) and their distances (DM_1 and DM_2).

the distance corresponding to the expected percentage change is determined by using the estimation procedure given in [62].

Suppose that M_1 and M_2 are the measured dielectric properties from the distances DM_1 and DM_2, respectively and the expected percentage change in dielectric properties (C) falls between M_1 and M_2 (see Figure 4.10). To obtain the distance (DC) corresponding to the expected percentage change, a linear line is defined using the points (M_1, M_2, DM_1 and DM_2). The distance (DC) corresponding to the expected change in dielectric property is calculated from the linear line equation.

First, the percent change in the measured dielectric property of the double-layered configuration was analyzed regarding the increase in the dielectric property of the second layer (olive oil). The percent change in the measured dielectric properties of the configuration and the corresponding distances (D_n) of the probe tip at five frequency points are listed in Table 4.5. Table 4.5 indicates 5% increment in relative permittivity and conductivity of the configuration from 1.36 to 3.28 mm and from 4.8 to 5.1 mm probe tip distances from the first layer (D_n), respectively, at the five frequency points. 10% increase in the measured relative permittivity and conductivity was observed from 0.87 to 2.31 mm and from 4.4 to 5.2 mm and 20% increase from 0.67 to 1.67 mm and from 0.37 to 4.6 mm, respectively. As the probe tip approached to the first layer, the effect of this layer became dominant resulting in an 80% increase in the measured relative permittivity between 0.40 and 0.41 mm and measured conductivity between

Table 4.5 : Specified increase levels for retrieved relative permittivity and conductivity of double-layered rat breast tissue and olive oil configuration and the corresponding distances (D_n) at 0.5, 1.05, 2.04, 3.03 and 6 GHz frequency points.

Freq (GHz)	Distance (mm) for Rat Breast Tissue-Olive Oil									
	Relative Permittivity					Conductivity (S/m)				
	5%	10%	20%	80%	90%	5%	10%	20%	80%	90%
0.5	3.28	2.31	1.67	0.44	0.42	4.8	4.4	3.6	1.77	1.67
1.05	2.31	1.36	0.77	0.41	0.38	5.2	5.1	0.37	0.36	0.35
2.04	1.36	0.87	0.67	0.4	0.38	4.9	4.5	3.5	1.77	1.62
3.03	2.29	1.36	0.77	0.4	0.38	5.0	4.6	3.9	2.07	1.87
6	2.31	1.36	0.77	0.41	0.38	5.1	4.9	4.6	2.6	2.29

Table 4.6 : Specified decrease levels for retrieved relative permittivity and conductivity of double-layered rat breast tissue and olive oil configuration and the corresponding distances (D_n) at 0.5, 1.05, 2.04, 3.03 and 6 GHz frequency points.

Freq (GHz)	Distance (mm) for Rat Breast Tissue-Olive Oil									
	Relative Permittivity					Conductivity (S/m)				
	5%	10%	20%	80%	90%	5%	10%	20%	80%	90%
0.5	0.02	0.06	0.1	0.29	0.67	0.03	0.05	0.09	0.18	0.31
1.05	0.02	0.06	0.1	0.27	0.57	0.03	0.05	0.09	0.17	0.18
2.04	0.02	0.06	0.1	0.27	0.47	0.03	0.05	0.09	0.18	0.31
3.03	0.02	0.06	0.1	0.28	0.57	0.03	0.05	0.09	0.17	0.23
6	0.02	0.07	0.1	0.29	0.57	0.03	0.05	0.09	0.17	0.21

0.36 and 2.6 mm distances. Furthermore, 90% increase in relative permittivity is seen between 0.38 and 0.42 mm and similar increase in conductivity between 0.35 and 2.29 mm is observed indicating that the probe tip was located at the region where the measurements reflect the dominance of the first layer.

Secondly, the percent change in the measured dielectric property of the double-layered configuration was evaluated with respect to the decrease in the dielectric property of the first layer (rat breast tissue). In Table 4.6, the measured relative permittivity and conductivity of the double-layered configuration decreased by 5% at 0.02 mm and at 0.03 mm probe tip distances respectively, for the given five frequency points. 10% decrease in permittivity from 0.06 to 0.07 mm and same percent decrease in conductivity, 20% observed at 0.1 mm. Likewise, 20% decrease in measured relative permittivity and conductivity is seen at 0.1 mm and at 0.09 mm probe tip distances, respectively. As the probe tip moved

Table 4.7 : The relative permittivity and conductivity of pure materials (rat wet skin tissue and triton X-100) at five frequency points.

Frequency (GHz)	Relative Permittivity		Conductivity (S/m)	
	Rat wet skin	Triton X-100	Rat wet skin	Triton X-100
0.5	30.5	5.8	0.33	0.05
1.05	27.7	5.1	0.49	0.07
2.04	25.5	4.6	0.91	0.14
3.03	23.9	4.3	1.30	0.18
6	20.4	3.8	2.67	2.41

away from the first layer, the effect of the second layer happened to be more dominant, leading to 80% decrease in measured relative permittivity between 0.27 and 0.29 mm probe tip distance and 80% decrease in measured conductivity between 0.17 and 0.18 mm. In addition, the measured relative permittivity and conductivity decreased by 90% between 0.47 and 0.67 mm probe distance and between 0.18 and 0.31 mm respectively, indicating that the second layer has more effect in this region.

4.4.2 Sensing depth analysis: Rat wet skin tissue–triton X-100

The relative permittivity and conductivity of pure materials (rat wet skin tissue and triton X-100) used for this scenario are listed in Table 4.7. Furthermore, similar to the previous section, the sensing depth of the probe was analyzed based on measured dielectric property change of both layers. Triton X-100 is not expected to interact with the tissue in a short period of time at room temperature [79]. In Figure 4.11, the change in dielectric property of rat wet skin tissue–triton X-100 double-layered configuration is given for five frequency points against the probe distance from the surface of the first layer (D_n). The percent change in the measured dielectric property of the rat wet skin tissue-triton X-100 configuration was first analyzed based on the increase in dielectric property of the second layer (triton X-100). Table 4.8, denotes the 5%, 10%, 20%, 80% and 90% increment points in the measured dielectric properties and their corresponding distances (D_n) at five frequency points. From the table, 5% increase in the measured relative permittivity at 1.23 mm and same percent increase in conductivity is observed between 1.33 and 1.43 mm probe tip distances. 10% and 20% increase in the measured relative permittivity are occurred at 1.11 mm and at 0.94 mm, respectively. Also, 10% and 20% increase in conductivity are observed from 1.23 to 1.33 mm and from 1.04 to

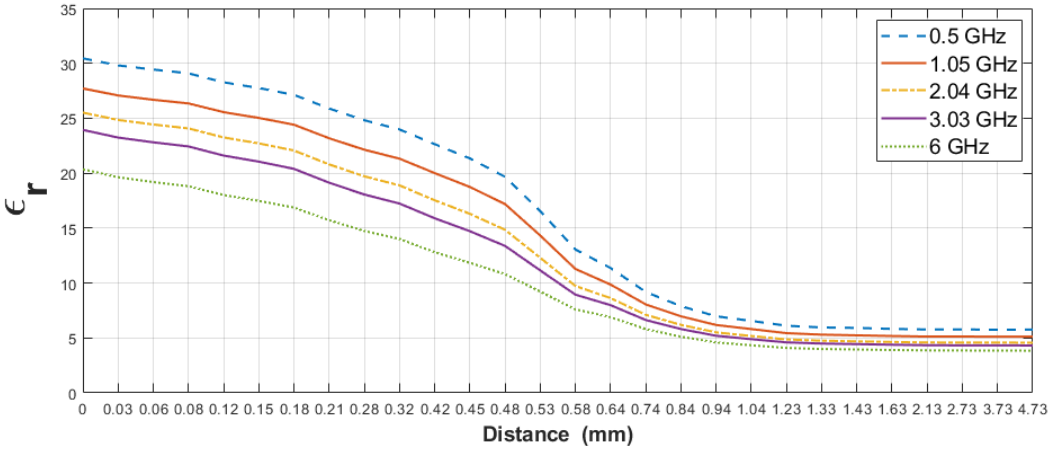

(a)

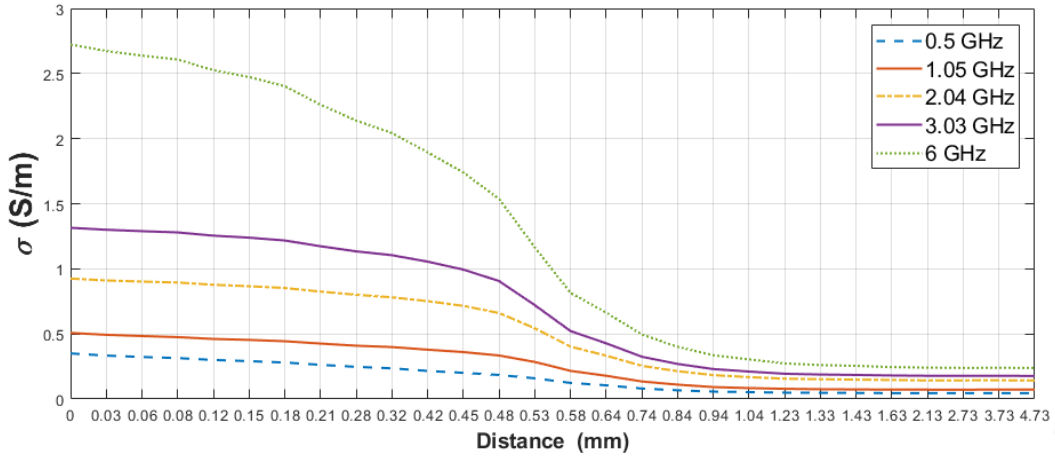

(b)

Figure 4.11 : Retrieved dielectric properties of the double-layered rat wet skin tissue and triton X-100 configuration: (a) Relative permittivity, (b) conductivity as a function of probe's distance from first layer (D_n) at 0.5, 1.05, 2.04, 3.03 and 6 GHz.

1.23 mm, respectively. Due to the close proximity of the probe to the first layer, 80% and 90% increase in the relative permittivity was observed between 0.64 and 0.69 mm probe tip distance and between 0.61 and 0.66 mm, respectively. Similarly, 80% and 90% increase conductivity was seen between 0.81 and 0.74 mm distances and between 0.72 and 0.78 mm, respectively. These values clearly show that the first layer was dominant with these distances (D_n).

The second analysis was based on the percent change in the measured dielectric property of double-layered configuration with respect to the decrease in dielectric property the first layer (rat wet skin tissue). Table 4.9, show 5% decrease in measured relative permittivity and conductivity of the double-layered configuration from 0.06 to

Table 4.8 : Specified increase levels for retrieved relative permittivity and conductivity of double-layered rat wet skin tissue and triton X-100 configuration and the corresponding distances (D_n) at 0.5, 1.05, 2.04, 3.03 and 6 GHz frequency points.

Freq	Distance (mm) for Rat Wet Skin Tissue-Triton X-100									
	Relative Permittivity					Conductivity (S/m)				
(GHz)	5%	10%	20%	80%	90%	5%	10%	20%	80%	90%
0.5	1.23	1.11	0.94	0.69	0.66	1.33	1.23	1.04	0.74	0.72
1.05	1.23	1.11	0.94	0.68	0.65	1.33	1.23	1.04	0.76	0.74
2.04	1.23	1.11	0.94	0.67	0.64	1.43	1.23	1.04	0.74	0.72
3.03	1.23	1.11	0.94	0.66	0.63	1.43	1.23	1.04	0.75	0.73
6	1.23	1.11	0.94	0.64	0.61	1.43	1.33	1.23	0.81	0.78

Table 4.9 : Specified decrease levels for retrieved relative permittivity and conductivity of double-layered rat wet skin tissue and triton X-100 configuration and the corresponding distances (D_n) at 0.5, 1.05, 2.04, 3.03 and 6 GHz frequency points.

Freq	Distance (mm) for Rat Wet Skin Tissue-Triton X-100							
	Relative Permittivity				Conductivity (S/m)			
(GHz)	5%	10%	20%	80%	5%	10%	20%	80%
0.5	0.08	0.18	0.32	1.33	0.03	0.08	0.18	0.84
1.05	0.08	0.15	0.28	1.23	0.06	0.15	0.28	0.94
2.04	0.08	0.15	0.21	1.04	0.12	0.21	0.42	0.94
3.03	0.08	0.12	0.21	1.04	0.12	0.21	0.42	0.84
6	0.06	0.12	0.18	1.23	0.08	0.15	0.28	0.74

0.08 mm and from 0.03 to 0.12 mm, respectively. Similarly, 10% decrease in relative permittivity and conductivity from 0.12 to 0.18 mm and from 0.08 to 0.21 mm probe distances, respectively, and 20% decrease from 0.18 to 0.32 mm and from 0.18 to 0.42 mm probe distances, respectively. Finally, 80% decrease the relative permittivity was observed between 1.04 and 1.33 mm and 80% decrease in conductivity between 0.74 and 0.94 mm. The high percentage decrease is due to the dominant nature of the second layer since the probe tip moved further away from the first layer. It should be noted the 90% decrease in the dielectric property was not calculated since the dielectric property of triton X-100 is higher than the calculated values.

4.5 Discussion

This study was performed to examine how various adnexal structures that can be formed on wet skin and around breast tissues can affect measurements. Moreover, two double-layered configurations were prepared to determine the effect of the dielectric property contrast between layers on the probe's sensing depth. The first configuration was composed of rat breast tissue (ε_r = 39.35 and σ = 0.8607 S/m at 1.05 GHz) and olive oil (ε_r = 2.73 and σ = 0.0034 S/m at 1.05 GHz). In the second configuration, rat wet skin tissue (ε_r = 26.86 and σ = 0.4812 S/m at 1.05 GHz) and triton X-100 (ε_r = 5.11 and σ = 0.0722 S/m at 1.05 GHz) were used. For the first configuration, the difference between the layers are 36.62 units for relative permittivity and 0.8573 S/m for conductivity. The difference between the layers for the second configuration are 21.75 units for the relative permittivity and 0.409 S/m for conductivity. From these results, the difference of relative permittivity between the layers decreased 40% in the second configuration. Similarly, the difference of conductivity was declined 52% in the second configuration. To analyze the impact of contrast between the layers, the dielectric property change of the two configurations was compared at the frequency point of 1.05 GHZ as given at Figure 4.12. The dielectric properties of both configurations were plotted in the distance range of 0–0.32 mm (D_n). Since the most important change was observed at the close proximity of the probe tip, the most precise increment was implemented at this interval even though manual measurements were performed. Therefore, the distances are only the same at this interval for both configurations. As seen in Figure 4.12, since rat breast tissue-olive oil has a larger dielectric property difference a significant change was observed between 0–0.32 mm, the rat wet skin tissue-triton X-100 shows a more gradual change due to the relatively smaller dielectric property difference between the layers. In [64], the dielectric property contrast between first and second layers of the double-layered configuration were examined independent of frequency, and similar results were also observed.

In addition, the dielectric property based on the percentage change was plotted using the data from Tables 4.5–4.9 at the result Sections 4.4.1 and 4.4.2. The Figure 4.13

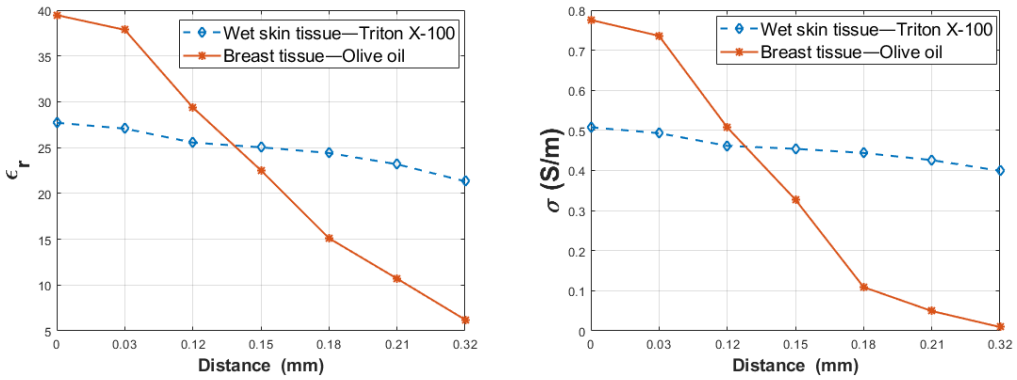

(a) **(b)**

Figure 4.12 : The comparison dielectric property alteration of rat wet skin tissue-triton X-100 and rat breast tissue-olive oil as a function of probe tip distance (D_n): (a) relative permittivity and (b) conductivity.

demonstrates the probe tip distances from the first layer (D_n) as a function of dielectric property percentage change in double-layered configuration at the 1.05 GHz frequency point. As seen in Figure 4.13, 20%, 80%, and 90% changes occur at smaller distances for rat breast tissue and olive oil, while the same percentage changes are observed at larger distances for the rat wet skin tissue and triton X-100. Furthermore, the intersection between wet skin tissue and triton X-100 alterations is observed at the 52% relativity permittivity change point and 0.8 mm probe tip distance from the first layer (D_n) as shown in Figure 4.13a. Similarly, intersection for the rat breast tissue and olive oil alteration is noticed at the 84% change point and 0.4 mm distance. For the conductivity, as given in Figure 4.13b, while the intersection of rat breast tissue and olive oil happens at 82% change and 0.35 mm distance point, the intersection of rat wet skin tissue and triton X-100 alterations happens at 67% change and 0.8 mm distance. The percentage change of relative permittivity for both configurations were examined in the frequency range of 0.5–6 GHz and it was concluded that the results are similar to Figure 4.13a. However, the change of the percentage based on conductivity of olive oil in the same frequency range is different from each other, contrary to the triton X-100 alteration. This difference between conductivity changes can be caused by the very low conductivity of olive oil. Although the small conductivity of olive oil caused difficulty in percentage analysis, the conductivity at 1.05 GHz showed percentage change similar to the relative permittivity variations. As also explained in the study [64], conductivity shows ambiguity at sensing depth studies. Therefore,

relative permittivity changes should be prioritized since they give more precise results. When measuring the relative permittivity of the skin or breast tissues, it was examined that a thin layer (such as collagen, white adipose or subcutaneous tissue) formed on targeted tissue, even if it has 0.4–0.8 mm thickness, can confound the results between 52% and 84%. To avoid these errors, it is important to establish a-priori information regarding the tissue or sample of interest. For rat tissues, even though the animal's anatomy is known well, small layers that cannot be recognized by the naked eye can have a significant impact on the results. For more accurate measurement results, the location of tissue to be measured must be precisely determined and measurements must be taken from areas surrounding the target point as well for cross-validation purposes. Moreover, the tissue can be scratched lightly before taking the measurement to remove the layer that may be formed on the target tissue. Therefore, there is a need to formulate a protocol for experiments to reduce errors caused by tissue heterogeneity. Another option is to catalogue sample specific sensing depth information and use the appropriate information in machine learning algorithms or choose the probe with the appropriate aperture size. Alternatively, the measured dielectric properties with known probe sensing depth can be used for heterogeneity grading or tumor grading.

4.6 Conclusions

Acquiring the dielectric property of biological tissue accurately is a prerequisite for microwave detection, diagnosis and treatment methods in the medical field. Even though the open-ended coaxial probe method provides essential advantages, the technique still suffers from having high measurement error and low repeatability. Rats are commonly preferred experimental animals since they have numerous advantages. The studies for breast cancer with rat models are significant due to the characteristic of rats, which is the extent of having more hormone responsiveness with histopathology and premalignant stages similar to the human breast cancer model [40]. To avoid acquiring incorrect data caused by a heterogeneous formation beneath the rat's pelt, dielectric measurement must be implemented rigorously. In addition, leaking of milk from the gland and body fluids or bleeding during the experiment can confound the measurement. To analyze the impact of any layer formed over the rat tissues (breast

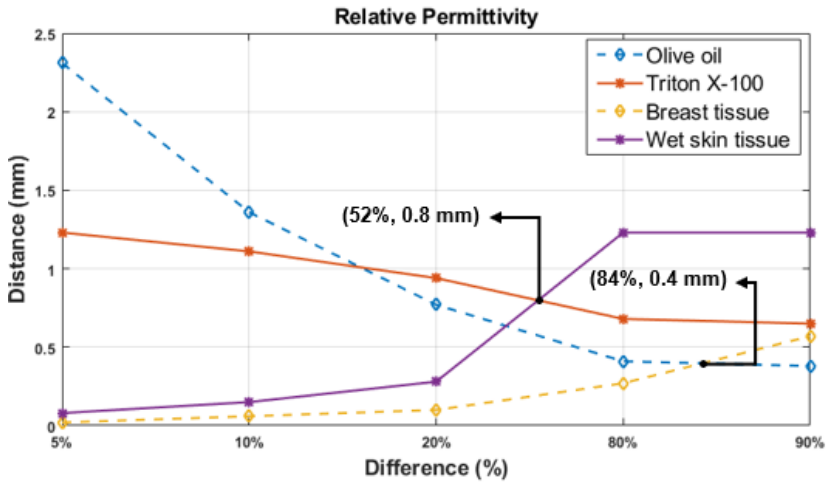

(a)

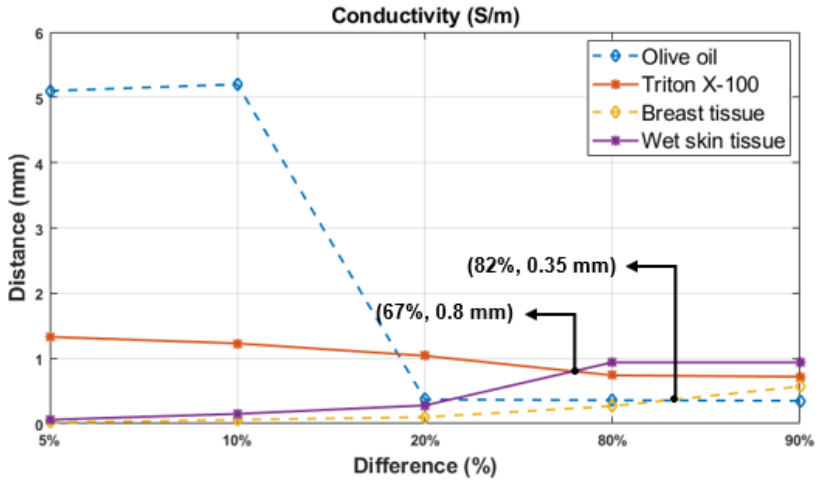

(b)

Figure 4.13 : The probe tip distances from rat tissue layers (D_n) are shown as a function of five percentage change points in dielectric property of the materials used for double-layered configurations (olive oil, triton X-100, rat breast and wet skin tissue): (a) relative permittivity and (b) conductivity.

and wet skin) during the measurements, we performed sensing depth analysis of the 2.2 mm-diameter open-ended coaxial probe.

To this end, this work investigates the sensing depth of 2.2 mm-diameter open-ended coaxial probe for animal experiment. Unlike previously reported studies, the experiments consisted of a simple measurement setup without forming a special experiment setup tank. The double-layered samples included rat breast and wet skin tissue as a first layer and liquids (olive oil and triton X-100) with relatively low

dielectric properties added as second layers. The difference of relative permittivity and conductivity between the layers decreased 40% and 52%, respectively, in the second configuration. Liquids with low dielectric properties provides substantial insight for potential change in measured dielectric properties since the liquids mimic the effect of adipose tissue which can cover the top of the healthy tissues and tumors. Five percent thresholds in dielectric property changes; 5%, 10%, 20%, 80% and 90% were tracked to define the sensing depth at five frequency points. The wide change from 5% to 90% increase in relative permittivity was taken place for the olive oil between 3.28 to 0.42 mm probe tip distance from the breast tissue at 0.5 GHz. Similarly, from 5% to 90% increase in conductivity for the olive oil was calculated in the distance range of 5.2–0.38 mm at 1.05 GHz. The dielectric property alteration of triton X-100 was in the range of 1.43–0.61 mm probe tip distance. Furthermore, the percent decrease in dielectric properties for rat breast and skin tissues was in the distance range of 0.02–1.33 mm. We can also state that a membrane layer (between 0.4–0.8 mm thickness) on the wet skin tissue and breast tissue will potentially affect the measurement results of dielectric property by 52–84%. These findings also suggests the layer that is in immediate contact with the probe tip will have the most significant effect on dielectric property measurements.

5. CHARACTERIZATION OF OPEN-ENDED COAXIAL PROBE SENSING DEPTH WITH RESPECT TO APERTURE SIZE FOR DIELECTRIC PROPERTY MEASUREMENT OF HETEROGENEOUS TISSUES [1]

The open-ended coaxial probe (OECP) method is frequently used for microwave dielectric property (DP) characterization of the high permittivity and conductivity materials due to inherent advantages including minimal sample preparation requirements and broadband measurement capabilities. However, the OECP method is known to suffer from high measurement error. One well-known contributor to the high error rates is tissue heterogeneity that can potentially be managed through selection of a probe with proper sensing depth (SD). The SD of the OECP is dependent on many factors including sample DPs and probe aperture diameter. Although the effect of sample DPs to SD have been investigated to some extend in the literature, the probe aperture diameters, particularly small diameters, have not been fully explored. To this end, the SD of probes with three different apertures (0.5, 0.9 and 2.2 mm-diameters) were analyzed in this study. Probes SD were first investigated with simulations using double-layered sample configuration (skin tissue and olive oil). Next, experiments were performed using a commercial OECP with 2.2 mm aperture diameter. The SD is categorized based on 5%, 20% and 80% DP change. Among these threshold values, 5% DP change was selected as the bench mark for SD categorization. The findings suggest that probes with smaller aperture size and correspondingly smaller SD should be utilized when measuring DPs of thin and multilayered samples, such as healthy and diseased skin tissues to increase the measurement accuracy.

5.1 Introduction

Each biological tissue has a unique set of dielectric properties (DPs) based on their molecular structure. Particularly at microwave frequencies, biological tissues can be characterized based on their water content. The interaction of the biological tissues

[1]This chapter is based on the paper "Aydinalp, C., Joof, S.,Dilman, I., Akduman, I. and Yilmaz, T. 2022. Characterization of open-ended coaxial probe sensing depth with respect to aperture size for dielectric property measurement of heterogeneous tissues, Sensors, 22, 760"

with the electromagnetic fields can be determined based on its DPs [80,81]. Therefore, tissue types or anomalies can theoretically be identified by analyzing the interaction between the field and tissue. Based on this principle, DP characterization of both healthy and diseased tissues have been a research interest for scientists primarily to enable the development of microwave diagnostic and therapeutic applications [22,61]. The DPs of many different tissue types including but not limited to breast, liver, and skin were characterized with the open-ended coaxial probe (OECP) for cancer diagnosis and treatment [22,52,53,82,83].

Accurate characterization of DPs is of importance for proper design and evaluation of microwave diagnostic and treatment modalities. The most common form of measurement technique for biological tissue DPs is the OECP due to its minimum requirements for sample preparation, broadband measurement capabilities, ease of use, and many other advantages. Despite the listed benefits, the OECP method suffers from high measurement inaccuracies stemming from the nature of the sample under test (SUT) or from equipment failure [42]. Tissue-related errors mainly emerge from the complex nature of biological tissue in some cases the heterogeneity, surface type, and size of the SUT. In others, state of the SUT such as ex vivo and in vivo, inconsistent tissue temperatures during the experiment and probe-tissue interaction such as the contact or pressure between probe tip and tissue can effect the accuracy. Equipment-related errors is primarily associated with the following measurement malpractices including choice of probe with an incompatible sensing depth (SD) to the tissue type, use of low quality connector or RF cable between the Vector Network Analyzer (VNA) and the probe, increase of noise levels by setting an high intermediate frequency (IF) filter bandwidth on the VNA. Part of the equipment-related errors can be minimized via system calibration. To this end, the appropriate equipment selection, especially proper probe selection with proper SD, is vital for accurate DP characterization of the SUT. Studies on probe SD with a variety of probe aperture sizes have been reported with diverse settings under different terminologies [62,63,83–86]. In [63], two probes with different aperture sizes (2.2 and 3.58 mm-diameters) were compared for accurate DP characterization of breast tissues. Reported study in [63] were conducted using pure alcohols and de-ionized water in order to identify sensing volume of two probes. It was concluded that the required sample thickness for 2.2 and

3.58 mm-diameter probes were 0.75 to 1.5 mm and 1.25 to 3.0 mm for de-ionized water and alcohol, respectively. In [62], effective penetration depth of 18 and 21 mm-diameter probes were compared. The reported effective penetration depth of 18 and 21 mm-diameter probes were 1.84 and 2.75 mm, respectively. Another comparison study for 2.2, 9.5, and 19 mm-diameter probes was performed by [84] and the results showed that the sensing radius of the probes expands linearly with the inner radius of the outer conductor. It was also determined that the effect of inner conductor on sensing radius was higher than the insulator. In [84], the results indicated that the sensing radius for 2.2, 9.5 and 19 mm-diameter probes were 1.4, 1.5, and 2.25 mm, respectively. Furthermore, in the same study, neural network model was presented to predict the sensing radius based on aperture size of these three probes. In [83], the DP measurements of human epidermis (palm and wrist) were performed with 3 and 1 mm-diameter probes. It was concluded that the thickness of the samples should be more than 1 and 3 mm for the 1 and 3 mm-diameter probes, respectively. In another study by the authors [85], the SD of the 2.2 mm-diameter probe was investigated using two double-layered configurations mimicking the skin tissue heterogeneity. The SD was determined based on three thresholds in percent increase of measured DPs. Obtained results suggested that the DP contrast between the two layers affects the SD. That is, high contrast causes a rapid change, while low contrast causes a slower change in the measured DPs. In yet another study by the authors [86], the SD of 2.2 mm-diameter probe with double-layered configurations using ex vivo rat breast and skin tissues were characterized. It was concluded that any membrane layer with 0.4 to 0.8 mm thickness on the SUT can potentially impact the DP measurement results by 52% to 84%.

Despite the many studies that have attempted to characterize the SD of the OECP with respect to different definitions—that is, radius, tissue and frequency—there is still a need to define the SD of probes with small aperture radii. The use of an appropriate probe dimension is of importance for the accurate DP measurement of thin multilayered-tissues such as skin tissue. This approach can potentially eliminate equipment and tissue -related errors. Therefore, the aim of this work is to investigate the SDs of OECPs with small aperture radii in order to achieve the following:

- To define the SDs of OECPs with small radii to enable the selection of appropriate probes during the DP characterization of highly heterogeneous, skin-like tissues composed of multiple thin layers;
- To form an SD definition via the examination of the three different percentage change thresholds in retrieved/measured DPs for different probe dimensions;
- To investigate the significance of tissue layers located immediately at the probe aperture during SD characterization—e.g., how thin and high DP contrast layers positioned on top of the tissue affect the probe SD.

Towards this end, an experiment was designed to analyze SD of the 2.2 mm-diameter probe with a double-layered sample. The double-layered configuration consists of skin tissue and olive oil as the first and second layers, respectively. Three probes with different aperture sizes (2.2, 0.9 and 0.5 mm outer diameters) were simulated using Ansys HFSS 2020 R2 software (Customer Number: 316232, Canonsburg, PA, USA) using a similar double-layered configuration to mimic a heterogeneous multilayered sample. Next, the SD of each probe was characterized with based on both simulation and experimental result.

The remainder of this paper is organized as follows: In Section 5.2, the simulations and experiments are described in detail. Section 5.3 shows experiment results obtained by the 2.2 mm-diameter probe based on 5%, 20% and 80% increase in measured DP of olive oil from 0.5 to 8 GHz frequency range. Similar method is applied to simulated response of 2.2, 0.9 and 0.5 mm-diameter probes. In Section 5.4, the SD analysis are presented based on probe's aperture and finally the conclusions are drawn in Section 5.5.

5.2 Materials and Methods

In this section, the simulations and experimental setup are explained in detail. Simulations with three probes along with DP retrieval from S-parameter response via in-house algorithm are given in Section 5.2.1. The double-layered sample configuration and the measurement protocol are described in Section 5.2.2.

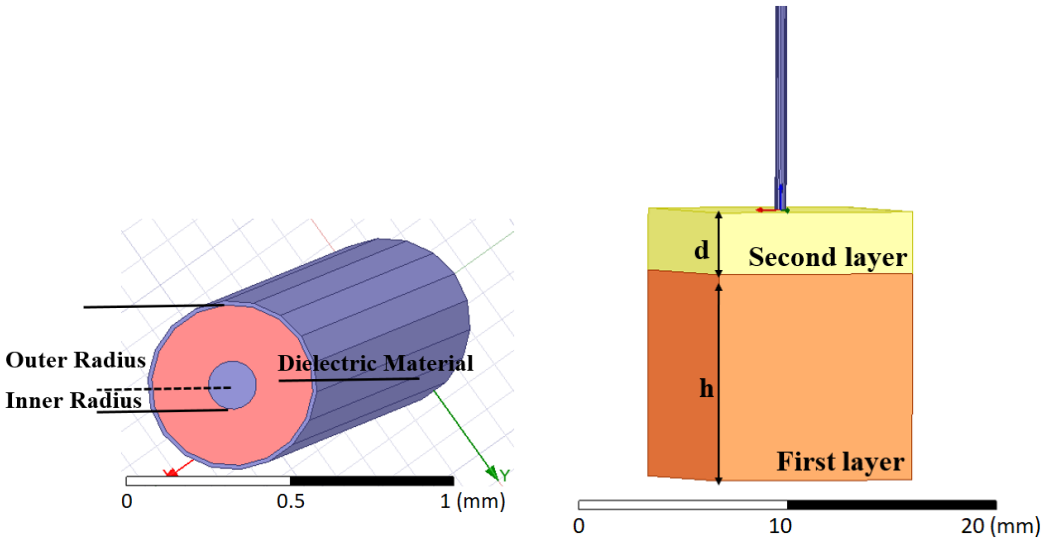

(a) **(b)**

Figure 5.1 : Simulated open-ended coaxial probe and configuration of double-layered sample. (a) Open-ended coaxial probe (OECP). (b) Double-layered sample with the first layer being skin tissue with d_1 thickness and the second layer is the olive oil with d_2 thickness.

5.2.1 Simulation configuration

The OECPs with three different aperture sizes and terminated with double-layered configurations were simulated with Ansys HFSS, 3D electromagnetic (EM) software (Canonsburg, PA, USA). As shown in Figure 5.1a, the OECPs were composed of two conductors with a dielectric material sandwiched in between. A commonly used dielectric material PTFE (ε_r=2.1) was implemented in the simulations of the probe. Since the desired outer radius of probes were known, inner radius were calculated to fix the probe input impedance to 50Ω. The length of probes were assigned as 40 mm in order to optimize computing process. The final dimensions of the probes are listed in Table 5.1. S-parameters of all probes were simulated with double-layered configuration composed of skin and olive oil. The dielectric properties of the materials used for the double-layered configuration at 4 GHz are given in Table 5.2. The effects of probes aperture size was analyzed by changing the second layer thickness *d* as illustrated in Figure 5.1b.

The simulations were performed from 0.5 to 20 GHz with 0.25 GHz increments. To adjust the distance between the probe tip and first layer, the thickness of the second

Table 5.1 : Simulated probe dimensions with different aperture sizes.

Outer Radius (mm)	Inner Radius (mm)	Dielectric Type	ε_r
0.25	0.075		
0.45	0.134	PTFE	2.1
1.1	0.328		

Table 5.2 : The relative permittivity and conductivity of skin and olive oil used to compose the double-layered configurations at 4 GHz for simulations.

Layers	Materials	Relative Permittivity (ε_r)	Conductivity (S/m)
First layer [87]	Skin	32.89	2.29
Second Layer [71]	Olive oil	3.00	0.04

layer (d), shown in Figure 4.1b, was varied. The second layer thickness d was selected in three different ranges: 0.01-1 mm with 0.05 mm increments, 1-3 mm with 0.2 mm increments and 3-5 mm with 1 mm increments.These step sizes and ranges were selected to reduce simulation time and to provide the thicknesses in which essential changes in dielectric properties occur. These ranges and increments were not linearly or logarithmically determined. It should be noted that, while the thickness of the second layer determined the distance between probe aperture and the first layer in the simulations, the probe is immersed to the second layer to adjust the distance between aperture and the first layer during measurements. Finally, to retrieve complex dielectric properties from S-parameters obtained from simulation, Debye relaxation model parameters were iteratively computed with the in-house algorithm described in [85].

5.2.2 Experiment setup

All DP measurements reported in this work were performed with the Agilent N5230A PNA-L Series Network Analyzer (Santa Clara, CA, USA) and commercial Agilent slim form probe kit (Santa Clara, CA, USA) using the 85070E DP measurement software. The experiment setup is shown in Figure 5.2. Before the measurements were performed, the system was calibrated based on the software's three step standard calibration procedure; that is, open circuit, short circuit and de-ionized water measurement, respectively.

During the measurements, an adjustable stand and a digital caliper (Mitutoyo absolute digimatic caliper 0–150 mm with 0.01 mm digital step size) were used to adjust and record the position of the double-layered samples. In the experimental setup, the

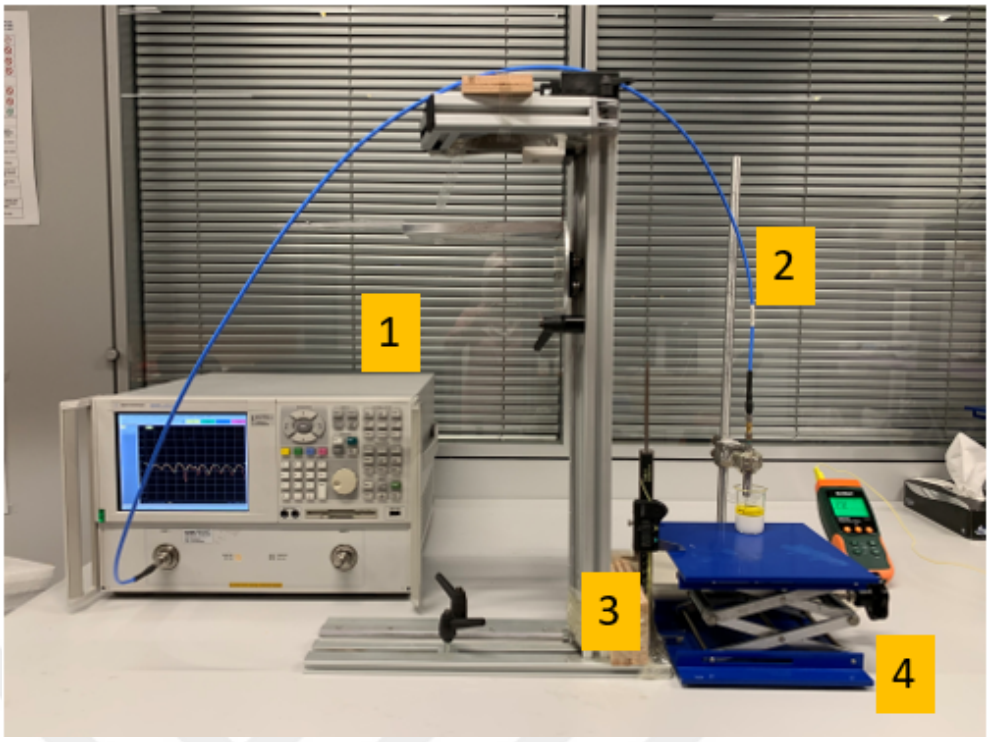

Figure 5.2 : Experimental setup: (1) Agilent N5230A PNA-L Series Network Analyzer, (2) Agilent Slim Form Probe (2.2 mm-diameter aperture size), (3) digital caliper and (4) an adjustable stand.

position of caliper and probe were firmly fixed in order to minimize the error caused by any movement. It should be noted that the VNA was turned on 4 hours before the measurements in order to minimize error due to drift in VNA measurements.

5.2.3 Measurement samples and protocol

The SD analysis was performed with the double-layered sample consisting of a skin-mimicking phantom and olive oil. The measured dielectric properties of the pure layers are listed in Table 5.3. Characterization of the skin mimicking phantom, used as the bottom (first) layer in the measurement sample along with phantom recipe, is described in [66]. Once the phantom was formed and placed in the measurement beaker, it was kept at room temperature (24$\pm$2°C) for five days until it was solidified. Next, the double-layered configuration, shown in Figure 5.2, was formed by adding the olive oil as the upper (second) layer. Olive oil is a liquid with low dielectric properties that can provide a realistic contrast in dielectric properties when used as a mimicking layer to represent the effect of the keratin layer on the skin. Due to its high viscosity and non-solvent properties, it was possible for us to form two separate layers using the olive oil and phantom while preventing the mixing on the boundary of two materials.

Table 5.3 : The relative permittivity and conductivity of skin and olive-oil in double-layered configuration for sensing depth (SD) experiment at 4 GHz.

Materials	Relative Permittivity (ε_r)	Conductivity (S/m)
Skin	34.17	4.00
Olive oil	2.67	0.02

Additionally, olive oil is transparent, which allowed us to clearly inspect the movement of the probe inside the layer by eye. During dielectric property measurements, the steps given in [85] was followed.

5.3 Results

In this section, the SD of all 3 probes with 0.5, 0.9 and 2.2 mm-diameter aperture sizes were determined. The axial electric field magnitude obtained from simulations using three probes with different apertures and double-layered configuration are given in this section. Furthermore, the analysis were conducted with the relative permittivity obtained from simulation and experiment results by selecting various frequency points. The percent change in the relative permittivity of the double-layered configuration were examined at each frequency point with respect to the second layer thickness below the probe tip (d).

5.3.1 Electric field distribution

To understand the field behaviour around different probe aperture tips with different sample types, simulated axial electric field magnitudes at 2 GHz are shown in Figure 5.3. Figure 5.3a, Figure 5.3d, Figure 5.3g and Figure 5.3j represent the analysis of the 0.5 mm-diameter probe with bare skin tissue layer, with only olive oil layer, double-layered configuration with 0.3 mm olive oil layer and double-layered configuration with 3 mm olive oil layer, respectively. Similar analysis are presented in Figure 5.3b, Figure 5.3e, Figure 5.3h and Figure 5.3k for the 0.9 mm-diameter probe and Figure 5.3c, Figure 5.3f, Figure 5.3i and Fig 5.3l for the 2.2 mm-diameter probe. The simulation results indicate that electric field distribution on the single layer configurations differed from the double-layered configurations.

The field distribution was approximately 70 dB around the three different probe tips, and the magnitude of field gradually decreased to 10 dB at distant points from the probe tip. As seen in Figure 5.3g, when the thickness of the olive oil layer was equal

to 0.3 mm, the electric field distribution in both layers (olive oil and skin tissue) was found to be around 70 dB for the 0.5 mm-diameter probe. However, when the thickness of the olive oil layer was increased to 3 mm, the electric field distribution on the skin layer decreased to 10 dB as shown in Figure 5.3j. Using the same double-layered sample the thickness of olive oil layer was set to 3 mm, the simulation results for the 0.9 mm-diameter probe indicate that the field distribution on the skin layer fluctuates between 10-18 dB as seen in Figure 5.3k. Lastly, the simulation results for the 2.2 mm-diameter probe when the thickness of olive oil layer was set to 3mm show that the field distribution on the skin layer changes between 10-30 dB as depicted in Figure 5.3l. The maximum electric field distribution at the skin tissue layer for each probe with double-layered configuration were 10, 18 and 30 dB for the 0.5, 0.9 and the 2.2 mm-diameter probes, respectively. Having higher value of electric field distribution at deeper position is one of the factors affecting SD. Based on these results, the electric field distribution of the 2.2 mm-diameter probe at a distant point from the aperture is higher when compared to the electric field strength of the 0.9 and 0.5 mm-diameter probes indicating that the SD of the 2.2 mm probe is larger.

5.3.2 2.2 mm-diameter probe simulation and experimental results

Analysis of the 2.2 mm-diameter probe through simulation results were performed via evaluating the retrieved relative permittivity based on three threshold values 5%, 20% and 80% with respect to the change in thickness of the second layer (distances from the first layer (d)). The percent changes and corresponding distances from the first layer (d) at five frequency points 0.5, 2, 4, 10 and 20 GHz are given in Table 5.4.

Obtained results for the five frequency points indicate that the retrieved relative permittivity of olive oil increased by 5%, 20%, and 80% between 0.66 mm to 1 mm, 0.36 to 0.86 mm, and 0.16 to 0.36 mm thicknesses, respectively.

To investigate the SD of the probe experimentally, 5 frequency points were chosen between 0.5 and 8 GHz. Similar to the simulations, three percent increases (5%, 20% and 80%) in the measured relative permittivity with respect to the dielectric properties of pure olive oil (ε_r= 2.67 at 4 GHz) were recorded. As shown in Table 5.5, 5% increase in relative permittivity of olive oil was observed at 0.81 mm for the five frequency points. By moving the adjustable stand upwards, the thickness of second layer (olive

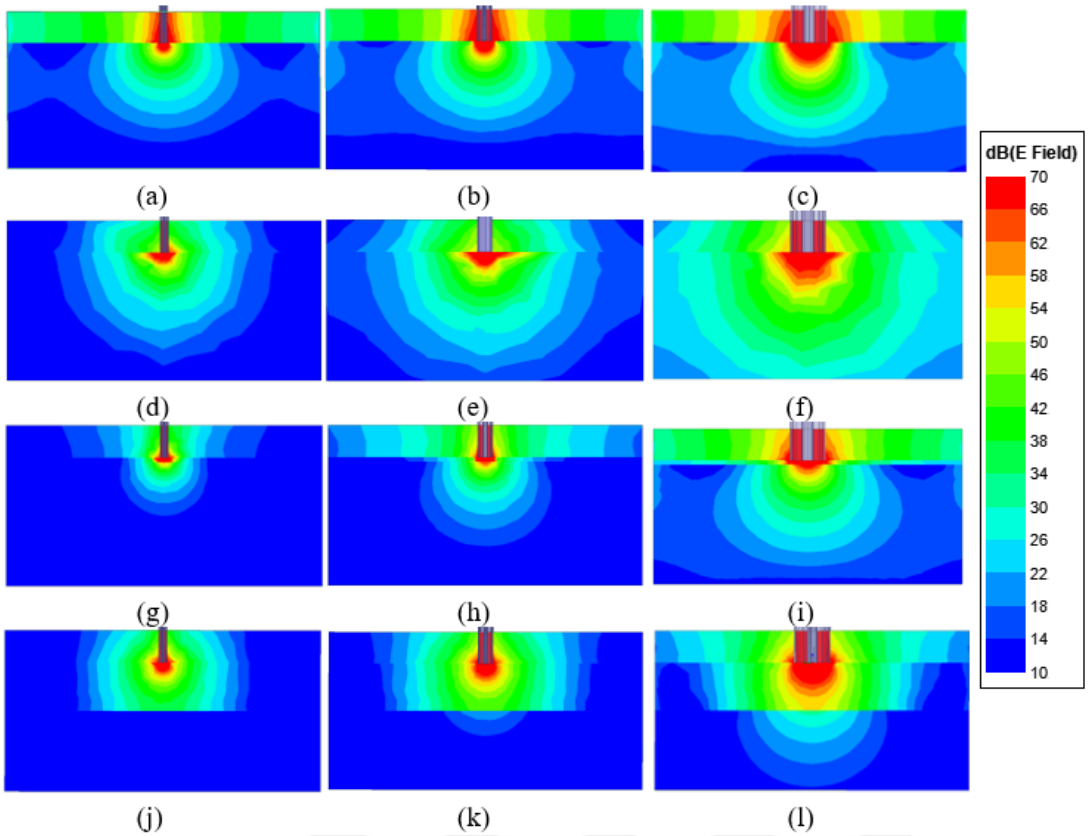

Figure 5.3 : The electric field strength when 0.5 , 0.9 and 2.2 mm-diameter probes placed against single layer: (a)-(c) skin tissue layer, (d)-(f) olive oil layer, and double layer configurations: (g)-(i) olive oil layer with thickness of 0.3 mm and (j)-(l) olive oil layer with thickness of 3 mm.

Table 5.4 : Retrieved relative permittivity change of skin-olive oil double-layered configurations with 2.2 mm-diameter probe at 0.5, 2, 4, 10 and 20 GHz frequency points.

Frequency	Thickness for 5% increase	Thickness for 20% increase	Thickness for 80% increase
0.5	1	0.86	0.36
2	0.76	0.56	0.26
4	0.71	0.46	0.21
10	0.66	0.41	0.21
20	0.66	0.36	0.16

oil) was decreased and the measured relative permittivity increased by 20% at 0.67 mm. Additionally, 80% increase in measured relative permittivity was obtained when the thickness of the second layer was between 0.20 and 0.22 mm.

The simulation results given in in Table 5.4 indicate that the frequency has an impact on the SD represented by the percent increase in relative permittivity according to the thickness of the second layer. However, a similar effect on SD with respect to

Table 5.5 : Measured relative permittivity change of skin-olive oil double-layered configurations with 2.2 mm-diameter probe at 0.5, 2, 4, 6 and 8 GHz frequency points.

Frequency	Thickness for 5% increase	Thickness for 20% increase	Thickness for 80% increase
0.5	0.81	0.67	0.22
2	0.81	0.67	0.22
4	0.81	0.67	0.22
6	0.81	0.67	0.20
8	0.81	0.67	0.22

thicknesses could not be detected in the experimental results due to the limitation of the frequency range (0.5–8 GHz). In order to prevent the cable loss and due to equipment limitations, the frequency was limited to the indicated band. The power level of signals was set to 0 dBm. Regarding the noise reduction during measurements, with the IF bandwidth set to 10 Hz, the noise level was significantly reduced and the sweep time was 18 s. Each measurement was acquired after five sweeps, which is 18×5 s. It should be noted that under experimental conditions it is expected that the measurement sensitivity will be diminished and it will be heightened during DP calculation. Thus, it can be stated that the disagreement could be due to noise during measurements. In [62, 64], the sensing depth was investigated based on the frequency. In [62], based on the simulation results, it was concluded that frequency-dependence occurs above 6 GHz and [64] stated that frequency-dependence can be discussed based on the materials characteristics by analyzing experimental results. In addition, the results obtained from our simulation show the critical changes observed from 0.5 to 4 GHz are 0.82, 0.62 and 0.27 mm for 5%, 20% and 80% increases in relative permittivity, respectively. Similarly, we acquired approximately the same thicknesses in the experiment results for 5%, 20% and 80% increases at the same frequency points.

5.3.3 0.9 mm-diameter probe simulation results

A second set of simulations were performed with the 0.9 mm-diameter probe. The sensing depth analysis were carried out for 0.5, 2, 4, 10 and 20 GHz frequency points. In Table 5.6, the thicknesses (d) are listed when the change in the retrieved relative permittivity of second layer reached 5%, 20% and 80% increase at the five frequency points.

Table 5.6 : Retrieved relative permittivity change of skin-olive oil double-layered configurations with 0.9 mm-diameter probe at 0.5, 2, 4, 10 and 20 GHz frequency points.

Frequency	Thickness for 5% increase	Thickness for 20% increase	Thickness for 80% increase
0.5	0.66	0.21	0.11
2	0.56	0.26	0.11
4	0.56	0.21	0.11
10	0.56	0.21	0.11
20	0.51	0.21	0.06

Table 5.7 : Retrieved relative permittivity change of skin-olive oil double-layered configurations with 0.5 mm-diameter probe at 0.5, 2, 4, 10 and 20 GHz frequency points.

Frequency	Thickness for 5% increase	Thickness for 20% increase	Thickness for 80% increase
0.5	0.31	0.11	0.06
2	0.31	0.16	0.06
4	0.31	0.11	0.06
10	0.31	0.11	0.06
20	0.31	0.11	0.06

It was observed that, the retrieved relative permittivity with the 0.9 mm-diameter probe increased 5%, 20%, and 80% between 0.51 to 0.66 mm, 0.21 to 0.26 mm, 0.06 to 0.11 mm distances, respectively at five frequency points.

5.3.4 0.5 mm-diameter probe simulation results

The final set of simulations were performed with 0.5 mm-diameter probe. In Table 5.7 the thicknesses where the change in retrieved relative permittivity of second layer reached 5%, 20% and 80% increases with 0.5 mm-diameter probe are listed at five frequency points. As seen from the Table 5.7, the retrieved relative permittivity of olive oil increased 5%, 20%, and 80% at 0.31, 0.11, and 0.06 mm distances, respectively.

5.4 Discussion

SD analysis based on the OECP's aperture size is important for choosing an appropriate probe to minimize tissue and equipment-related errors. In this context, several studies have been presented in the literature. Comparison of previously reported work on OECP SD is given in Table 5.8. The results (Depth (mm)) given in the table is

based on the definition or terminology used. Also, the type of data acquisition method (experiment (Exp.) and simulation (Sim.)), the size of the probe aperture (Aper. Size (mm)), the type of sample configuration (Sam. Config.) and the relative permittivity of the samples (Sample's ε') are also given in Table 5.8. In the literature, aperture sizes larger than 1 mm was investigated. In this study, the sensing depth of three different probe apertures are compared to assist in the equipment and tissue-oriented design of the experimental setup. To this end, 0.5, 0.9 and 2.2 mm-diameter probe and a double-layered material to represent tissue heterogeneity are designed using HFSS simulation software. Furthermore, the commercially available 2.2 mm-diameter probe was utilized to validate simulation results.

The proposed double-layered skin-olive oil sample was designed and simulated with the 0.5, 0.9 and 2.2 mm-diameter probes. The retrieved relative permittivity and conductivity from the simulation results as a function of the second layer thickness d are shown in Figure 5.4. When the thickness d on the graph is equal to 0, it refers to the probe tip being terminated by the first layer. Even though the SD was examined from 0 to 5 mm thicknesses of the second layer, the (thickness) axes in Figure 5.4 were plotted from 0 to 1.2 mm to clearly depict the graph. This is due to the rapid changes in dielectric properties at smaller thicknesses. In order to plot and demonstrate the rapid DP changes for SD analysis, critical thickness values (0, 0.01–1 mm with 0.05 mm increments and 1.2 mm) were selected for the thickness axes. Therefore, the thickness axes in Figure 5.4 are not linearly or logarithmically plotted. For the 0.5 mm-diameter probe, a retrieved DP approximately close to that of olive oil was reached when the thickness of the second layer was 0.31 mm. However, at the same thickness (d = 0.31 mm), the DP value acquired via the 2.2 mm diameter probe was 80% higher than the value of olive oil. Therefore, it can be inferred that at the same thickness, the probe with a bigger aperture size can sense the first layer (skin tissue); thus, a probe with a larger aperture size is expected to have a larger SD.

In [83], two different probes with 1 and 3 mm-diameter aperture sizes were used to define the proper thickness of the sample that does not affect the measurement of relative permittivity. Double-layered sample configuration including porcine muscle as the bottom layer and porcine fat as the upper layer were utilized. The proper thickness for the porcine fat layer was determined as 1 and 3mm for the 1 and 3 mm- diameter

probe, respectively. The study defined the term proper thickness for a double-layered biological tissue and their results indicated that the Probe aperture size is proportional to the SD.

In [63], the sensing depth from the simulation and experiment results of the 2.2 and 3.58 mm-diameter probes for glass-ethanol, glass-methanol, and glass-deionized water (d.water) double-layered configurations was presented. Higher SD values for the probe with the larger aperture size from both the simulation and experiment results irrespective of the sample configuration were obtained. Furthermore, $\pm 10\%$ was chosen as the acceptable level of error in the real and imaginary parts of the complex permittivity.

In [62], from the simulation results, the effective penetration depth (20% reduction from expected dielectric property value) was found to be 0.158, 0.483 and 0.866 mm for the 1.19, 3.58 and 6.35 mm-diameter probes, respectively. The obtained 20% change in relative permittivity from our simulation results for the 0.5, 0.9 and 2.2 mm probes was 0.11, 0.21, 0.46 mm, respectively. The effective penetration depth obtained in [62] is higher than sensing depth in our work for the same percentage change in relative permittivity. This difference is related to the different probe dimensions (inner and outer conductor diameters) used in the simulations. Even though different values were obtained from both work, the results still indicate that the sensing depth/effective penetration depth increases as the probe aperture size increases.

For this work, the thicknesses of three different levels of percentage increase for retrieved relative permittivity of skin-olive oil double-layered configurations at 4 GHz with three different probes was presented and listed in Table 5.9. According to the results, the increase in retrieved dielectric properties from 5% to 80% was slower for the 2.2 mm-diameter probe. Based on these results, the 2.2 mm-diameter probe is more sensitive to the dielectric property of the skin phantom layer below the olive oil phantom layer.

These findings suggest that sensing depth is dependent on the probe aperture; that is, the SD increases with the increase in probe aperture for such a configuration. Lastly, to analyze the critical variation of the dielectric property, the thickness of the olive oil layer was set to $d_1 = 0.01$, $d_2 = 0.06$ and $d_3 = 0.11$ and simulated with the three

Table 5.8 : List of literature studies on different aperture sizes, sample configurations and different terminologies to define the sensing depth of the OECP.

Ref.	Definition	Type	Aper. Size (mm)	Sam. Config.	Sample's ε'	Depth (mm)
[83]	"Proper thickness of target-sample" is thickness the target sample where the influence of non-targeted region is no longer sensed by the probe.	Exp.	1.0	porcine muscle-porcine fat	Porcine muscle ε'=∼52 porcine fat ε'=∼8 at 0.5 GHz.	1.0
			3.0			3.0
[63]	"Sensing volume" was defined by monitoring the changes in the S_{11} between ± 0.5-± 1.0 error which is ± 10% error in terms of the ε' and ε''.	Sim.	2.2	Glass-ethanol	Glass ε'=4.82, ethanol ε'=9.6, methanol ε'=24.2, d.water ε'=79.2 at 3 GHz. Below the glass beaker, there is epoxy stand ε'=4.0 at 5 GHz.	0.5-1.0
				Glass-methanol		1.0-1.5
				Glass-d.water		1.25-1.5
			3.58	Glass-ethanol		1.0-1.5
				Glass-methanol		∼1.75
				Glass-d.water		∼2.5
		Exp.	2.2	Glass-ethanol		0.75-1.0
				Glass-methanol		1.0-1.5
				Glass-d.water		∼1.5
			3.58	Glass-ethanol		1.25-1.5
				Glass-methanol		∼2.25
				Glass-d.water		∼2.5-3.0
[62]	"Effective penetration depth" was defined as when 20% error is observed between the measured and expected linearly changing ε'.	Sim	1.19	Acrylic-0.9% saline	Acrylic ε'=3.0 0.9% saline ε'=78.1 d.water ε'=78.8 at 2 GHz.	0.158
			3.58			0.483
			6.35			0.866
		Exp.	18.0	Acrylic-d.water		1.84
			21.0			2.74
			2.16	Teflon-d.water	Teflon ε'=2.1 d.water ε'=78.8 at 2 GHz.	0.28
This work	"Sensing depth" is defined as when 5% change in the targeted ε' is observed.	Sim.	2.2	Skin tissue-olive oil	Skin tissue ε'=32.89, olive oil ε'=3.0 at 4 GHz	0.71
			0.9			0.56
			0.5			0.31
		Exp.	2.2	Skin-mimicking phantom-olive oil	Skin-mimicking phantom ε'=34.7, olive oil ε'=2.67 at 4 GHz	0.81

different probes. The results of the dielectric properties obtained from the simulations at the given olive oil thicknesses are plotted with respect to frequency in Figure 5.5. Additionally, the dielectric property results based on the olive oil thickness and probe apertures are listed in Table 5.10. As seen from the table, the dielectric properties of first layer (skin) have greater effect on the double-layered results performed with the 2.2 mm-diameter probe.

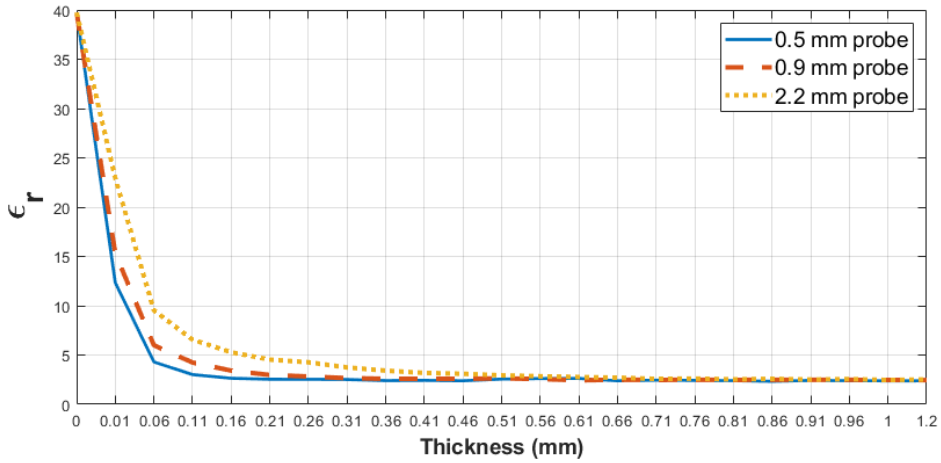

(a)

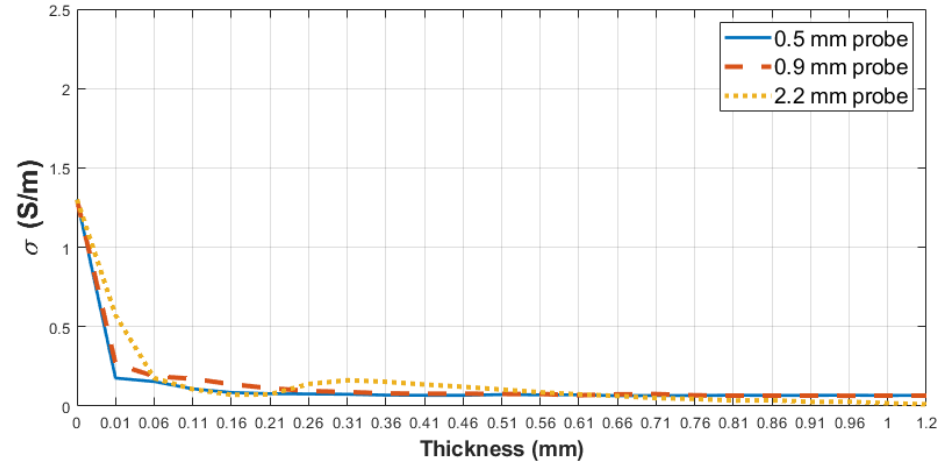

(a)

Figure 5.4 : Retrieved dielectric property changes obtained from the simulated skin-olive oil phantoms with 0.5, 0.9, and 2.2mm probes: (a) Retrieved relative permittivity change and (b) retrieved conductivity change as a function of second layer thickness *d* below the probe tips at 4 GHz.

As shown in Table 5.10, at 0.11 mm thickness of olive oil, the retrieved relative permittivities are 3.02, 4.24, and 6.56 for 0.5, 0.9, and 2.2 mm-diameter probes, respectively. Simulated results acquired by the 0.5 mm-diameter probe converged to the dielectric properties of olive oil at the smallest thickness under the same conditions.

Table 5.9 : Thickness of three different increase levels for retrieved relative permittivity of skin-olive oil double-layered configurations at 4 GHz with three different probes.

Probe aperture (mm)	Thickness for 5% increase	Thickness for 20% increase	Thickness for 80% increase
0.5	0.31	0.11	0.06
0.9	0.56	0.21	0.11
2.2	0.71	0.46	0.21

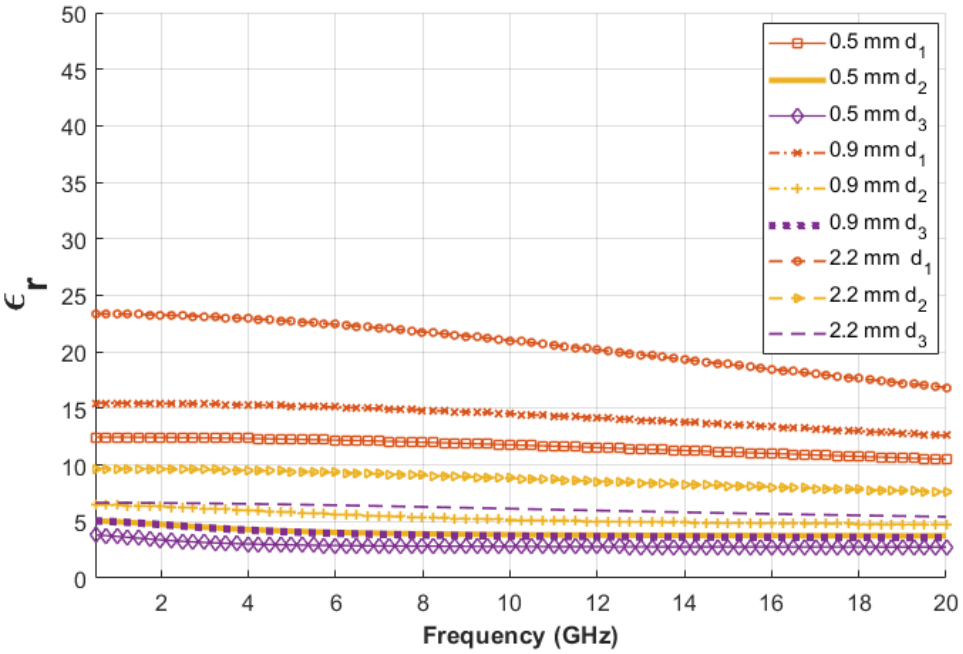

Figure 5.5 : The comparison of skin-olive oil retrieved relative permittivity through simulation of 0.5, 0.9 and 2.2 mm-diameter probes as a function of frequency when the second layer thicknesses (d_1, d_2 and d_3) are 0.01, 0.06 and 0.11 mm.

Table 5.10 : Three different thicknesses and retrieved relative permittivity of skin-olive oil double-layered configurations at 4 GHz with three probes.

Thickness (mm)	Relative Permittivity (ε_r)		
	0.5 mm Probe	0.9 mm Probe	2.2 mm Probe
0.01	12.34	15.32	22.95
0.06	4.29	5.98	9.52
0.11	3.02	4.24	6.56

5.5 Conclusion

The OECP method is superior to other dielectric property measurement techniques for dielectric property characterization of biological tissues due to its measurement simplicity. However, the method suffers from equipment- and tissue-related errors. Minimizing the effect of skin tissue heterogeneity and the sensing depth of the probe is an important amendment for classifying skin tissue anomalies and detection of skin cancer through dielectric property discrepancy. Therefore, there is a need to understand the effect of sensing depth in order to implement the appropriate probe for the application. Towards this end, the sensing depth of three different probe aperture sizes were compared in this work. Probes with 0.5, 0.9 and 2.2 mm-diameter were simulated with double-layered skin tissue and olive oil sample configuration. The experimental validation was performed with the 2.2 mm-diameter probe with the skin phantom and olive oil configuration. The obtained results show that the sensing depth is proportional to the probe aperture and smaller probe aperture can potentially aid in diminishing the heterogeneity of the tissue and allow accurate dielectric property characterization of thin skin tissue layers. As an example, 5% increase in retrieved relative permittivities were obtained at 0.31, 0.56 and 0.71 mm thicknesses for 0.5, 0.9 and 2.2 mm-diameter probes, respectively. Based on these results, we can state that using a 0.5 mm-diameter probe can provide more accurate results when a thin skin layer measurement is performed. However, the membrane or any tissue fluid that may be present on the tissue surface during measurement with a 0.5 mm-diameter probe may affect the measurement result more than expected. Therefore, measurement protocols should be established to prepare the measurement surface for tissues that consist of a multi-layered structure or that may have a membrane or any other layer on the measurement surface. Alternatively, tissue heterogeneity can be determined using probes with multiple aperture sizes.

6. MICROWAVE DIELECTRIC PROPERTY RETRIEVAL FROM OPEN-ENDED COAXIAL PROBE RESPONSE WITH DEEP LEARNING[1]

This work presents a technique for dielectric property retrieval through Debye parameter reconstruction from open-ended coaxial probe (OECP) response. Debye parameters were obtained with the application of a deep learning (DL) model to the reflection coefficient response of the OECP when terminated with a material under test. The OECP was modelled with the well-known admittance technique from 0.5 to 6 GHz with 20 MHz resolution. A dataset was generated using the admittance technique and obtained data was utilized to design the DL model. As part of the standard procedure, the dataset was separated to train, validate, and test parts by allocating the 80%, 10%, and 10% of the dataset to each section, respectively. Obtained percent relative error for Debye parameters were 1.86±3.01%, 3.33±9.52%, and 2.07±7.42% for ε_s, ε_∞ and τ, respectively. To further test the constructed DL model, OECP responses were measured at the same frequency band when it was terminated with five different standard liquids, four mixtures, and a gel-like material. Reconstructed Debye parameters from the DL model were used to retrieve the complex dielectric properties and obtained results were compared with the literature data. Obtained mean percent relative error was ranging from 1.21±0.06 to 10.89±0.08 within the frequency band of interest.

6.1 Introduction

Microwave dielectric properties (DP), also referred to as complex permittivity, are critical system design parameters for the development of microwave diagnostic, imaging, treatment devices, and RF/microwave circuits. Therefore, inaccurate determination of the complex permittivity can render information resulting in poor system reliability. Based on the nature of the sample and frequency of interest different techniques can be employed to measure the DP. One such widely utilized technique is

[1]This chapter is based on the paper "Aydinalp, C., Joof, S., Akinci, M. N., Akduman, I. and Yilmaz, T. 2021. Microwave Dielectric Property Retrieval from Open-Ended Coaxial Probe Response with Deep Learning, IEEE Access, vol. 10, pp. 1216-1227"

open-ended coaxial probe (OECP) method. The technique is used for the complex permittivity characterization of many different materials including but not limited to liquids, biological tissues, ice, and concrete [22, 39, 88–91]. Provided that the full contact between the material under test (MUT) and the probe aperture is ensured, the method does not require strict sample preparation procedures. Additionally, the OECP technique is capable of performing wideband measurements of the MUTs complex permittivity. While these advantages make the method a widely preferred tool for complex permittivity characterization, the OECP method is known to suffer from large measurement error. Commercially available probes report $\pm 5\%$ accuracy under ideal conditions [68]. It is reported that the measurement error can increase up to 30% [92]. Sources of error include but not limited to the mathematical approach, calibration degradation, sample heterogeneity. Since the DP are not measurable quantities, complex permittivities are derived from the other measurable quantities. Thus, the mathematical approach can be a major contributor to the measurement error. Addressing the mathematical approach can aid in the improvement of the measurement accuracy of the OECP technique.

In the OECP technique, reflected signals from the MUT are measured and converted to the complex permittivity. Different mathematical approaches have been implemented to retrieve the complex permittivity from measured reflection coefficients including the full-wave method and the equivalent circuit model [93, 94]. Full-wave analysis provides higher accuracy results for wideband but suffers from poor convergence and slow computing performances when processing large quantities of data. The equivalent circuit model provides faster computing; however, suffers from low accuracy and limited bandwidth [59, 95, 96].

In [69], an admittance model is proposed to mathematically represent the relationship between the MUT complex permittivity and the measured reflection coefficients at the probe aperture. Different solution approaches including the quasi-static approximation, Taylor Series approach, stochastic approach, and particle swarm optimization (PSO) were proposed in the literature to retrieve the complex permittivity from the admittance model [59, 91, 97–100]. While iterative solution techniques can converge under certain constraints, such as being valid until a certain probe diameter, heuristic approaches are likely to be stuck in a local minima. Moreover, these methods

have high computational complexity; for non-linear inverse estimation problems, they reach the solution either (i) in an iterative manner by means of linear or quadratic approximations of the problem at each step or (ii) solving the forward problem many times for each estimation. In contrast to these approaches, the deep neural network model proposed in this work offers a non-iterative and nonlinear solution of the inverse estimation problem by directly learning the non-linearity of the problem from the data generated with the admittance model [101]. Moreover, after the training phase, it needs only simple operations (summations, multiplications and activation function evaluations) and it does not require a solution of forward problem, which makes it easily adoptable in hardware. To this end, deep neural networks have been successfully employed in the literature for high dimensional microwave modelling, such as extracting the parameters of microwave filters [49]. Therefore, we believe that the deep neural networks can be utilized in similar nonlinear inverse problems in electromagnetic, to potentially improve the computation time and to reduce complexity of solution while enhancing the ease of implementation.

In this paper, we propose an alternative method to find Debye parameters which are used to represent the complex permittivity of materials for a wide frequency range. The Debye parameters are retrieved from the reflection coefficient of the probe through deep learning (DL) model designed by utilizing a synthetically generated dataset. The reflection coefficients were numerically calculated using the admittance model proposed in [69] and the designed DL model was then tested with the measurement data. Briefly, 276×17732 input dataset was generated corresponding to the 3×17732 output Debye parameters dataset. The scattering parameters of the probe were calculated between 0.5–6 GHz, with 20 MHz steps. The dataset was divided into three sections, 80% was used for training and 10% was used for validation. After the training procedure had ended, the remaining 10% of the dataset was used for testing. Obtained percent relative errors of the proposed model were $1.86\pm3.01\%$, $3.33\pm9.52\%$, $2.07\pm7.42\%$ for prediction of the Debye parameters ε_s (static dielectric permittivity), ε_∞ (dielectric permittivity at high frequencies), and τ (relaxation time constant), respectively. Finally, the trained deep learning model was tested with measurement data and it was found that the retrieved complex dielectric parameters had a percent mean relative error of approximately less than 10%.

In the literature, an artificial neural network model is proposed in [102] to compute the complex permittivity from the measured reflection coefficients for biomedical applications. In the proposed study [102], 102 experiment samples including standard liquids and biological tissues were measured in order to train, validate and test the neural network model. Prediction accuracy of $\pm 5\%$ was obtained for the complex permittivity. The study in [102] was limited with collected data from the experiments; therefore, the predictions of the trained neural network model was restricted. Composing a large dataset through measurements that include different materials, frequencies, and probes is labor intensive and costly. To the best of authors' knowledge, this work presents the first large scale study performed by designing a deep learning model using numerically generated data. Also, this work proposes to retrieve the Debye parameters from the reflection coefficient response of the OECP. The contributions of the paper and the added advantages are as follows:

1. One main contribution of this work is generation of dataset for training the deep neural network, which estimates the Debye parameters. In particular, unlike to [102], the input and output dataset was not measured but synthetically generated by means of a calibration procedure. Designing such procedures is an important topic for inverse electromagnetic estimation problems [103], since it produces large amount of data required to train the deep learning model. Therefore, a more robust model is built in this work since a wide range of Debye parameters and reflection coefficients can be conveniently generated.

2. Since the probe is theoretically modelled, the proposed method provides design flexibility and ability to generate dataset for any desired probe with different dimensions.

3. Generating synthetic data shortens the time required for the collection of training data. For example, 276×17732 input dataset mentioned above was generated approximately in 50 mins on a computer with 192 GB RAM, $2\times$ Intel(R) Xeon(R) X5690 3.47 GHz CPU. Furthermore, due to the features of deep neural networks, very large datasets can be easily trained using high-performance computing platforms such as GPUs.

4. Synthetic training approach proposed here is also flexible in data type and data production method. For instance, the dielectric permittivity model can be changed (Cole-Cole, Debye or multipole Debye) simply by using the target model for complex permittivity calculation or the simulation method can be different (instead of using the admittance model [69], numerical electromagnetic software such as HFSS or CST can be employed).

5. Different from the verification of previously proposed dielectric retrieval methods, which is usually performed by measuring few standard liquids, this work presents a statistical verification of the DL-based dielectric property retrieval technique both with synthetically generated and measured data.

The remainder of this paper is organized as follows: Section 6.2.1 presents the admittance model. Process for synthetic dataset generation is explained in section 6.2.2. Measurement procedure and the experimental setup are given in section 6.2.3. The design of the deep learning model is presented in section 6.2.4. Results are given in section 6.3 and conclusions are drawn in section 6.4.

6.2 Material and Methods

In the following section, we first present the theoretical background for retrieving the Debye parameters from the reflection coefficient using the OECP and admittance model. Second, based on the theoretical model, the dataset was generated to train, validate, and test the deep learning model. Furthermore, to test the deep learning model with measurement data, experiments were conducted to acquire the reflection coefficients of standard liquids, mixtures, and a gel-like material. Finally, the design process for the deep learning model to retrieve the Debye parameters from the reflection coefficient is given in detail.

6.2.1 Admittance model for the open-ended coaxial probe

The configuration of the OECP consists of two concentric cylindrical conductors with a dielectric material placed between the conductors. When the OECP is utilized to obtain the dielectric properties of a MUT, the relation between the complex permittivity of MUT and the admittance of the probe is given by the classical admittance model as

shown below in (6.1) [69]:

$$\frac{Y(\varepsilon)}{Y_0} = \frac{ik_0^2\varepsilon_c}{k_d \ln(b/a)} \int_0^\infty \frac{[J_0(\zeta a) - J_0(\zeta b)]^2}{\zeta\sqrt{\zeta^2 - k_0^2\varepsilon_c}} d\zeta \tag{6.1}$$

where $Y(\varepsilon)$ represents admittance of the probe when terminated with MUT, Y_0 is the probe characteristic admittance, a and b represent the inner and outer radius of the conductors, respectively. $J_0(\cdot)$ is the first order Bessel function, k_d denotes the wave number of the dielectric material (between conductors) and k_0 represents the free space wave number. ε_c is the complex dielectric permittivity of the MUT which can be expressed in terms of Debye parameters:

$$\varepsilon_c(\omega) = \varepsilon_\infty + \frac{\varepsilon_s - \varepsilon_\infty}{1 + i\omega\tau} \tag{6.2}$$

where ω represents the angular frequency, ε_s is the static constant, ε_∞ is the infinite frequency dielectric constant and τ is the characteristic relaxation time. Debye equation (6.2) can be used for generating the complex dielectric constant. The admittance of the probe can then be derived from admittance model (6.1). As result of the impedance difference between the reference medium and the MUT, the reflection coefficient Γ at the probe's aperture can be expressed in terms of the ratio between the admittance of the MUT $Y(\varepsilon)$ and the probe characteristic admittance Y_0:

$$\frac{Y(\varepsilon)}{Y_0} = \frac{1+\Gamma}{1-\Gamma} \tag{6.3}$$

From (6.3) corresponding reflection coefficient can be derived. However, it should be noted that this represents the calculated reflection coefficient and does not correspond to a measured reflection coefficient. For a measured reflection coefficient, there is a need to adjust the reference plane of measurement through calibration in order to utilize (6.3) for measurements. Therefore, a calibration procedure is required to acquire the reflection coefficient (Γ_c) at the probe's aperture. Please note that Γ_c will be used to denote the calibrated reflection coefficient throughout this paper. Suppose, ρ represents the reflection coefficient obtained from the MUT and ρ_1, ρ_2, ρ_3 are the reflection coefficients corresponding to three known material terminations. The reflection coefficient at probe's aperture (Γ_c) can be obtained from the measured reflection coefficients ρ, ρ_i, $(i = 1,2,3)$ with the following expression:

$$\Gamma_c = \frac{\rho - S_{11}}{\rho S_{22} + S_{12}S_{21} - S_{11}S_{22}} \tag{6.4}$$

where S_{11}, S_{12}, S_{21} and S_{22} represent the unknown scattering parameters of the network [92], which can be evaluated with the subsequent equations:

$$S_{11} = \frac{\Gamma_1\Gamma_2\rho_3(\rho_1-\rho_2)+\Gamma_1\Gamma_3\rho_2(\rho_3-\rho_1)+\Gamma_2\Gamma_3\rho_1(\rho_2-\rho_3)}{\Gamma_1\Gamma_2(\rho_1-\rho_2)+\Gamma_1\Gamma_3(\rho_3-\rho_1)+\Gamma_2\Gamma_3(\rho_2-\rho_3)} \tag{6.5}$$

$$S_{12}S_{21} = \frac{(\rho_1-S_{11})(1-S_{22}\Gamma_1)}{\Gamma_1} \tag{6.6}$$

$$S_{22} = \frac{\Gamma_1(\rho_2-S_{11})+\Gamma_2(S_{11}-\rho_1)}{\Gamma_1\Gamma_2(\rho_2-\rho_1)} \tag{6.7}$$

where Γ_1, Γ_2, and Γ_3 are the calculated reflection coefficients of the known materials using (6.1) and (6.3). For a measurement from a MUT, once the scattering parameters are calculated from the given expressions above, (6.4) is used to calculate the reflection coefficient at the aperture.

6.2.2 Procedure for obtaining the deep learning dataset

In this section, the expected reflection coefficient (Γ) due to material's complex permittivities (ε_c) is calculated using the admittance model. To do so, Debye parameters corresponding to a wide range of complex permittivity values were systematically generated. Note that the Debye parameters are frequently used for mathematical modelling of frequency dispersive complex permittivity. The theoretical relation between the Debye parameters and reflection coefficient at the probe's aperture can be expressed using (6.1), (6.2) and (6.3). Using any given set of Debye parameters (ε_s, ε_∞, τ), the corresponding reflection coefficient (Γ) at the probe's aperture can be directly calculated. The following steps were implemented to generate the required dataset. First, Debye parameters were generated by varying ε_s from 5–120 units, ε_∞ from 1–10 units, τ from 20–180 ps with constant step size of $\frac{5}{\sqrt[3]{2}}$, $\frac{1}{\sqrt[3]{2}}$ and $\frac{4}{\sqrt[3]{2}}$, respectively. The step sizes were determined by trial and error. Note that the step size is a critical parameter for training the model. We ran several simulations by training and testing the initial network with multiple datasets generated by using different step sizes. If the Debye parameters are generated with smaller step sizes, the difference between the corresponding calculated reflection coefficients becomes minimal. The initial network cannot interpret these differences. Conversely, if the Debye parameters are generated with larger step sizes, the discrepancy between the calculated reflection

coefficients becomes too large and the number of generated data will not be adequate for training the network. Therefore, the step size is an important part of the dataset generation and it must be optimized using an initial network, when using the proposed approach. It should also be noted that in this trial and error process the point that we noticed is to divide the output space (the space spanned by $\varepsilon_s - \varepsilon_\infty - \tau$) into equal pieces as much as possible in all three parameters. Lastly, the limits of the Debye parameters were selected based on the widely used pure standard liquids presented in the literature and based on the frequency of interest in this work.

Next, generated Debye parameters were combined and a total of 17748 Debye parameter sets were obtained. Then, the complex dielectric properties were produced using Debye parameter sets. The frequency range was selected from 0.5 to 6 GHz with 20 MHz resolution (a total of 276 frequency points). Synthetically generated complex permittivity values were then placed in (6.1) to obtain the corresponding admittance. It should be noted that the dimensions of the probe (a and b in (6.1)) were chosen based on the commercially available Dielectric Assessment Kit (DAK). The outer radius of the probe (a) is 1.75 mm and inner radius (b) is 0.465 mm [104]. Finally, (6.3) was used to obtain the reflection coefficient. Through the application of this process, a dataset composed of reflection coefficients and corresponding Debye parameters was obtained. The dimensions of the dataset were 276×17748 (Γ) matrix (input of the deep learning model) corresponding to 3×17748 Debye parameters (output of the deep learning model).

6.2.3 Experiment setup and protocol for reflection coefficient measurements

Since the deep learning algorithm is modelled based on the generated theoretical data, it is critical to evaluate the model's performance with real measurements. Therefore, an experiment setup shown in Fig. 6.1 (a) was used to collect the reflection coefficient responses of the probe with standard pure liquids. The experiment setup consisted of N5230A PNA Series Network Analyzer (Santa Clara, CA, USA) and the commercial Speag DAK 3.5 mm-diameter open-ended coaxial probe (Zurich, Switzerland), shown in Fig. 6.1 (a) and (b). The frequency range of the analyzer was set from 0.5 to 6 GHz with 20 MHz increments; that is, 276 frequency points consistent with the synthetically generated data. An IF bandwidth of 10 Hz was selected to reduce the error due to

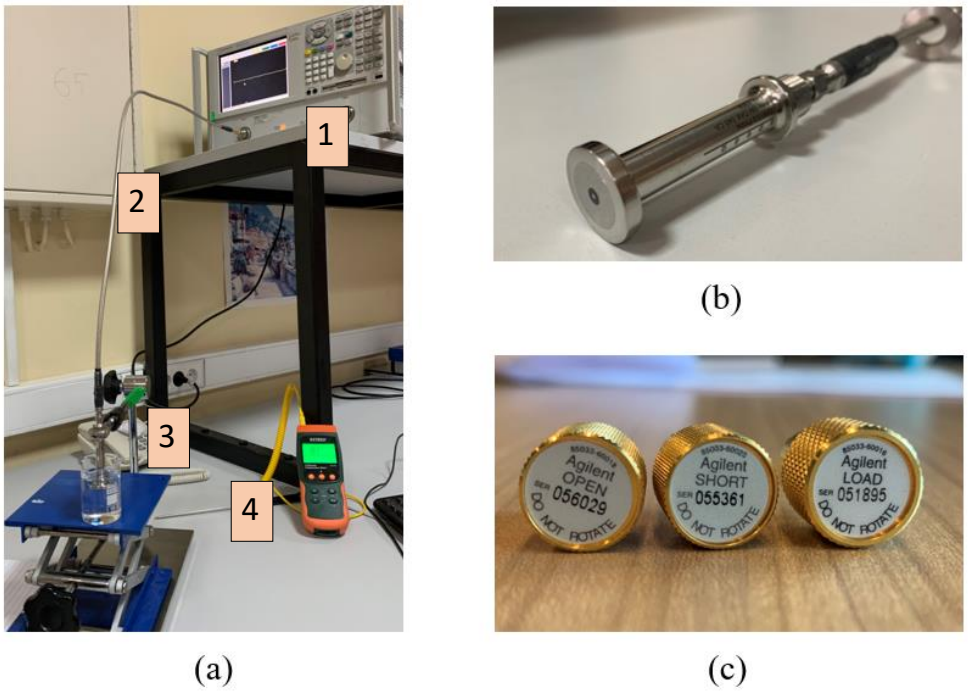

Figure 6.1 : Experimental setup and its components. (a) Experiment setup 1. N5230A PNA Series Network Analyzer, 2. RF cable, 3. sample: standard liquid and 4. EXTECH thermometer, (b) DAK 3.5 probe, and (c) mechanical calibration kit.

noise. The analyzer and probe were connected via an RF cable. Before connecting cable to the probe, the Agilent 85033E 3.5 mm standard mechanical calibration kit (Santa Clara, CA, USA), as seen in Fig. 6.1 (c), was used for RF calibration with the aim to transfer the measurement reference plane to the end of the cable.

Obtaining the reflection coefficient for any MUT requires the calibration of the probe. The standard protocol for calibrating the OECP is a three-step process (open circuit, short circuit and distilled water). Probe calibration procedure for obtaining the reflection coefficient Γ_c is given in section 6.2.1. To apply the given procedure in the section, measured reflection coefficients for the MUT (ρ) and the reflection coefficients of three known materials (ρ_1, ρ_2, ρ_3) were collected. The ρ_1, ρ_2, ρ_3 were measured by allowing the probe to radiate in free space (Open), terminating the probe's aperture with a copper strip (Short) and with a reference material (distilled water) respectively. The measured pure materials were DMSO, ethanol, ethylene glycol, formamide and methanol. The temperatures of the materials were 17.8$\pm$0.2°C at the time of the measurement. The mixtures were prepared via volume fractions:

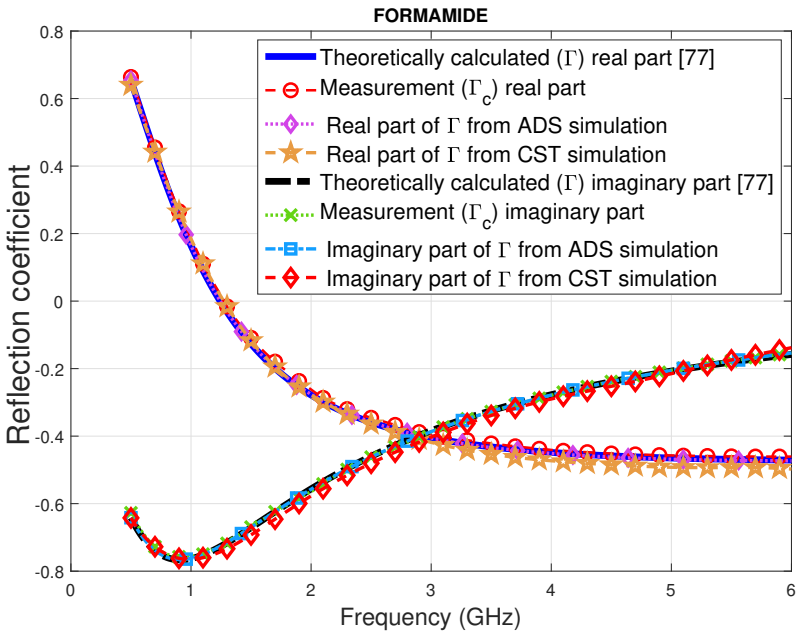

Figure 6.2 : Comparison of theoretically calculated reflection coefficients, the reflection coefficients obtained from commercial software (CST and ADS) and the measured calibrated reflection coefficients of formamide. The Debye parameters of formamide given in literature were used for the simulations and theoretical data.

formamide (90%)–1-buthanol (10%), formamide (70%)–1-buthanol (30%), DMSO (23%)–ethanol (77%) and DMSO (54%)–1-butanol (%46) at temperatures of 24.5±0.9 °C. Apart from the liquids/solutions, a gel-like material was prepared by mixing deionized water (15 ml) and triton X-100 (15 ml) at 23.5°C. Each measurement, (3 reflection coefficients for calibration step and the measurement of the samples) were repeated five times for statistical verification purposes. As an example of the consistency between the theoretical calculation and calibration, Fig. 6.2 depicts the comparison of the theoretically calculated Γ and the Γ_c obtained from the calibrated reflection coefficient of formamide. Additionally, comparison of the real and imaginary parts of the reflection coefficients obtained from the full-wave simulation software (CST Microwave Studio) and from the equivalent circuit model via Advanced Design System (ADS) [105] are given in Fig.6.2 in order to verify our results with benchmark simulation approaches. From this figure, it can be concluded that the theoretically generated reflection coefficients, the obtained reflection coefficients from commercial software tools, and the measured reflection coefficient of formamide are in good agreement.

6.2.4 Deep learning model design

Recently, many different studies have adopted deep learning to model nonlinear input-output relationships. This work presents the design of a deep neural network with 5 hidden layers as seen in Fig. 6.4. The inputs of the network were the real and imaginary parts of the reflection coefficients. As described in section 6.2.2, the input dataset was generated through the admittance model [69]. Before training the network, as a constraint, generated data with $\varepsilon_s < \varepsilon_\infty$ were omitted from the data set since it is known that most materials possess $\varepsilon_s > \varepsilon_\infty$ property. This approach shrank the dataset to 276×17732 reflection coefficients as input data and 3×17732 Debye parameters as the corresponding output data. Next, the dataset was divided into three sections, 80% was used for training and 10% was used for validation. After the training procedure was ended, the remaining 10% of the synthetically generated dataset was used for testing the designed network. Further, validation of the designed network was performed with the measured reflection coefficient data collected from a number of well-known liquids. As explained in section 6.2.3, in order to collect a measurement dataset compatible with the synthetically generated data, reflection coefficients of the commercially available DAK probe were measured between 0.5 to 6 GHz, with steps of 20 MHz. Thus, the obtained number of input parameters and the frequencies were consistent with the synthetic dataset.

The strategy of setting the neural network can be summarized as follows:

1) Normalize the output parameters with respect to its maximum value. For this study, ε_s, ε_∞ and τ were normalized by 120, 10, and 180 ps, respectively. This approach was applied in order to increase the numerical stability of training.

2) Number of inputs is determined by the number of frequencies for which the measurements are performed. (For this study, the number of inputs was 2×276 since the input parameters are complex numbers.) The number of outputs is the number of parameters that is to be extracted. Note that in this work, the dielectric properties (DP) is mathematically represented with the Debye equation and the number of Debye parameters is three; thus, the number of outputs were three. The design can be started with a single hidden layer, whose size is determined

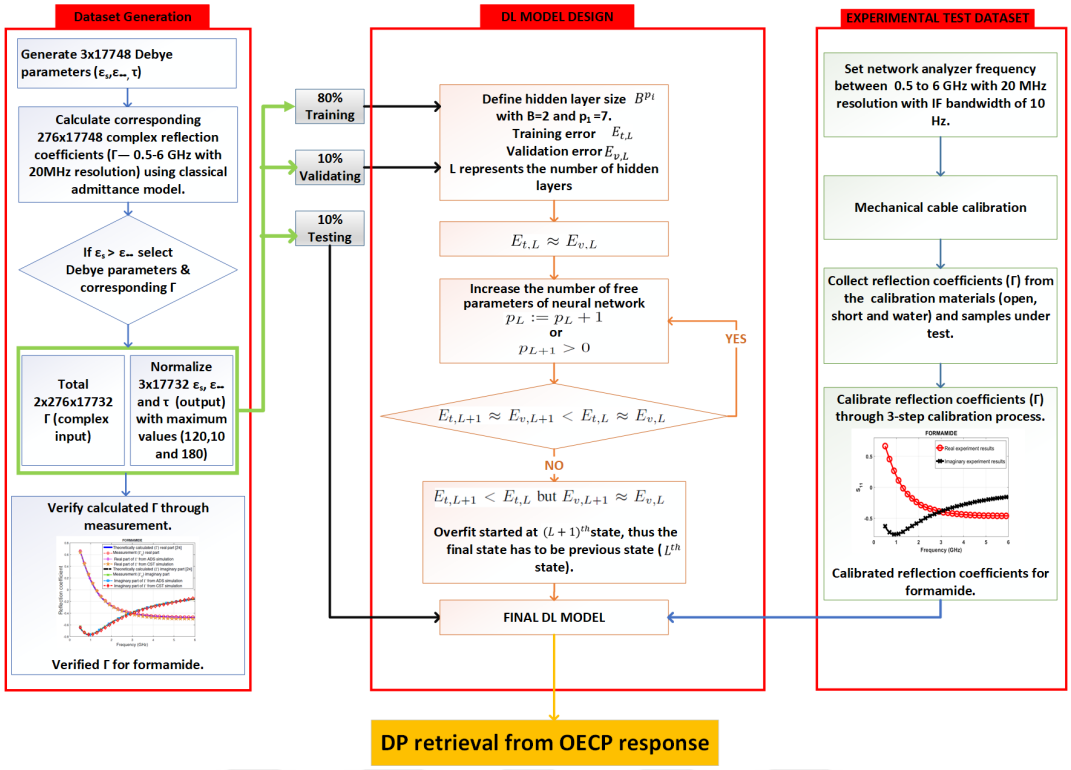

Figure 6.3 : Flowchart of the Deep Learning (DL) model along with the training and testing approach charts.

as $B^{p_i}, B, p_i \in N$ (i.e. integer powers of an integer) where i is the order of the related layer. In this study, $B = 2$ and we started with $p_1 = 7$.

3) Assume that there are L many hidden layers, let the training error for this case is $E_{t,L}$ and validation error for this case is $E_{v,L}$. If $E_{t,L} \approx E_{v,L}$ then increase the number of free parameters of neural network either by choosing $p_L := p_L + 1$ or by setting $p_{L+1} > 0, p_{L+1} \in N$.

4) If $E_{t,L+1} \approx E_{v,L+1} < E_{t,L} \approx E_{v,L}$, then go step 3. If $E_{t,L+1} < E_{t,L}$ but $E_{v,L+1} \approx E_{v,L}$ then the neural networks start to overfit the data; thus, go to the previous state and choose the final design with L layers. Fig. 6.3 shows a flowchart of the algorithm for designing DL model used in this work along with dataset production for training and testing steps.

Following the guidelines given above, the deep neural network model shown in Fig. 6.4 was designed. Please note that using batch normalization (BN) and Relu layer (ReLu) after each dense layer (DN), improves the model. Thus, after each dense layer, these two blocks were applied to the data subsequently. Finally, a regression layer (RL) was applied. The given model was trained on GPU using Matlab's Deep Neural

Table 6.1 : The mean and standard deviation of the percent relative errors for Debye parameters (ε_s, ε_∞ and τ) of the test set (10% of the synthetic dataset).

Debye parameters	Mean (%)	Std dev. (%)
ε_s (units)	1.86	3.01
ε_∞ (units)	3.33	9.52
τ (ps)	2.07	7.42

Network Toolbox on a computer with 32 GB RAM, 16 GB Intel(R) UHD Graphics 630 GPU, 2.6 GHz CPU. In the training, maximum of 200 epochs were applied to the model and Adam optimizer was used with least mean square error cost function. The training lasted approximately 10 mins and at the end of training the model had a loss of 0.02 for both training and validation data, indicates that the model did not overfit. Finally, to further show that the model can represent the nonlinear relationship between reflection coefficients and Debye parameters, test data (10% of the synthetic dataset) was processed by the trained network. For each case, the predicted Debye parameters were compared with the actual values and the percent relative error for each parameter was computed ($\frac{|Predicted-Exact|}{|Exact|} \times 100\%$). There were approximately 1700 sample in the test data and the histograms of percent relative error for each parameter are given in Fig. 6.5. Additionally, the mean and standard deviation of the percent relative errors of the test data are given in Table 6.1. As can be seen from these results, the designed model can accurately determine the Debye parameters.

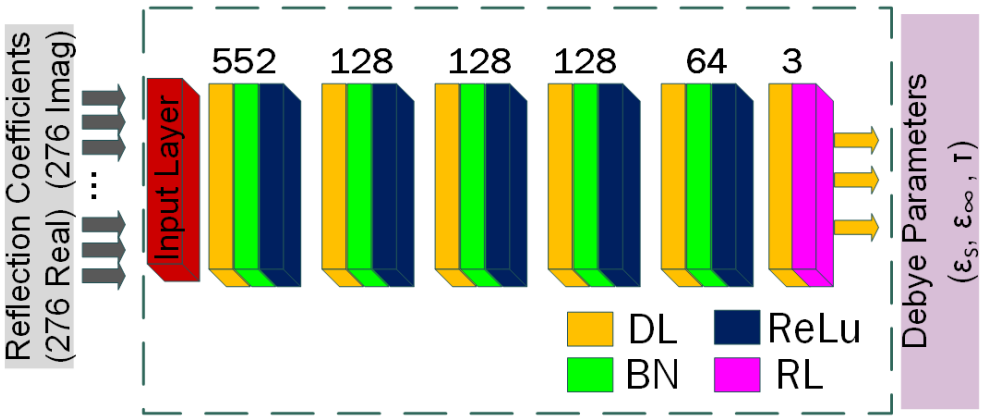

Figure 6.4 : Designed deep learning model with dense layer (DN), batch normalization (BN), Relu layer (ReLu) and regression layer (RL) for predicting Debye parameters from reflection coefficients.

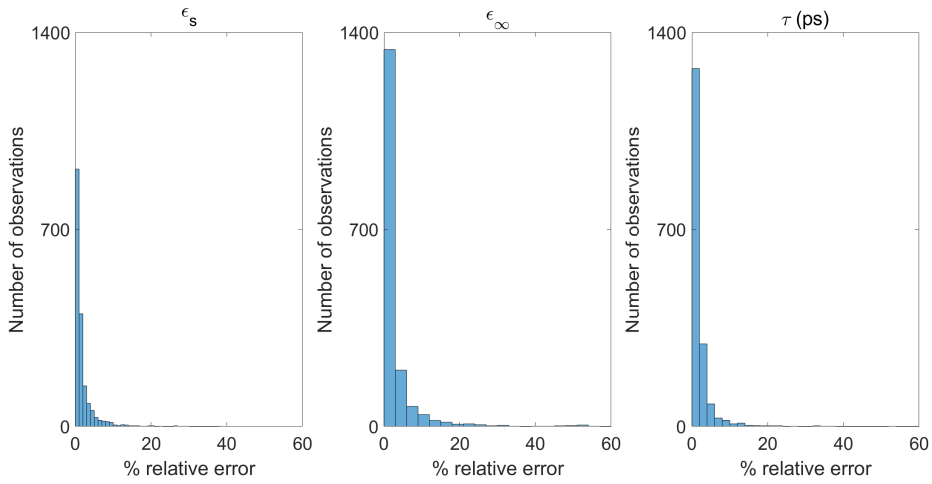

Figure 6.5 : Histograms of percent relative errors for each output parameter (ε_s, ε_∞ and τ) obtained for 1700 samples in the test set (10% of the synthetic dataset).

Table 6.2 : Complex permittivity comparison of formamide retrieved using the Deep Learning (DL) model from the reflection coefficients obtained via the theoretical model, full-wave software (CST), equivalent circuit model (ADS) and from the measured reflection coefficients. The results are compared with Debye parameters of formamide given in literature.

Freq. (GHz)	Data Generation Methods									
	Ref. [77]		Mea.-DL		Theo.-DL		CST–DL		ADS–DL	
	ε'	ε''	ε'	ε''	ε'	ε''	ε'	ε''	ε'	ε''
0.5	110	13.75	107.4	13.6	110.4	14.54	108.45	12.52	110.72	14.19
3	71.38	50.84	68.24	51.05	68.61	51.93	73.94	50.4	70.25	52.47
6	36.81	46.55	34.11	47.36	34.46	46.18	38.2	50.44	35.02	48.05

6.3 Results and Discussion

In this section, first, the DL method is verified by comparing the complex permittivity (ε' and ε'') of formamide retrieved by using reflection coefficients obtained through different approaches; that is, the theoretical model, full-wave solution (CST), equivalent circuit model (ADS) [105] , and the measured reflection coefficient. The complex permittivity results retrieved from DL model are also compared with the Debye parameters of formamide from [77]. The results are given in Table 6.2 and a good agreement is obtained with the literature as well as the different approaches.

To further test the optimized deep learning model with measured data, a dataset was generated by using 5 standard liquids; namely, dimethyl sulfoxide (DMSO), ethanol,

Table 6.3 : Comparison of Debye parameters given in literature and mean of the retrieved Debye parameters from the designed neural network (NN) for standard liquids. MPE±SPE for the calculated complex permittivity (ε_c) from retrieved Debye parameters with respect to literature values from 0.5 to 6 GHz.

Standard Liquids	ε_s (units)		ε_∞ (units)		τ (ps)		ε_c
	Ref.	NN-res.	Ref.	NN-res.	Ref.	NN-res.	MPE±SPE (%)
Dimethyl sulfoxide [106]	47.13	46.81	6.8	4.98	21.6	19.86	1.21±0.06
Ethanol [107]	25.07	22.82	4.2	4.00	143.24	150.22	10.89±0.08
Ethylene Glycol [108]	35.85	37.34	4.23	4.79	99.62	115.14	6.08±0.02
Formamide [77]	111.8	109.23	6.9	5.26	42.00	42.9	3.68±0.03
Methanol [107]	33.64	37.01	5.7	4.94	53.05	57.21	8.53± 0.02

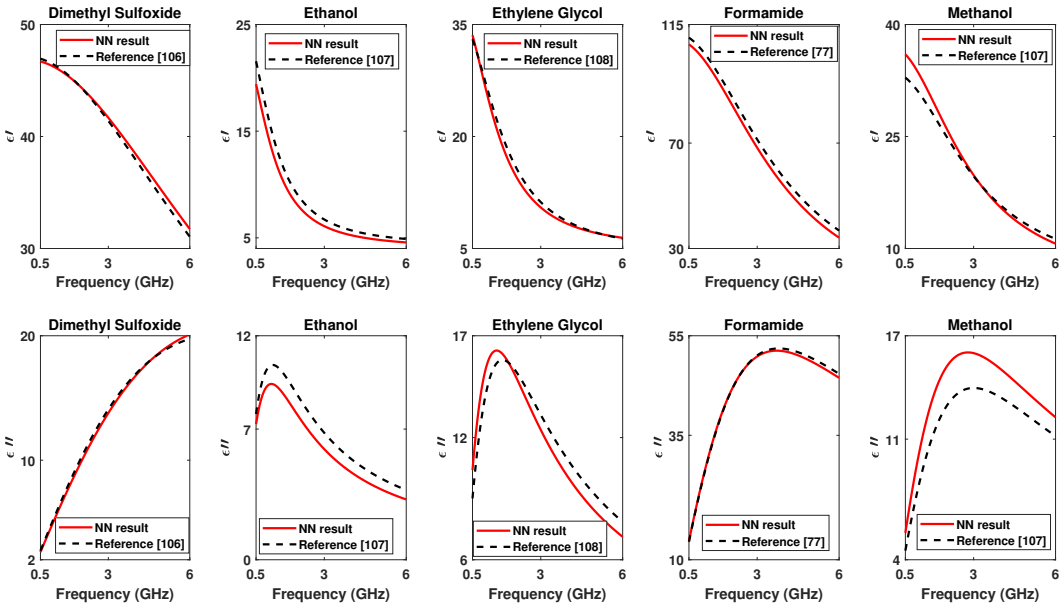

Figure 6.6 : Comparisons of calculated complex permittivities from the retrieved mean of Debye parameters and literature values of complex permittivities for five standard liquids: dymethyl sulfoxide, ethanol, ethylene glycol, formamide and methanol.

ethylene glycol, formamide, and methanol; and 4 mixtures. To compose the dataset, 5 reflection coefficient measurements with the commercially available DAK probe were collected from each of the liquids/mixtures, and the calibration standards; that is, open, short and distilled water. Then, 5 measurements for each material were combined with the calibration (open+short+water+material) to obtain a total of 625 different measurement. Thus, the obtained test datasets generated from experiments were

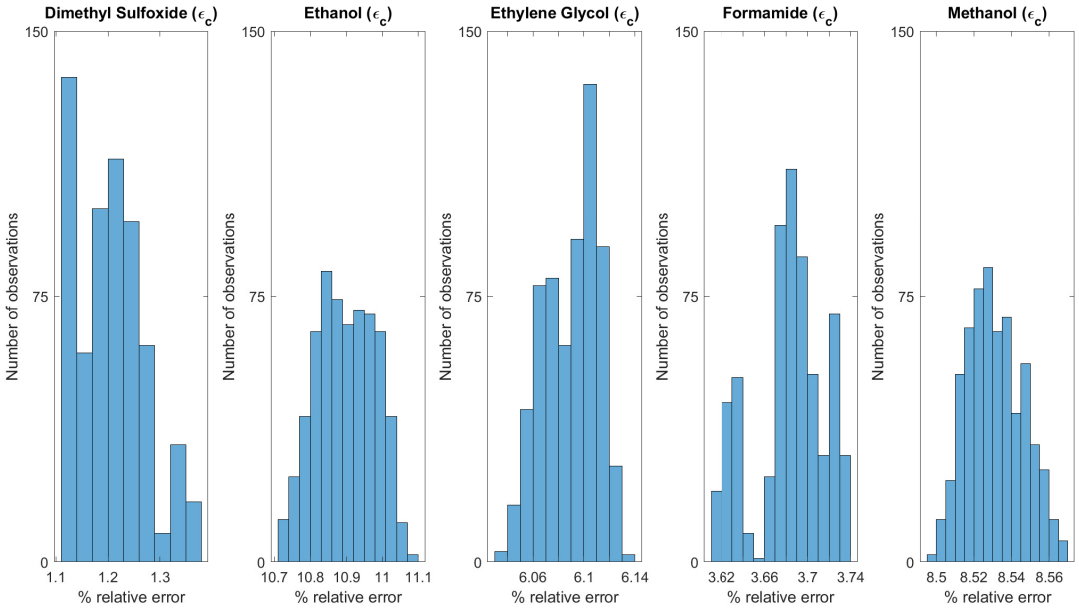

Figure 6.7 : The calculated E_{single} of eq.(6.8) of deep learning model by testing over 625 measurements for each standard liquid.

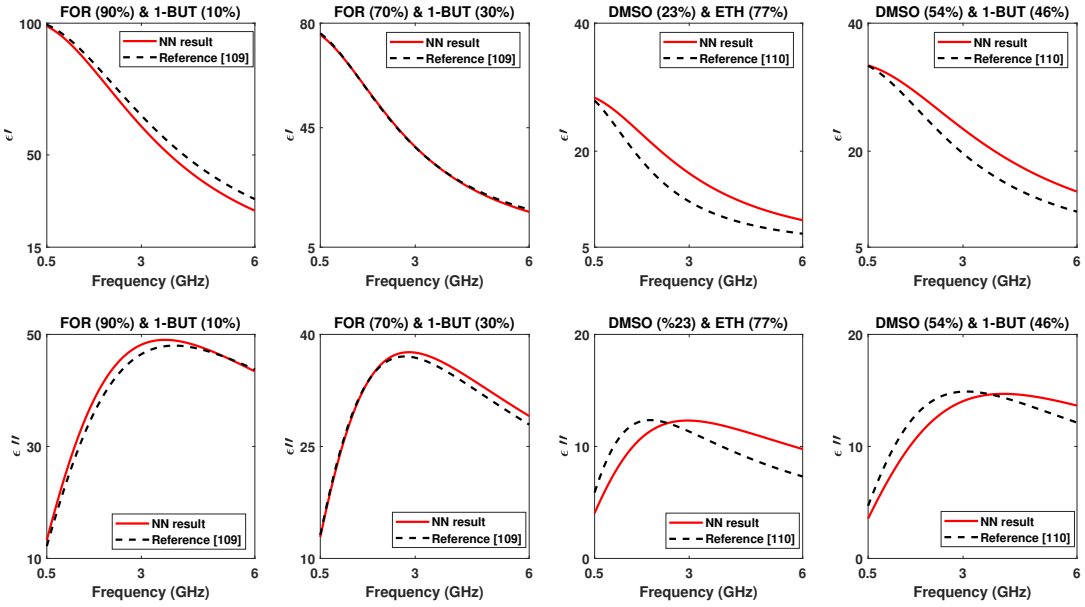

Figure 6.8 : Comparisons of calculated complex permittivities from the retrieved mean of Debye parameters and literature values of complex permittivities for three liquid mixtures: formamide (90%) & 1-butanol (10%), formamide (70%) & 1-butanol (30%), DMSO (23%) & ethanol (77%) and DMSO (54%) & 1-butanol (46%).

composed of 5×625 measurements for standard liquids and 4×625 measurements for mixtures. Apart from these two dataset, the deep learning model was tested with a gel-like material with the same data collection process.

Table 6.4 : Comparison of Debye parameters given in literature and mean of the retrieved Debye parameters from the designed neural network (NN) liquid mixtures. MPE±SPE for the calculated complex permittivity (ε_c) from retrieved Debye parameters with respect to literature values from 0.5 to 6 GHz.

Liquid Mixtures (Vol. frac. %)	ε_s (units)		ε_∞ (units)		τ (ps)		ε_c
	Ref.	NN-res.	Ref.	NN-res.	Ref.	NN-res.	MPE±SPE (%)
Formamide (90) & 1-Butanol (10) [109]	101.0	100.69	5.0	2.64	41.1	43.9	5.9± 0.18
Formamide (70) & 1-Butanol (30) [109]	79.0	78.14	4.9	3.29	58.3	56.95	1.75 ±0.05
* DMSO (23) & Ethanol (77) [110]	29.4	29.35	4.7	4.4	80.8	53.6	8.9±0.06
** DMSO (54) & 1-Butanol (46) [110]	34.1	33.83	4.3	4.43	51.5	39.11	4.83± 0.02

$*$ The parameter of β equals 0.77 in Debye equation [110] $**$ The parameter of β equals 0.84 in Debye equation [110].

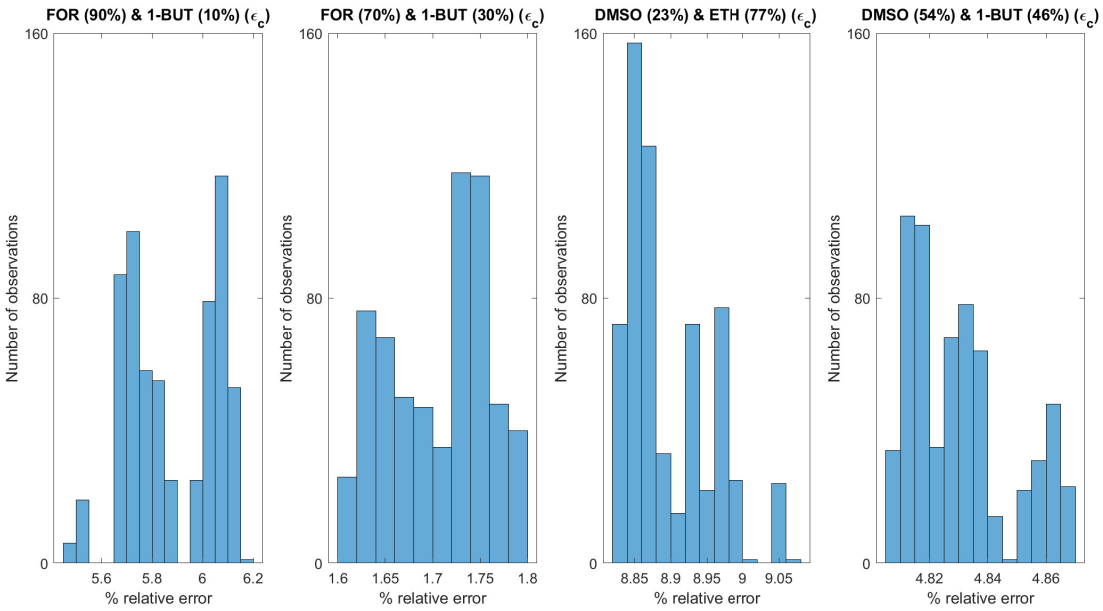

Figure 6.9 : The calculated E_{single} of eq.(6.8) of deep learning model by testing over 625 measurements for each liquid mixture.

The first dataset (5×625) was fed to the optimized deep neural network and the mean of the obtained network outputs; that is, mean Debye parameters corresponding to the dataset and literature values for five standard liquids are listed in Table 6.3. Furthermore, the complex permittivity was computed from the retrieved Debye parameters using equation (6.2). The mean of percent relative error (MPE)

and standard deviation of percent relative error (SPE) for the calculated complex permittivity from the retrieved Debye parameters are also given in Table 6.3. The MPE was calculated from 0.5-6 GHz using the equation of:

$$E_{single} = \frac{\sum_{Freq} \frac{|Predicted - Exact|}{|Exact|}}{276} \times 100 \tag{6.8}$$

$$MPE = \frac{\sum_{Measurements} E_{single}}{625} \tag{6.9}$$

where 'Predicted' is the complex permittivity calculated from the Debye parameters acquired from the deep learning neural network model and 'Exact' is the complex permittivity computed using Debye parameters obtained from the literature. Similarly, the SPE is calculated as:

$$SPE = \frac{\sum_{Measurements} (E_{single} - MPE)^2}{625} \tag{6.10}$$

As seen in Table 6.3, all MPEs are below 11%. Moreover, the SPEs for complex permittivity is below 0.08 units, which demonstrates that the deep learning model is robust enough to predict Debye parameters from reflection coefficients. In Fig. 6.6, a comparison of real (ε') and imaginary (ε'') parts of the complex permittivity calculated from the retrieved neural network Debye parameters and literature values are shown for five standard liquids from 0.5 to 6 GHz. To further investigate the accuracy of the deep learning model, the histograms for E_{single} of eq.(6.8) is given in Fig. 6.7. The maximum E_{single} was 11.1% for ethanol and the minimum E_{single} was 1.1% DMSO.

The second test dataset (4×625) includes the prepared mixtures. The mean of the estimated Debye parameters from neural network (NN) corresponding to the dataset and the literature values are listed in Table 6.4. Also, in the last column of Table 6.4, the MPE and SPE for the calculated complex permittivity from the retrieved Debye parameters is given. The results from Table 6.4 indicate that the obtained MPEs for all the mixtures are below 8.9%. Furthermore, the SPEs for complex permittivity is below 0.18 units. Comparison of the real (ε') and the imaginary (ε'') parts of the complex permittivity, which are computed from the retrieved Debye parameters and the literature, are shown in Fig. 6.8. The histograms E_{single} in complex permittivity for each mixture are given in Fig. 6.9. The maximum E_{single} for the calculated complex permittivity was 9.05% for the DMSO and ethanol mixture (volume ratio 2.3:7.7) and

the minimum E_{single} obtained from the formamide and 1-butanol mixture (volume ratio 7:3) is 1.6%. As seen from the histograms, the error of prediction from the deep learning model has differed in a small range for each sample.

The obtained results are an indication that the proposed approach is robust and can be used to retrieve the dielectric properties of materials with the OECP technique. When this study is compared with the previously reported work in the literature, to the best of authors' knowledge, only one reported work carried out a study utilizing NN to retrieve complex permittivity with OECP response [102]. However, the reported study only used measurements; therefore, train and test data were restricted with the measurements and availability of the materials. Also, in [102], the complex permittivity values of methanol were calculated from 0.5 to 5 GHz frequency range from three samples. The obtained real and imaginary values for methanol at 2.45 GHz were approximately 24 and 15 units, respectively. The computed real and imaginary values from the Debye parameters of methanol retrieved from the deep learning algorithm proposed in this work at 2.46 GHz are 23 and 15.9 units, respectively. To further expand the comparison, a gel-like solution containing 15 ml Triton X-100 and 15 ml de-ionized water was prepared. At 2.45 GHz, [102] reported 35 and 8 units for real and imaginary parts of DP, respectively. In this work, the retrieved real and imaginary DP values from the trained NN at 2.46 GHz are 33.4 and 10.4 units, respectively. It should also be noted that, unlike [102], our work provides statistical analysis of 625 different combinations of methanol measurements.

In [106], the traditional approach for dielectric property characterization with iterative solution techniques was implemented. Furthermore, the Debye parameters of DMSO between 30 MHz and 5 GHz frequency band were reported with approximately 95% confidence level using linear interpolation via Monte Carlo modelling. The calculated MPE between obtained results in this work and [106] is 1.21 ± 0.06 for DMSO. As seen in Table 6.3, the maximum error was observed in the complex permittivity of ethanol. Instead of the single-pole Debye (3 parameters), the Debye-Γ (4 parameters) can potentially offer a more suitable relaxation equation for ethanol as mentioned in [106]. In [108], the measurement of ethylene glycol was performed using the transmission line (TL) approach from 0.3 to 3 GHz. The Debye parameters were calculated from the complex permittivity by solving a system of nonlinear equations

using MATLAB's fsolve function. The calculated Debye parameters for ethylene glycol differ from the work in [108] as much as 1.51 units, 0.56 units and 15.52 ps for ε_s, ε_∞ and τ, respectively. These differences can be due to the different approaches used in obtaining the Debye parameters. In [77], the complex permittivity of formamide was measured from 10 MHz to 70 GHz frequency range and the best fit was represented by a single-Debye type dispersion. As seen in Table 6.3, the retrieved Debye parameters difference in [77] and this work is 2.57 units, 1.64 units and 0.9 ps for ε_s, ε_∞ and τ, respectively. In [109], formamide and 1-butanol were mixed with different volume fractions. The measurements were taken over the frequency range of 0.2 to 13.5 GHz. In this work, two different mixtures were prepared in fractions of 9:1 and 7:3. The results in Table 6.4 indicate that the MPE$\pm$SPE is 5.9$\pm$0.18 and 1.75$\pm$0.05 for these mixtures. In another study [110], the dielectric properties of the mixture of DMSO and monohydric alcohol were analyzed. In this work, DMSO and ethanol mixture was prepared with a volume fraction of 2.3:7.7, corresponding to a molar fraction of 2:8. The results show that the MPE$\pm$SPE is 8.9$\pm$0.05. Similarly, DMSO and 1-butanol mixture solution was prepared with a volume fraction of 5.4:4.6, that is molar fraction of 6:4. The obtained results indicate MPE$\pm$SPE of 4.83$\pm$0.02. Consequently, the results obtained from this work match well with the literature data, which were obtained through different methods.

As a final example, the trained NN is compared with the brute force look up table (LUT) approach. The LUT has two problems: (i) it requires a data table to be held in memory and (ii) for each estimation, the points that are close to the data point has to be determined, which requires evaluating the distance between the data point and the points in the LUT. These two problems become worse with increasing the dimension of the measured data. In contrast to this, a trained NN consists of simple computations (multiplications, summations and activation function evaluations). From another perspective, LUT is similar to memorization, it tries to separate all instances of data points by dividing the output space into Voronoi cells with respect to a metric, while NN is akin to generalization (or vary much similar to learning with aid of a complicated formula). The goal of NN is to find a nonlinear function that can map the input to output. To further explore the difference, the DMSO example in Table 6.3 is re-estimated with the LUT approach. 80% of the dataset (17732×0.8 S-parameters

simulations, each of which includes 276 frequencies) are used to form a LUT. With the perspective defined above, we can think that there are 17732×0.8 many points in $R^{276\times 2}$ in LUT. Then, the Euclidean distance between DMSO measurement in Table 6.3 and each data point in LUT is calculated and the Debye parameters of DMSO are assigned as the Debye parameters of the closest point in LUT. To assess the robustness of the LUT based method, it was evaluated 50 times (with different selections of 17732×0.8 many S-parameters simulations from 17732 simulations) and the average Debye parameters are estimated as $\varepsilon_s = 48.7$, $\varepsilon_\infty = 7.35$ and $\tau = 24.0$ ps with an MPE of 3.37 % (this was 1.21 % for DMSO using NN as seen from Table 6.3). In terms of computational speed, NN based method spends 3.8 ms on average, while LUT spends 24.0 ms on average for one single dielectric property estimation. From the point-view of memory consumption, the LUT needs much more resources than the NN, since it needs a large table ($276 \times 17732 \times 0.8 + 3 \times 17732 \times 0.8 = 3.9 \times 10^6$ many complex numbers) to be held in memory to decide the best suitable estimation; while NN requires to hold the coefficients of designed network ($552 \times 128 + 128 \times 128 + 128 \times 128 + 128 \times 64 + 64 \times 3 = 1.2 \times 10^5$ many real number). In conclusion, the cost of using NN is to train a neural network, yet after training NN is more efficient than LUT approach both in terms of time and memory performance.

6.4 Conclusion

In this work, an alternative approach is proposed for obtaining Debye parameters from the reflection coefficient response of the OECP when terminated with a material by utilizing a deep learning model. A synthetically generated dataset was used to design the deep learning model. The synthetic dataset was produced by modeling the OECP with the traditional admittance model [69]. Theoretically modeling the OECP enabled us to effortlessly create a large-scale dataset utilized for designing the deep learning model. A combination of 29 ε_s, 12 ε_∞ and 51 τ Debye parameters were used to compose Debye models representing a wide range of materials. Among the generated Debye parameters 17732 samples were selected from the generated dataset and reflection coefficients were calculated from 0.5 to 6 GHz with 267 frequency points using the admittance model. A total number of 276×17732 input dataset (reflection coefficients) and 3×17732 output dataset (Debye parameters) was produced. To

design the deep neural network, 80, 10, 10 % of the dataset was used for training, validating and testing the model, respectively. The model has (mean)±(std.dev) percent relative errors between 1.86 ± 3.01, 3.33 ± 9.52 and 2.07 ± 7.42 for predicting ε_s, ε_∞ and τ of test set (10% of the generated dataset), respectively. In order to test the designed deep learning model with experimental results, 625 input dataset (reflection coefficients) was prepared using measurements collected from five different standard liquids, four mixtures and a gel-like material. Collected measurements were performed in the frequency range of 0.5 to 6 GHz with 20 MHz resolution. The complex dielectric constants are obtained from the Debye parameters retrieved using the optimized deep learning model and the calculated complex permittivities were compared with reference data obtained from the literature. Obtained minimum and maximum (mean)±(std.dev) complex permittivity percent relative errors are 1.21 ± 0.06 and 10.89 ± 0.08, respectively.

7. CONCLUSIONS

In this thesis, we investigate the detection of biological tissue anomalies based on microwave dielectric properties discrepancy between the healthy and abnormal tissues in terms of analyzing tissue- and equipment-related error.

The first part of the thesis present the sensing depth analysis of the 2.2 mm-diameter probe for skin cancer detection. In order to examine the impact of the sensing depth and skin tissue heterogeneity on the dielectric property measurements, we implemented simulations and experiments using two double-layered sample configurations. In the simulation, the axial magnitude of electric field strength was evaluated when the probe tip is terminated with four different sample configurations. Furthermore, the reflection coefficients obtained from simulations were applied into in-house algorithm to investigate sensing depth of the probe with dielectric property of the samples. Moreover, we prepared two different double-layered sample configurations including skin-mimicking phantom as a first layer and olive oil/triton X-100 as a second layer for the experimental measurements. Different from previously reported studies, we carried out the experiments using a simple measurement setup without forming a special experiment setup tank. The analysis to define the sensing depth were perfomed with three percent thresholds in relative permittivity changes 5, 20, and 80%. The distance results achieved from both the simulation and experiment at 2 GHz for 5%, 20% and 80% increase in dielectric properties of olive oil and triton X-100 are 0.66–1.2 mm, 0.36–0.86 mm and 0.14–0.42 mm, respectively, from the first layer (first reference point; that is, the top surface of skin phantom). Therefore, we concluded that a membrane layer or keratin layer on the skin tissue has a potential effect of 80% on the dielectric property measurement. Furthermore, the results show that the layer in immediate contact with the probe tip has the most critical impact on dielectric property measurements.

In the second part of this thesis, the sensing depth of 2.2 mm-diameter open-ended coaxial probe was investigated for animal experiment. Rats are widely used as

experimental animals for breast cancer research because their hormone responses with histopathology and premalignant stages are similar to the human breast cancer model. However, a heterogeneous formation beneath the rat's pelt, leakage of milk from the gland and bodily fluids or bleeding during the experiment can mislead the measurement results. To this end, the double-layered samples were prepared that included rat breast and wet skin tissue as a first layer and liquids (olive oil and triton X-100) added as second layers. Liquids with relatively low dielectric properties provide important information for the potential change in dielectric properties measurement, as the liquids mimic the effect of adipose tissue, which can overlay healthy tissues and tumors. Five percent thresholds for relative permittivity and conductivity changes (5%, 10%, 20%, 80% and 90%) were examined at five frequency points to find the appropriate definition of sensing depth. The change from 5% to 90% increase in relative permittivity for the olive oil was reported between 3.28 to 0.42 mm probe tip distance from the breast tissue at 0.5 GHz. Also, the changes from 5% to 90% increase in conductivity for the olive oil was taken place in the distance range of 5.2–0.38 mm at 1.05 GHz. Similarly, the dielectric property changes of triton X-100 was in the distance range of 1.43–0.61 mm. Apart from these changes, the percent decrease in dielectric properties for rat breast and skin tissues was addressed in the distance range of 0.02–1.33 mm. Any membrane layer (between 0.4–0.8 mm thickness) on the wet skin tissue and breast tissue can mislead the measurement results of dielectric property by 52–84%.

In the third part of thesis, the main contribution is to designate the sensing depth of the open-ended coaxial probe in order to use an appropriate probe for the experiments. Therefore, it can reduce the errors caused by the tissue heterogeneity for skin cancer detection.

Three probes with different aperture sizes (0.5, 0.9 and 2.2 mm-diameter) and double-layered sample configuration (skin tissue and olive oil) were simulated to analyze sensing depth of the probes. Furthermore, the simulation was validated by the experiment performed with the 2.2 mm-diameter probe and the double-layered configuration. Consequently, the probe aperture proportionally affected the sensing depth. If the dielectric property of thin skin tissue layers is a target for measurements, the smaller probe aperture required selecting to reduce errors related to the

heterogeneity of the tissue. Yet, when measuring with a smaller aperture probe, if there is a layer of membrane or any tissue fluid on the target tissue surface, the measurement result will be affected more than expected. Thus, it is necessary to establish a measurement protocol for tissues consisting of a multilayer structure or which may have a membrane or any other layer on the measurement surface. In addition, it is possible to determine tissue heterogeneity using probes with multiple aperture sizes.

In the forth and last part of the thesis, we propose an alternative approach to retrieve Debye parameters from the reflection coefficient response of the open-ended coaxial probe by using a deep learning model. The large-scale training, validating and testing dataset were synthetically generated by theoretically modeling open-ended coaxial probe with the traditional admittance model. $2\times276\times17732$ reflection coefficients as total input and 3×17732 Debye parameters as total output are generated. To design the deep neural network, the dataset is split into 80%, 10% and 10% to train, validate and test the model, respectively. The designed model was analyzed by percent relative errors using (mean)$\pm$(std.dev). The results for predicting ε_s, ε_∞ and τ was found 1:86$\pm$3:01, 3:33$\pm$9:52 and 2:07$\pm$7:42, respectively. The designed deep learning model was also tested with experimental measurements collected from five different standard liquids, four mixtures and a gel-like material. The minimum and maximum (mean)$\pm$(std.dev) complex permittivity percent relative errors are 1.21$\pm$0.06 and 10.89$\pm$0.08, respectively.

REFERENCES

[1] **Fricke, H.** and **Morse, S.** (1926). The electric capacity of tumors of the breast, *The Journal of Cancer Research*, *10*.

[2] **England, T. S.** and **Sharples, N. A.** (1949). Dielectric properties of the human body in the microwave region of the spectrum, *Nature*, *163*.

[3] **Cook, H. F.** (1951). The dielectric behaviour of some types of human tissues at microwave frequencies, *British Journal of Applied Physics*, *2*, 295.

[4] **Foster, K. R.**, **Schepps, J. L.**, **Stoy, R. D.**, and **Schwan, H. P.** (1979). Dielectric properties of brain tissue between 0.01 and 10 GHz, *Physics in Medicine and Biology*, *24*.

[5] **Halter, R. J.**, **Zhou, T.**, **Meaney, P. M.**, **Hartov, A.**, **Barth, R. J.**, **Rosenkranz, K. M.** ... **Paulsen, K. D.** (2009). The correlation of in vivo and ex vivo tissue dielectric properties to validate electromagnetic breast imaging: Initial clinical experience, *Physiological Measurement*, *30*.

[6] **Misra, D.**, **Chabbra, M.**, **Epstein, B. R.**, **Microtznik, M.**, and **Foster, K. R.** (1990). Noninvasive electrical characterization of materials at microwave frequencies using an open-ended coaxial line: Test of an improved calibration technique, *IEEE transactions on microwave theory and techniques*, *38*, 8–14.

[7] **Technologies, K.** (2015). Application Note: Basics of Measuring the Dielectric Properties of Materials, *5989-2589En*.

[8] **Peyman, A.**, **Holden, S.**, and **Gabriel, C.** (2005). Mobile telecommunications and health research programme: Dielectric properties of tissues at microwave frequencies, *Microwave Consultants Limited: London, UK*.

[9] **Gabriel, S.**, **Lau, R. W.**, and **Gabriel, C.** (1996). The dielectric properties of biological tissues: II. Measurements in the frequency range 10 Hz to 20 GHz, *Physics in Medicine and Biology*, *41*.

[10] **Stuchly, M. A.**, **Athey, T. W.**, **Samaras, G. M.**, and **Taylor, G. E.** (1982). Measurement of radio frequency permittivity of biological tissues with an open-ended coaxial line: Part II-Experimental results, *IEEE Transactions on Microwave Theory and Techniques*, *30*, 87–92.

[11] **Schulsinger, D. A.** (2015). *Kidney stone disease: Say NO to stones!*

[12] **Hospital, M. P.** (2018). *Patient Guide about Kidney Stones*, `http://www.bobrektasitedavisi.net/bobrek-taslari/`.

[13] **Basiri, A.**, **Taheri, M.**, and **Taheri, F.** (2012). What is the state of the stone analysis techniques in urolithiasis?, *Urology Journal*, *9*.

[14] **Saçlı, B.**, **Aydınalp, C.**, **Cansız, G.**, **Joof, S.**, **Yilmaz, T.**, **Çayören, M.** ... **Akduman, I.** (2019). Microwave dielectric property based classification of renal calculi: Application of a kNN algorithm, *Computers in Biology and Medicine*, *112*.

[15] **Yilmaz, T.**, **Sacli, B.**, **Cansiz, G.**, **Joof, S.**, **Aydinalp, C.**, **Cayoren, M.** ... **Onal, B.** (2019). Microwave dielectric spectroscopy of renal calculi: A large scale study on dielectric properties from 500 MHz to 18 GHz, *IEEE Transactions on Dielectrics and Electrical Insulation*, *26*.

[16] **Meyers, P. A.** and **Gorlick, R.** (1997). Osteosarcoma, *Pediatric Clinics of North America*, *44*.

[17] **Ottaviani, G.** and **Jaffe, N.** (2009). The epidemiology of osteosarcoma, volume152.

[18] **Freeman, C. R.**, **Gledhill, R.**, **Chevalier, L. M.**, **Whitehead, V. M.**, and **Esseltine, D. L.** (1980). Osteogenic sarcoma following treatment with megavoltage radiation and chemotherapy for bone tumors in children, *Medical and Pediatric Oncology*, *8*.

[19] **Messerschmitt, P. J.**, **Garcia, R. M.**, **Abdul-Karim, F. W.**, **Greenfield, E. M.**, and **Getty, P. J.** (2009). Osteosarcoma, *Journal of the American Academy of Orthopaedic Surgeons*, *17*.

[20] **Peyman, A.**, **Gabriel, C.**, **Grant, E. H.**, **Vermeeren, G.**, and **Martens, L.** (2009). Variation of the dielectric properties of tissues with age: The effect on the values of SAR in children when exposed to walkie-talkie devices, *Physics in Medicine and Biology*, *54*.

[21] **Meaney, P. M.**, **Goodwin, D.**, **Golnabi, A. H.**, **Zhou, T.**, **Pallone, M.**, **Geimer, S. D.** ... **Paulsen, K. D.** (2012). Clinical microwave tomographic imaging of the calcaneus: A first-in-human case study of two subjects, *IEEE Transactions on Biomedical Engineering*, *59*.

[22] **Yilmaz, T.** and **Alkan, F. A.** (2020). In vivo dielectric properties of healthy and benign rat mammary tissues from 500 mhz to 18 ghz, *Sensors (Switzerland)*, *20*.

[23] **Jithin, D.**, **Hussein, M. I.**, **Awwad, F.**, and **Irtini, R.** (2017). Dielectric characterization of breast cancer cell lines using microwaves.

[24] **Egot-Lemaire, S.**, **Pijanka, J.**, **Sulé-Suso, J.**, and **Semenov, S.** (2009). Dielectric spectroscopy of normal and malignant human lung cells at ultra-high frequencies, *Physics in Medicine and Biology*, *54*.

[25] **Odelstad, E.**, **Raman, S.**, **Rydberg, A.**, and **Augustine, R.** (2014). Experimental Procedure for Determination of the Dielectric Properties of Biological Samples in the 2-50 GHz Range, *IEEE Journal of Translational Engineering in Health and Medicine*, *2*.

[26] **Macit, Z.**, **Aydinalp, C.**, **Yilmaz, T.**, **Sert, A. B. O.**, and **Kok, F. N.** (2019). Microwave Dielectric properties of Osteosarcoma Cell Line (SAOS-2) Suspensions.

[27] **MacIt, Z.**, **Aydinalp, C.**, **Yilmaz, T.**, **Sert, A. B. O.**, and **Kok, F. N.** (2020). Broadband Microwave Dielectric Property Comparison of Human Fetal Osteoblastic (hFOB) and Osteosarcoma (SaOS-2) Cell Lines.

[28] **Macit, Z.**, (2019). Microwave dielectric property characterization of healthy and cancerous bone cells with open-ended coaxial probe, M.Sc. Thesis, Fen Bilimleri Enstitüsü.

[29] **Ghoncheh, M.**, **Pournamdar, Z.**, and **Salehiniya, H.** (2016). Incidence and mortality and epidemiology of breast cancer in the world, *Asian Pacific Journal of Cancer Prevention*, *17*.

[30] **Abeel, T.**, **Helleputte, T.**, **de Peer, Y. V.**, **Dupont, P.**, and **Saeys, Y.** (2009). Robust biomarker identification for cancer diagnosis with ensemble feature selection methods, *Bioinformatics*, *26*.

[31] **Hwang, K.-B.**, **Cho, D.-Y.**, **Park, S.-W.**, **Kim, S.-D.**, and **Zhang, B.-T.** (2002). *Applying Machine Learning Techniques to Analysis of Gene Expression Data: Cancer Diagnosis*.

[32] **Ramos-Pollán, R.**, **Guevara-López, M. A.**, **Suárez-Ortega, C.**, **Díaz-Herrero, G.**, **Franco-Valiente, J. M.**, **Rubio-Del-Solar, M.** ... **Ramos, I.** (2012). Discovering mammography-based machine learning classifiers for breast cancer diagnosis, *Journal of Medical Systems*, *36*.

[33] **Elmore, J. G.**, **Barton, M. B.**, **Moceri, V. M.**, **Polk, S.**, **Arena, P. J.**, and **Fletcher, S. W.** (1998). Ten-year risk of false positive screening mammograms and clinical breast examinations, *New England Journal of Medicine*, *338*(16), 1089–1096.

[34] **Kriege, M.**, **Brekelmans, C. T.**, **Boetes, C.**, **Besnard, P. E.**, **Zonderland, H. M.**, **Obdeijn, I. M.** ... **Klijn, J. G.** (2004). Efficacy of MRI and Mammography for Breast-Cancer Screening in Women with a Familial or Genetic Predisposition, *New England Journal of Medicine*, *351*.

[35] **Fear, E. C.**, **Hagness, S. C.**, **Meaney, P. M.**, **Okoniewski, M.**, and **Stuchly, M. A.** (2002). Enhancing breast tumor detection with near-field imaging, *IEEE Microwave Magazine*, *3*.

[36] **Surowiec, A. J.**, **Stuchly, S. S.**, **Barr, J. R.**, and **Swarup, A.** (1988). Dielectric Properties of Breast Carcinoma and the Surrounding Tissues, *IEEE Transactions on Biomedical Engineering*, *35*.

[37] **Campbell, A. M.** and **Land, D. V.** (1992). Dielectric properties of female human breast tissue measured in vitro at 3.2 GHz, *Physics in Medicine and Biology*, *37*.

[38] **Meaney, P. M.**, **Fanning, M. W.**, **Li, D.**, **Poplack, S. P.**, and **Paulsen, K. D.** (2000). A clinical prototype for active microwave imaging of the breast, *IEEE Transactions on Microwave Theory and Techniques*, *48*.

[39] **Lazebnik, M.**, **McCartney, L.**, **Popovic, D.**, **Watkins, C. B.**, **Lindstrom, M. J.**, **Harter, J.** ... **Hagness, S. C.** (2007). A large-scale study of the ultrawideband microwave dielectric properties of normal breast tissue obtained from reduction surgeries, *Physics in Medicine and Biology*, *52*.

[40] **Iannaccone, P. M.** and **Jacob, H. J.** (2009). *Rats!*, The Company of Biologists Ltd.

[41] **Onemli, E.**, **Joof, S.**, **Aydinalp, C.**, **Pastacı Özsobacı, N.**, **Ateş Alkan, F.**, **Kepil, N.** ... **Yilmaz, T.** (2022). Classification of rat mammary carcinoma with large scale in vivo microwave measurements, *Scientific reports*, *12*(1), 1–11.

[42] **Gioia, A. L.**, **Porter, E.**, **Merunka, I.**, **Shahzad, A.**, **Salahuddin, S.**, **Jones, M.** and **O'Halloran, M.** (2018). Open-ended coaxial probe technique for dielectric measurement of biological tissues: Challenges and common practices, *Diagnostics*, *8*, 40.

[43] **Schwan, H. P.** and **Li, K.** (1953). Capacity and Conductivity of Body Tissues at Ultrahigh Frequencies, *Proceedings of the IRE*, *41*.

[44] **Lazebnik, M.**, **Converse, M. C.**, **Booske, J. H.**, and **Hagness, S. C.** (2006). Ultrawideband temperature-dependent dielectric properties of animal liver tissue in the microwave frequency range, *Physics in Medicine and Biology*, *51*.

[45] **C Gabriel A Peyman, S. H.** (2000). Dielectric Properties of Tissues at Microwave Frequencies, *Mobile Telecommunications and Health Research Programme*.

[46] **Burdette, E. C.**, **Cain, F. L.**, and **Seals, J.** (1980). In Vivo Probe Measurement Technique for Determining Dielectric Properties at VHF Through Microwave Frequencies, *IEEE Transactions on Microwave Theory and Techniques*, *28*.

[47] **Semenov, S. Y.**, **Posukh, V. G.**, **Bulyshev, A. E.**, **Williams, T. C.**, **Sizov, Y. E.**, **Repin, P. N.** ... **Nazarov, A.** (2006). Microwave tomographic imaging of the heart in intact swine, *Journal of Electromagnetic Waves and Applications*, *20*.

[48] **Yilmaz, T.** (2020). Multiclass classification of hepatic anomalies with dielectric properties: From phantom materials to rat hepatic tissues, *Sensors*, *20*(2), 530.

[49] **Jin, J.**, **Zhang, C.**, **Feng, F.**, **Na, W.**, **Ma, J.**, and **Zhang, Q.-J.** (2019). Deep neural network technique for high-dimensional microwave modeling and applications to parameter extraction of microwave filters, *IEEE Transactions on Microwave Theory and Techniques*, *67*(10), 4140–4155.

[50] **Schwan, H. P.** (1957). *Electrical properties of tissue and cell suspensions*, volume 5, Elsevier.

[51] **Kraszewski, A.**, **Stuchly, M. A.**, **Stuchly, S. S.**, and **Smith, A. M.** (1982). In vivo and in vitro dielectric properties of animal tissues at radio frequencies, *Bioelectromagnetics*, *3*.

[52] **Yilmaz, T.**, **Kiliç, M. A.**, **Erdoğan, M.**, **Çayören, M.**, **Tunaoğlu, D.**, **Kurtoğlu, I.** ... **Kalkan, T.** (2016). Machine learning aided diagnosis of hepatic malignancies through in vivo dielectric measurements with microwaves, *Physics in Medicine and Biology*, *61*.

[53] **Mirbeik-Sabzevari, A.**, **Ashinoff, R.**, and **Tavassolian, N.** (2018). Ultra-wideband millimeter-wave dielectric characteristics of freshly excised normal and malignant human skin tissues, *IEEE Transactions on Biomedical Engineering*, *65*.

[54] **Aydinalp, C.**, **Joof, S.**, **Yilmaz, T.**, **Özsobaci, N. P.**, **Alkan, F. A.**, and **Akduman, I.** (2019). In vitro dielectric properties of rat skin tissue for microwave skin cancer detection, *2019 International Applied Computational Electromagnetics Society Symposium (ACES)*, Ieee, pp.1–2.

[55] **Sugitani, T.**, **Kubota, S. I.**, **Kuroki, S. I.**, **Sogo, K.**, **Arihiro, K.**, **Okada, M.** ... **Kikkawa, T.** (2014). Complex permittivities of breast tumor tissues obtained from cancer surgeries, *Applied Physics Letters*, *104*.

[56] **Meaney, P. M.**, **Gregory, A. P.**, **Epstein, N. R.**, and **Paulsen, K. D.** (2014). Microwave open-ended coaxial dielectric probe: Interpretation of the sensing volume re-visited, *BMC Medical Physics*, *14*.

[57] **Grove, T. T.**, **Masters, M. F.**, and **Miers, R. E.** (2005). Determining dielectric constants using a parallel plate capacitor, *American Journal of Physics*, *73*.

[58] **Karacolak, T.**, **Cooper, R.**, **Unlu, E. S.**, and **Topsakal, E.** (2012). Dielectric properties of porcine skin tissue and in vivo testing of implantable antennas using pigs as model animals, *IEEE Antennas and Wireless Propagation Letters*, *11*, 1686–1689.

[59] **Athey, T. W.**, **Stuchly, M. A.**, and **Stuchly, S. S.** (1982). Measurement of radio frequency permittivity of biological tissues with an open-ended coaxial line: Part I, *IEEE Transactions on Microwave Theory and Techniques*, *30*, 82–86.

[60] **Martellosio, A.**, **Pasian, M.**, **Bozzi, M.**, **Perregrini, L.**, **Mazzanti, A.**, **Svelto, F.** ... **Bellomi, M.** (2016). Dielectric properties characterization from 0.5 to 50 GHz of breast cancer tissues, *IEEE Transactions on Microwave Theory and Techniques*, *65*, 998–1011.

[61] **Lazebnik, M.**, **Popovic, D.**, **McCartney, L.**, **Watkins, C. B.**, **Lindstrom, M. J.**, **Harter, J.** ... **Hagness, S. C.** (2007). A large-scale study of the ultrawideband microwave dielectric properties of normal, benign and malignant breast tissues obtained from cancer surgeries, *Physics in medicine & biology*, *52*(20), 6093.

[62] **Meaney, P. M.**, **Gregory, A. P.**, **Seppälä, J.**, and **Lahtinen, T.** (2016). Open-ended coaxial dielectric probe effective penetration depth determination, *IEEE transactions on microwave theory and techniques*, *64*, 915–923.

[63] **Hagl, D. M.**, **Popovic, D.**, **Hagness, S. C.**, **Booske, J. H.**, and **Okoniewski, M.** (2003). Sensing volume of open-ended coaxial probes for dielectric characterization of breast tissue at microwave frequencies, *IEEE Transactions on Microwave Theory and Techniques*, *51*.

[64] **Porter, E.** and **O'Halloran, M.** (2017). Investigation of histology region in dielectric measurements of heterogeneous tissues, *IEEE Transactions on Antennas and Propagation*, *65*, 5541–5552.

[65] **Gioia, A. L.**, **O'Halloran, M.**, **Elahi, A.**, and **Porter, E.** (2018). Investigation of histology radius for dielectric characterisation of heterogeneous materials, *IEEE Transactions on Dielectrics and Electrical Insulation*, *25*, 1064–1079.

[66] **Aydinalp, C.**, **Joof, S.**, and **Yilmaz, T.** (2019). Sensing depth analysis of open-ended coaxial probe for skin cancer detection, *2019 23rd International Conference on Applied Electromagnetics and Communications (ICECOM)*, IEEE, pp.1–5.

[67] **Gandhi, O. P.** and **Riazi, A.** (1986). Absorption of millimeter waves by human beings and its biological implications, *IEEE Transactions on microwave theory and techniques*, *34*, 228–235.

[68] **Keysight**, Keysight, (2018). N1501A Dielectric Probe Kit 10 MHz to 50 GHz, `https://literature.cdn.keysight.com/litweb/pdf/5992-0264EN.pdf?id=2605692`.

[69] **Levine, H.** and **Papas, C. H.** (1951). Theory of the circular diffraction antenna, *Journal of applied physics*, *22*, 29–43.

[70] **Garrett, D. C.**, **Bourqui, J.**, and **Fear, E. C.** (2017). Antenna calibration method for dielectric property estimation of biological tissues at microwave frequencies, *Progress In Electromagnetics Research*, *158*, 73–87.

[71] **Šegatin, N.**, **Pajk Žontar, T.**, and **Poklar Ulrih, N.** (2020). Dielectric Properties and Dipole Moment of Edible Oils Subjected to 'Frying'Thermal Treatment, *Foods*, *9*(7), 900.

[72] **Schwan, H. P.** and **Foster, K. R.** (1980). RF-field interactions with biological systems: electrical properties and biophysical mechanisms, *Proceedings of the IEEE*, *68*, 104–113.

[73] **O'rourke, A. P.**, **Lazebnik, M.**, **Bertram, J. M.**, **Converse, M. C.**, **Hagness, S. C.**, **Webster, J. G.** and **Mahvi, D. M.** (2007). Dielectric properties of human normal, malignant and cirrhotic liver tissue: in vivo and ex vivo measurements from 0.5 to 20 GHz using a precision open-ended coaxial probe, *Physics in medicine & biology*, *52*(15), 4707.

[74] **Treuting, P. M.**, **Dintzis, S. M.**, and **Montine, K. S.** (2017). *Comparative anatomy and histology: a mouse, rat, and human atlas*, Academic Press.

[75] **Maynard, R. L.** and **Downes, N.** (2019). *Anatomy and Histology of the Laboratory rat in Toxicology and Biomedical Research*, Academic Press.

[76] **Hamzah, H.**, **Abduljabar, A.**, **Lees, J.**, and **Porch, A.** (2018). A compact microwave microfluidic sensor using a re-entrant cavity, *Sensors*, *18*, 910.

[77] **Jordan, B. P.**, **Sheppard, R. J.**, and **Szwarnowski, S.** (1978). The dielectric properties of formamide, ethanediol and methanol, *Journal of Physics D: Applied Physics*, *11*, 695.

[78] **Lu, Z.**, **Manias, E.**, **Macdonald, D. D.**, and **Lanagan, M.** (2009). Dielectric relaxation in dimethyl sulfoxide/water mixtures studied by microwave dielectric relaxation spectroscopy, *The Journal of Physical Chemistry A*, *113*, 12207–12214.

[79] **Vavken, P.**, **Joshi, S.**, and **Murray, M. M.** (2009). TRITON-X is most effective among three decellularization agents for ACL tissue engineering, *Journal of orthopaedic research*, *27*, 1612–1618.

[80] **Gabriel, C.**, **Gabriel, S.**, and **Corthout, y. E.** (1996). The dielectric properties of biological tissues: I. Literature survey, *Physics in medicine & biology*, *41*(11), 2231.

[81] **Jafary-Asl, A.** and **Smith, C.** (1983). Biological dielectrics in electric and magnetic fields, *Conference on Electrical Insulation & Dielectric Phenomena-Annual Report 1983*, IEEE, pp.350–355.

[82] **Mohammed, B.**, **Naqvi, S.**, **Manoufali, M.**, **Bialkowski, K.**, and **Abbosh, A.** (2018). Changes in epidermal dielectric properties due to skin cancer across the band 1 to 50 GHz, *2018 Australian Microwave Symposium (AMS)*, IEEE, pp.77–78.

[83] **Hwang, H.**, **Yim, J.**, **Cho, J.-W.**, **Cheon, C.**, and **Kwon, Y.** (2003). 110 GHz broadband measurement of permittivity on human epidermis using 1 mm coaxial probe, *IEEE MTT-S International Microwave Symposium Digest, 2003*, volume 1, IEEE, pp.399–402.

[84] **La Gioia, A.**, **Santorelli, A.**, **O'Halloran, M.**, and **Porter, E.** (2020). Predicting the Sensing Radius of a Coaxial Probe Based on the Probe Dimensions, *IEEE Transactions on Antennas and Propagation*, *68*(9), 6704–6716.

[85] **Aydinalp, C.**, **Joof, S.**, and **Yilmaz, T.** (2021). Towards Non-Invasive Diagnosis of Skin Cancer: Sensing Depth Investigation of Open-Ended Coaxial Probes, *Sensors*, *21*(4), 1319.

[86] **Aydinalp, C.**, **Joof, S.**, and **Yilmaz, T.** (2021). Towards Accurate Microwave Characterization of Tissues: Sensing Depth Analysis of Open-Ended Coaxial Probes with Ex Vivo Rat Breast and Skin Tissues, *Diagnostics*, *11*(2), 338.

[87] **Alekseev, S.** and **Ziskin, M.** (2007). Human skin permittivity determined by millimeter wave reflection measurements, *Bioelectromagnetics: Journal of the Bioelectromagnetics Society, The Society for Physical Regulation in Biology and Medicine, The European Bioelectromagnetics Association*, *28*(5), 331–339.

[88] **Stuchly, M. A.** and **Stuchly, S. S.** (1980). Coaxial line reflection methods for measuring dielectric properties of biological substances at radio and microwave frequencies-A review, *IEEE Transactions on instrumentation and measurement*, *29*(3), 176–183.

[89] **Blackham, D. V.** and **Pollard, R. D.** (1997). An improved technique for permittivity measurements using a coaxial probe, *IEEE Transactions on Instrumentation and Measurement*, *46*(5), 1093–1099.

[90] **Filali, B.**, **Boone, F.**, **Rhazi, J.**, and **Ballivy, G.** (2008). Design and calibration of a large open-ended coaxial probe for the measurement of the dielectric properties of concrete, *IEEE Transactions on Microwave Theory and Techniques*, *56*(10), 2322–2328.

[91] **Komarov, S. A.**, **Komarov, A. S.**, **Barber, D. G.**, **Lemes, M. J.**, and **Rysgaard, S.** (2016). Open-ended coaxial probe technique for dielectric spectroscopy of artificially grown sea ice, *IEEE Transactions on Geoscience and Remote Sensing*, *54*(8), 4941–4951.

[92] **Popovic, D.**, **McCartney, L.**, **Beasley, C.**, **Lazebnik, M.**, **Okoniewski, M.**, **Hagness, S. C.** and **Booske, J. H.** (2005). Precision open-ended coaxial probes for in vivo and ex vivo dielectric spectroscopy of biological tissues at microwave frequencies, *IEEE Transactions on Microwave Theory and Techniques*, *53*.

[93] **Grant, J.**, **Clarke, R.**, **Symm, G.**, and **Spyrou, N. M.** (1989). A critical study of the open-ended coaxial line sensor technique for RF and microwave complex permittivity measurements, *Journal of Physics E: Scientific Instruments*, *22*(9), 757.

[94] **Stuchly, M. A.**, **Brady, M. M.**, **Stuchly, S. S.**, and **Gajda, G.** (1982). Equivalent circuit of an open-ended coaxial line in a lossy dielectric, *IEEE Transactions on instrumentation and Measurement*, (2), 116–119.

[95] **Gajda, G.** and **Stuchly, S. S.** (1983). An equivalent circuit of an open-ended coaxial line, *IEEE transactions on instrumentation and measurement*, *32*(4), 506–508.

[96] **Monsefi, F.**, **Otterskog, M.**, and **Silvestrov, S.** (2013). Direct and Inverse Computational Methods for Electromagnetic Scattering in Biological Diagnostics, *arXiv preprint arXiv:1312.4379*.

[97] **Misra, D. K.** (1987). A quasi-static analysis of open-ended coaxial lines (short paper), *IEEE Transactions on Microwave Theory and Techniques*, *35*(10), 925–928.

[98] **Xu, Y.**, **Bosisio, R.**, and **Bose, T.** (1991). Some calculation methods and universal diagrams for measurement of dielectric constants using open-ended coaxial probes, *IEE Proceedings H (Microwaves, Antennas and Propagation)*, volume138, IET, pp.356–360.

[99] **Artioli, M.**, **Perez, M. D.**, **Reggiani, U.**, and **Sandrolini, L.** (2010). Particle Swarm Optimization method for complex permittivity extraction of dispersive materials, *2010 Asia-Pacific International Symposium on Electromagnetic Compatibility*, IEEE, pp.900–903.

[100] **Marcuvitz, N.** (1951). *Waveguide handbook*, 21, Iet.

[101] **Li, M.**, **Guo, R.**, **Zhang, K.**, **Lin, Z.**, **Yang, F.**, **Xu, S.** ... **Abubakar, A.** (2021). Machine Learning in Electromagnetics With Applications to Biomedical Imaging: A Review, *IEEE Antennas and Propagation Magazine*.

[102] **Bonello, J.**, **Demarco, A.**, **Farhat, I.**, **Farrugia, L.**, and **Sammut, C. V.** (2020). Application of artificial neural networks for accurate determination of the complex permittivity of biological tissue, *Sensors*, *20*(16), 4640.

[103] **Chen, X.**, **Wei, Z.**, **Li, M.**, and **Rocca, P.** (2020). A review of deep learning approaches for inverse scattering problems (invited review), *Progress In Electromagnetics Research*, *167*, 67–81.

[104] OVERVIEW SPEAG, Schmid & Partner Engineering AG, swiss, `https://speag.swiss/products/dak/overview/`.

[105] **Chen, L.-F.**, **Ong, C.**, **Neo, C.**, **Varadan, V.**, and **Varadan, V. K.** (2004). *Microwave electronics: measurement and materials characterization*, John Wiley & Sons.

[106] **Gregory, A.** and **Clarke, R.** (2009). Tables of the complex permittivity of dielectric reference liquids at frequencies up to 5 GHz; NPL Report MAT 23, *Innovation*, 1–87.

[107] **Buckley, F.** (1958). Tables of dielectric dispersion data for pure liquids and dilute solutions, *United States Department of Commerce,National Bureau of Standards, Circular,*, *589*, 7–8.

[108] **Mosavirik, T.**, **Soleimani, M.**, **Nayyeri, V.**, **Mirjahanmardi, S. H.**, and **Ramahi, O. M.** (2021). Permittivity Characterization of Dispersive Materials Using Power Measurements, *IEEE Transactions on Instrumentation and Measurement*, *70*, 1–8.

[109] **Lou, J.**, **Hatton, T. A.**, and **Laibinis, P. E.** (1997). Effective dielectric properties of solvent mixtures at microwave frequencies, *The Journal of Physical Chemistry A*, *101*(29), 5262–5268.

[110] **Guo-Zhu, J.** and **Jie, Q.** (2014). Dielectric constant of dimethyl sulfoxide-monohydric alcohol mixture solution at the microwave frequency, *Fluid Phase Equilibria*, *365*, 5–10.

CURRICULUM VITAE

Name SURNAME **:** Cemanur AYDINALP

EDUCATION **:**

- **B.Sc.** **:** 2011, Ankara University, Faculty of Science and Engineering, the Department of Electronics Engineering.
- **M.Sc.** **:** 2015, San Diego State University, Faculty of Electrical and Computer Engineering, the Department of Electrical Engineering

PROFESSIONAL EXPERIENCE AND REWARDS:

- 2019 CA17115 Conference Grant for 2019 International Applied Computational Electromagnetics Society Symposium (ACES) in Miami
- 2019 CA17115 Conference Grant for 23rd International Conference on Applied Electromagnetics and Communications (ICECOM-Dubrovnik) in Dubrovnik, Croatia.
- 2020 CA18223 Conference Grant for the 14th European Conference on Antennas and Propagation, (EuCAP2020) in Copenhagen, Denmark.
- 2021 CA17115 Conference Grant for 34. General Assembly and Scientific Symposium (GASS) of the International Union of Radio Science (Union Radio Scientifique Internationale-URSI) in Rome, Italy.
- 2021 COST Action SyMat CA18223 and the European School of Antennas (ESoA) in hybrid format ESoA-SyMat school on "Exploiting Symmetries in Artificial Materials for Antenna Applications," in Paris, France.
- 2021 COST Action MyWave CA17115 Short Term Scientific Mission (STSM) on " Training on numerical simulation software CST," in Malta.

PUBLICATIONS AND PRESENTATIONS ON THE THESIS:

- **Aydinalp, C.**, Joof, S., Akinci, M. N., Akduman, I. and Yilmaz, T. 2022. Microwave Dielectric Property Retrieval From Open-Ended Coaxial Probe Response With Deep Learning, *IEEE Access,* vol. 10, pp. 1216-1227.

- **Aydinalp, C.**, Joof, S., Dilman, I., Akduman, I. and Yilmaz, T. 2022. Characterization of Open-Ended Coaxial Probe Sensing Depth with Respect to Aperture Size for Dielectric Property Measurement of Heterogeneous Tissues, *Sensors,* 22(3), 760.

- **Aydinalp, C.**, Joof, S., and Yilmaz, T. 2021. Towards non-invasive diagnosis of skin cancer: Sensing depth investigation of open-ended coaxial probes, *Sensors,* 21(4), 1319.

- **Aydinalp, C.** , Joof, S., and Yilmaz, T.2021. Towards Accurate Microwave Characterization of Tissues: Sensing Depth Analysis of Open-Ended Coaxial Probes with Ex Vivo Rat Breast and Skin Tissues, *Diagnostics,* 11(2), 338.

- **Aydinalp, C.**, Joof, S., and Yilmaz, T. 2021. Microwave Dielectric Property Based Stage Detection of Skin Cancer, *XXXIVth General Assembly and Scientific Symposium of the International Union of Radio Science (URSI GASS),* August 28 – September 4 2021 Roma, Italy.

- **Aydinalp, C.**, Joof, S., Akduman, I. and Yilmaz, T. 2019. Sensitivity and Sensing Depth Analysis of Open-ended Contact Probes for Cancer Diagnosis, *Progress in Electromagnetics Research Symposium (PIERS),* June 17-20, 2019 Rome, Italy.

- **Aydinalp, C.**, Joof, S., Yilmaz, T., Özsobaci, N. P., Alkan, F. A. and Akduman, I. 2019. In Vitro Dielectric Properties of Rat Skin Tissue for Microwave Skin Cancer Detection, *In 2019 International Applied Computational Electromagnetics Society Symposium (ACES),* April 14-19, 2019 Miami (FL), USA.

- **Aydinalp, C.**, Joof, S., and Yilmaz, T. 2019. Sensing Depth Analysis of Open-Ended Coaxial Probe for Skin Cancer Detection, *23rd International Conference on Applied Electromagnetics and Communications (ICECOM),* September 30–October 2, 2019 Dubrovnik, Croatia.

OTHER PUBLICATIONS AND PRESENTATIONS:

- Onemli, E., Joof, S., **Aydınalp, C.**, Özsobaci, N. P., Alkan, F. A., Kepil, N., Rekik, I., Akduman, I. and Yilmaz, T. 2022. Classification of rat mammary carcinoma with large scale in vivo microwave measurements, *Scientific Reports,* 12, 349.

- Yilmaz, T., Saçlı, B., Cansız, G., Joof, S., **Aydınalp, C.**, Çayören, M., Akduman, I. and Onal, B. 2019. Microwave dielectric spectroscopy of renal calculi: A large scale study on dielectric properties from 500 MHz to 18 GHz,*IEEE Transactions on Dielectrics and Electrical Insulation,* 26(5), 1425 – 1433.

- Saçlı, B., **Aydınalp, C.**, Cansız, G., Joof, S., Yilmaz, T., Çayören, M., Onal, B. and Akduman, I.2019.Microwave dielectric property based classification of renal calculi: Application of a kNN algorithm, *Computers in Biology and Medicine,* 112, 103366.

- **Aydinalp, C.**, and Yilmaz, T. 2021. Detection of Diseased Tissues with Open-Ended Coaxial Probes, *XXXIVth General Assembly and Scientific Symposium of the International Union of Radio Science (URSI GASS),* August 28 – September 4 2021 Roma, Italy.

- Yilmaz, T., Onemli, E., and **Aydinalp, C.** 2021. Temperature-dependent Dielectric Property of Breast Tissue Phantoms for Hyperthermia Applications, *XXXIVth General Assembly and Scientific Symposium of the International Union of Radio Science (URSI GASS),* August 28 – September 4 2021 Roma, Italy.

- Macit, Z., **Aydinalp, C.**, Sert, A.B.O, Kok, F.N. and Yilmaz, T. 2019. Broadband Microwave Dielectric Property Comparison of Human Fetal Osteoblastic (hFOB) and Osteosarcoma (SaOS-2) Cell Lines, *14th European Conference on Antennas and Propagation (EuCAP),* March 15-20, 2020 Copenhagen, Denmark.

- Macit, Z., **Aydinalp, C.**, Sert, A.B.O, Kok, F.N. and Yilmaz, T. 2019. Microwave Dielectric properties of Osteosarcoma Cell Line (SAOS-2) Suspensions., *23rd International Conference on Applied Electromagnetics and Communications (ICECOM),* September 30–October 2, 2019 Dubrovnik, Croatia.

- Onal, G.E., Kelesoglu, A., Sacli, B., Cansiz, G., Joof, S., **Aydinalp, C.**, and Cayoren, M. 2017. Kidney Stone Classification with Electromagnetic Properties: Preliminary Results, *25th Telecommunication Forum (TELFOR),* November 21-22, 2017 Belgrade, Serbia.